The study of two transmembrane autophagy proteins and

the autophagy receptor, p62

UNIVERSITY OF
CAMBRIDGE

Gautam M. Runwal

St. John's College, Cambridge

September 2018

This dissertation is submitted for the degree of Doctor of Philosophy

Title: The study of two transmembrane autophagy proteins and the autophagy receptor, p62

Submitted by : Gautam M Runwal

Abstract

Autophagy is an evolutionarily conserved process across eukaryotes that is responsible for degradation of cargo such as aggregate-prone proteins, pathogens, damaged organelles, macromolecules etc. via its delivery to lysosomes. The process is known to involve the formation of a double-membraned structure, called autophagosome, that engulfs the cargo destined for degradation and delivers its contents by fusing with lysosomes. This process involves several proteins at its core which include two transmembrane proteins, ATG9 and VMP1. While ATG9 and VMP1 has been discovered for about a decade and half, the trafficking and function of these proteins remain relatively unclear. My work in this thesis identifies and characterises a novel trafficking route for ATG9 and VMP1 and shows that both these proteins traffic via the dynamin-independent ARF6-associated pathway. Moreover, I also show that these proteins physically interact with each other. In addition, the tools developed during these studies helped me identify a new role for the most common autophagy receptor protein, p62. I show that p62 can specifically associate with and sequester LC3-I in autophagy-impaired cells (ATG9 and ATG16 null cells) leading to formation of LC3-positive structures that can be misinterpreted as mature autophagosomes. Perturbations in the levels of p62 were seen to affect the formation of these LC3-positive structures in cells. This observation, therefore, questions the reliability of LC3-immunofluorescence assays in autophagy-impaired cells as method of assessing autophagy and points towards the homeostatic function played by p62 in autophagy-impaired cells.

Declaration

This dissertation is the result of my own work and includes nothing which is the outcome of work done in collaboration except as declared in the Preface and specified in the text.

It is not substantially the same as any that I have submitted, or, is being concurrently submitted for a degree or diploma or other qualification at the University of Cambridge or any other University or similar institution except as declared in the Preface and specified in the text. I further state that no substantial part of my dissertation has already been submitted, or, is being concurrently submitted for any such degree, diploma or other qualification at the University of Cambridge or any other University of similar institution except as declared in the Preface and specified in the text.

This thesis does not exceed 60,000 words.

Abstract

Autophagy is an evolutionarily conserved process across eukaryotes that is responsible for degradation of cargo such as aggregate-prone proteins, pathogens, damaged organelles, macromolecules etc. via its delivery to lysosomes. The process is known to involve the formation of a double-membraned structure, called autophagosome, that engulfs the cargo destined for degradation and delivers its contents by fusing with lysosomes. This process involves several proteins at its core which include two transmembrane proteins, ATG9 and VMP1. While ATG9 and VMP1 has been discovered for about a decade and half, the trafficking and function of these proteins remain relatively unclear. My work in this thesis identifies and characterises a novel trafficking route for ATG9 and VMP1 and shows that both these proteins traffic via the dynamin-independent ARF6-associated pathway. Moreover, I also show that these proteins physically interact with each other. In addition, the tools developed during these studies helped me identify a new role for the most common autophagy receptor protein, p62. I show that p62 can specifically associate with and sequester LC3-I in autophagy-impaired cells (ATG9 and ATG16 null cells) leading to formation of LC3-positive structures that can be misinterpreted as mature autophagosomes. Perturbations in the levels of p62 were seen to affect the formation of these LC3-positive structures in cells. This observation, therefore, questions the reliability of LC3-immunofluorescence assays in autophagy-impaired cells as method of assessing autophagy and points towards the homeostatic function played by p62 in autophagy-impaired cells.

Table of Contents

3. Studying ATG9 phosphorylation in HeLa cells

4. Characterisation of ATG9 CRISPR knockout cell line

5. LC3-I associates with p62 in autophagy-impaired cells

1.   Introduction

1.1.   Autophagy

Cellular homeostasis includes processes that are involved in maintaining the steady state inside the cell. A notable process amongst these, involved in roles beyond maintaining cellular homeostasis, is autophagy. Recent studies have shown autophagy to play a role in multitude of functions like degradation o aggregate-prone proteins, pathogens, damaged organelles, macromolecules etc. and not simply maintaining cellular homeostasis (Bento et al., 2016b; Ravikumar et al., 2009).

Autophagy is an evolutionarily conserved catabolic process responsible for the bulk degradation of cytosolic cargo by delivering them to lysosomes. There are three different types of autophagy: macroautophagy, microautophagy and chaperone-mediated autophagy, classified on the basis of the mode of cargo delivery to the lysosomes (Fig 1.1 a) (Jimenez-Sanchez et al., 2012).

1.1.1. Chaperone-mediated autophagy

Chaperone-mediated autophagy is a highly selective autophagic process that involves binding of the substrate to a chaperone and co-chaperones facilitating its transport across the lysosomal membrane. Studies have shown that starvation for about 8-10 hours activates CMA (Cuervo et al., 1995). The substrates destined for degradation by this mode of autophagy are characterised by a KFERQ-like motif that is recognised by the chaperone HSC70 (heat shock cognate protein of 70 kDa) and co-chaperones like CHIP (carboxy terminus of HSC70-interacting protein), HSP40 (heat shock protein 40), HOP (HSP70-HSP90 organising protein). This targets the substrate to the lysosomal membrane and promotes its interaction with LAMP2A (lysosomal-associated membrane protein type 2A), while promoting the unfolding of the substrate. This is followed by the translocation of the unfolded protein substrate across the lysosomal membrane into the lysosomal lumen for degradation (Jimenez-Sanchez et al., 2012; Kaushik and Cuervo, 2018).

1.1.2. Microautophagy

Microautophagy involves the engulfment of the cargo to be degraded via the invagination of the lysosomal membrane. While studies in yeast have provided some mechanistic insights into the process, its role in mammalian cells remains unclear. The yeast studies have shown the requirement of TOR and EGO protein complexes to regulate and facilitate microautophagy in yeast. This study also proposes that microautophagy plays a role in the decrease of the lysosomal size on macroautophagy induction (Dubouloz et al., 2005).

1.1.3. Macroautophagy

Macroautophagy constitutes the major form of autophagy in cells and hereafter will be referred to simply as 'autophagy' in this thesis. While this process was considered to be largely non-specific, recent studies have shown the process to be specific for certain substrates. A few examples of these processes include clearance of damaged organelles like mitochondria – mitophagy, peroxisomes – pexophagy, aggregate-prone proteins – aggrephagy, etc (Ashrafi and Schwarz, 2013; Jr et al., 2005; Stolz et al., 2014).

Autophagy involves the formation of double-membraned autophagosomes that engulf cargoes destined for lysosomal degradation. The autophagosome has been proposed to be derived from a cytoplasmic, cup-shaped structure named phagophore. The phagophore encapsulates and sequesters the cargo to be degraded by elongation of its edges, finally resulting in closure by sealing off the ends. The autophagosomes then fuse with lysosomes to form structures called 'autolysosomes', where the contents are degraded and recycled back in the form of amino acids and other similar macromolecules (Fig 1.1 b) (Rubinsztein et al., 2012).
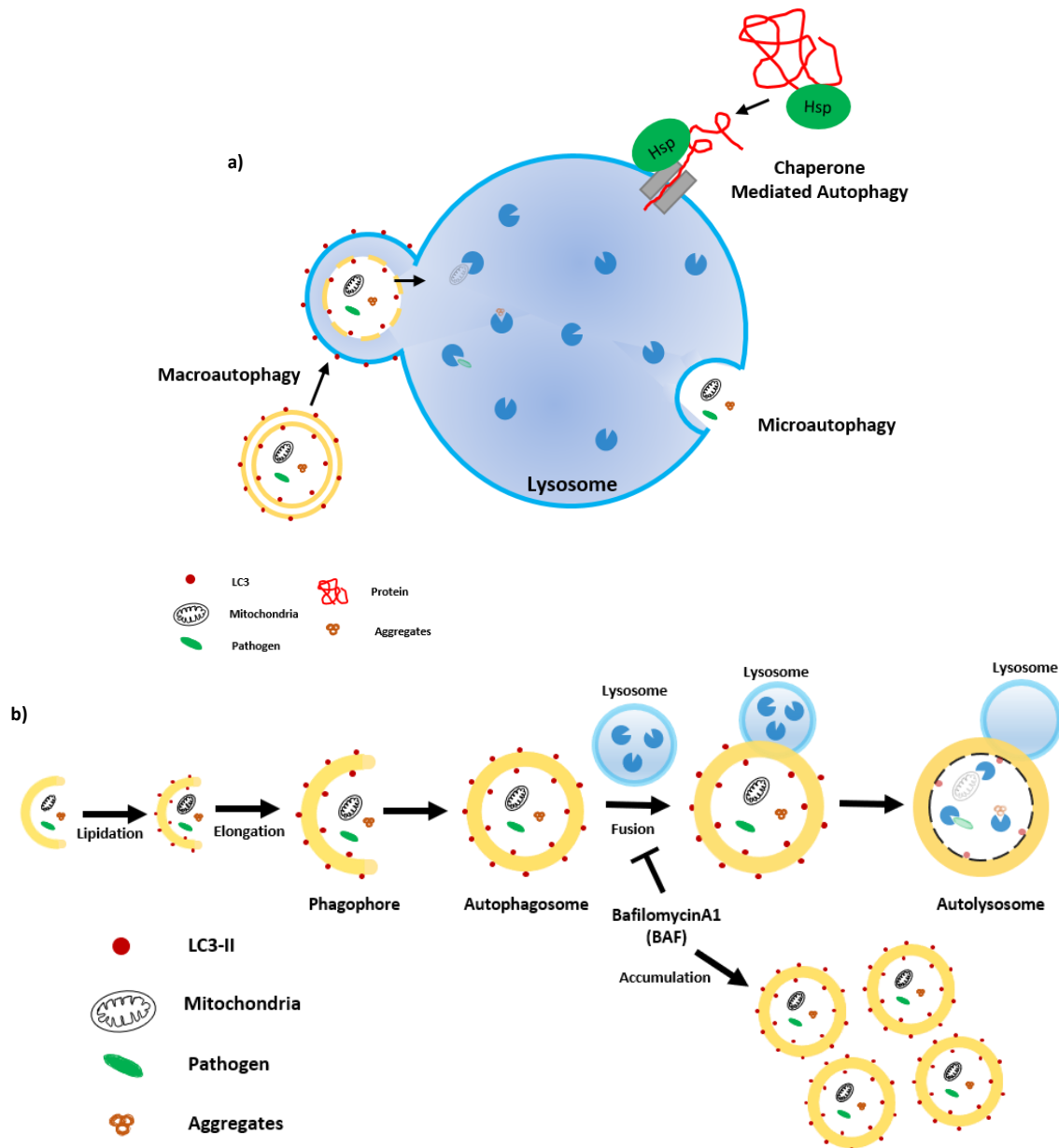
Fig 1.1 a) A schematic showing various forms of autophagy classified as chaperone-mediated, micro and macroautophagy. The schematic of chaperone-mediated autophagy shows the binding of the cargo to Hsp and its delivery to lysosomes. The schematic of microautophagy highlights the engulfment of cargo by micro-invagination of the lysosomal membrane. The schematic of the process of macroautophagy shows the general process of cargo degradation by its delivery to the lysosomes. Please refer to the legend for description of various symbols. b) A detailed schematic depicting the various steps involved in the process of macroautophagy as described in the section 1.1. The process involves formation of double-membrane cup-shaped structure to engulf cargo destined for degradation by the lysosomal hydrolases. The process has been identified to consist of distinct structures such as phagophore – a precursor for autophagosome formation and autophagosome – a double-membraned structure enclosing cargo to be degraded. Autolysosomes are formed upon fusion of completed autophagosomes with lysosomes. The LC3-II molecules labelling the cytosolic face of the autophagosomes are recycled back while the LC3-II molecules on the lumenal side are degraded by the lysosomal hydrolases. Please refer to the legend for description of various symbols.

1.2. Protein complexes involved in autophagy

The understanding of the autophagy machinery was vastly improved since the identification of the 'AuTophagy-related Genes - ATG' in yeast using genetic studies (Thumm et al., 1994; Tsukada and Ohsumi, 1993). While more than 35 autophagy genes have been identified to date, Apg1/Atg1 – a Ser/Thr kinase, was the first gene to be identified and studied. The products of these ATG genes usually exist as a part of a protein complex to achieve a defined function. The various protein complexes involved in the process of autophagy are as follows:

1.2.1. ULK1/2 complex

This complex consists of ULK1 (unc-51-like kinase 1) or its homologue ULK2 together with ATG13, ATG101 and FIP200 (focal adhesion kinase (FAK)-family interacting protein of 200 kDa). This complex can be activated in mammalian cells under nutrient-deprived conditions such as glucose (AMPK-dependent) or amino acid starvation (AMPK-independent). Upon glucose deprivation, AMPK (adenosine-monophosphate-activated protein kinase) phosphorylates ULK1/2 on Ser317 and 777, hence activating the complex and autophagy. However, under nutrient-rich conditions, the kinase mTOR (mammalian target of rapamycin) phosphorylates ULK1 on Ser757, which causes an inhibition of the interaction between ULK1 and AMPK resulting in an inhibition of autophagy (Fig 1.3) (Feng et al., 2014; Kim et al., 2011).

In addition, the activity of the ULK1/2 complex and its ability to bind FIP200 depends on the interaction between ULK1 and ATG13, which in turn relies on the phosphorylation state of ATG13. The phosphorylation of ATG13 has been shown to be regulated by mTOR and AMPK. More specifically, ATG13 is phosphorylated on the serine residue 258 by mTOR and on serine 224 by AMPK under nutrient availability thereby inhibiting the ULK1-FIP200-ATG13 complex formation and attenuating autophagy (Puente et al., 2016). Therefore, under nutrient-rich conditions mTOR associates with the ULK1-ATG13 complex leading to ATG13 phosphorylation, causing a disruption of ULK1-ATG13 binding which consequentially inactivates the complex. In contrast, under nutrient-deprived conditions, mTOR is released from the complex resulting in ATG13 dephosphorylation. This facilitates the binding of ATG13 with ULK1 to form an active complex which can then bind and phosphorylate FIP200.

This further results in the recruitment and activation of the VPS34/PI-3 kinase complex at the site of autophagosome formation. ULK1 complex has been shown to phosphorylate BECN1 on the residue S14 to facilitate full autophagic induction in mammalian cells and *C. elegans* (Hosokawa et al., 2009; Itakura and Mizushima, 2010; Koyama-Honda et al., 2013; Ravikumar et al., 2009; Rc et al., 2013).

1.2.2. VPS34/PI-3 kinase complex

The core of the VPS34/PI-3 kinase complex consists of VPS34 kinase, BECN1 (Beclin-1) and VPS15. This core can then combine with either ATG14, UVRAG or Rubicon, resulting in three different complexes. In context of autophagy, the complex with ATG14 constitutes the most widely studied, while the functions of the other two complexes have received less attention. The activity of the ATG14 complex is regulated by the binding of BECN1 to either AMBRA1 (activating molecule in BECN1-regulated autophagy protein 1) or BCL2 (B-cell lymphoma 2), which results in the activation or inhibition of the complex, respectively (Feng et al., 2014; Fimia et al., 2007; Itakura et al., 2008; Weidberg et al., 2011). The activity of this complex is essential for autophagy, since the inhibition of the complex by both pan-PI-3-kinase inhibitors (3-methyladenine (3-MA) or wortmannin) and VPS-34-specific inhibitors (PIK-III and SAR405) block autophagosome formation and LC3 lipidation (Blommaart et al., 1997; Dowdle et al., 2014; Ronan et al., 2014).

The primary function of this complex is the synthesis of PI3P at the site of autophagosome formation to facilitate canonical autophagy. The generation of PI3P at the autophagosome formation site then results in the recruitment of PI3P-binding proteins, like WIPI-family proteins (Feng et al., 2014). The recruited PI3P-binding proteins then help the autophagic cascade progress further. For instance, WIPI2 was shown to direct the localisation of ATG5-ATG12-ATG16 complex, which plays an important role in the process of LC3 lipidation (Fig 1.3) (Dooley et al., 2014). In addition, WIPI2 was also shown to be responsible for the trafficking of the transmembrane autophagic protein, ATG9, and depletion of WIPI2 from HEK cells causes disruption of retrograde ATG9 trafficking (Orsi et al., 2012).

While all of the above information describes the VPS34-dependent canonical autophagy, it is worth noting that there exists a non-canonical autophagic signalling pathway which is known

to be VPS34-independent (Codogno et al., 2011). A recent study showed that this non-canonical autophagic pathway relies on the activity of the PI3P effectors and their ability to recognise PI5P generated by PIKfyve (type III phosphatidylinositol 5-kinase) in cells. The observed defects in cells with VPS34 depletion were successfully rescued by increasing the endogenous levels of PI5P, implicating its important role in the cells (Vicinanza et al., 2015).

1.2.3. ATG5-ATG12-ATG16 complex

The ATG5-ATG12-ATG16 is a trimeric complex consisting of three proteins ATG5, ATG12 and ATG16. The formation of this complex precedes the LC3 lipidation step in autophagosome biogenesis (Fig 1.2). The process involves conjugation of ubiquitin-like molecule ATG12 on to ATG5, with the help of enzymes ATG7 (E1-like) and ATG10 (E2-like) (Mizushima et al., 1998a; Mizushima et al., 1998b; Tanida et al., 2001). The conjugated complex then interacts with ATG16 in a non-covalent fashion, inducing oligomerisation and formation of a complex of approximately 800kDa size in mammalian cells. The oligomerisation of the complex is achieved via the homodimerisation of ATG16, which in turn is facilitated by the presence of a coiled-coil (CC) domain at its N-terminus (Mizushima et al., 2003; Zavodszky et al., 2013).

One of the primary functions of ATG16 is to act as a scaffold for the expansion of growing autophagosomes along with ATG5-ATG12. ATG16 was shown to generate a two-dimensional scaffold that resembles a meshwork (Kaufmann et al., 2014; Mizushima et al., 2001). This complex is known to be tethered to the membrane of the immature phagophore but dissociates from completed autophagosomes. The membrane binding of this complex has been shown to be mediated by ATG5, inhibited by ATG12 and activated by ATG16 (Romanov et al., 2012). This complex further acts as an E3-like enzyme during the LC3 lipidation and determines the site for LC3-lipidation (Fig 1.3) (Dooley et al., 2014; Fujita et al., 2008).

1.2.4. LC3-PE conjugation system

Subsequent to the ATG5-ATG12-ATG16 complex formation, the process of autophagosome formation involves the lipidation of LC3, via a second ubiquitin-like reaction (Fig 1.2). The reaction begins with the processing of the precursor LC3 molecule to remove arginine residues causing the glycine residue located at the C-terminus to be exposed by ATG4 - a cysteine

protease. The exposed glycine on the processed LC3 (LC3-I) molecule is then activated by the E1-like enzyme ATG7 resulting in a transfer of the LC3-I on to ATG3 (an E2-like enzyme). In the final step of this process, the activated LC3-I molecule attached to ATG3 is then transferred to a phosphatidylethanolamine (PE) molecule to form LC3-II. The site of the LC3 lipidation is directed by the ATG5-ATG12-ATG16 complex (Dooley et al., 2014). This marks the completion of the cascade and the PE-conjugated LC3-II resides on the autophagosomes until they fuse with lysosomes, resulting in its recycling/degradation (Bento et al., 2016b; Feng et al., 2014). The difference in the mobilities of LC3-I and LC3-II forms of the protein has been exploited to develop a gold-standard assay for assessing autophagy. The assay involves checking the levels of LC3-II protein in cells using SDS-PAGE technique. While LC3-II has the same molecular weight as LC3-I, it runs faster on SDS-PAGE potentially due to increased hydrophobicity as a result of conjugation of LC3-I to PE molecule (Barth et al., 2010).

Besides the LC3-family of proteins, mammalian cells express another sub-family of ATG8-like proteins, namely the GABARAP-family. The members of this sub-family are also known to undergo similar post-translational modifications and might regulate other steps of autophagosome formation including phagophore extension and closure (Nguyen et al., 2016; Weidberg et al., 2011; Weidberg et al., 2010).
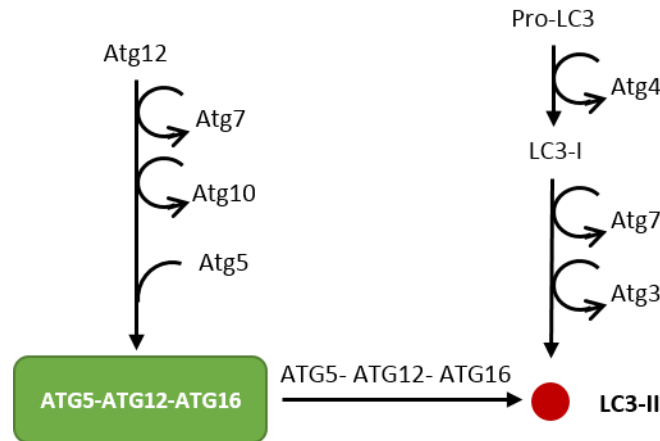
Fig 1.2. A schematic depicting the two ubiquitin-like reactions involved during the process of autophagosome formation. These reactions involve the transfer of two small ubiquitin-like molecules – ATG12 and LC3 with the help of E1-like and E2-like enzymes on to ATG5 and phosphatidylethanolamine molecule respectively. ATG5-ATG12-ATG16 complex acts as an E3-ligase for the ubiquitin-like reaction that results in LC3 lipidation. The enzymes involved in the ubiquitin-like reaction are ATG7 (E1-like)/ATG10 (E2-like) for ATG12-ATG5 conjugation and ATG7 (E1-like)/ATG3 (E2-like) for LC3 lipidation.

The aforementioned system defines the core autophagic processes that assist towards de novo autophagosome biogenesis and it is worth noting that the proteins involved in this process are mostly cytosolic. However, the autophagic system also comprises of the two transmembrane proteins, namely ATG9 and VMP1. These proteins constitute the primary focus of my thesis and I will now describe the known functions and trafficking routes for both in the next section.
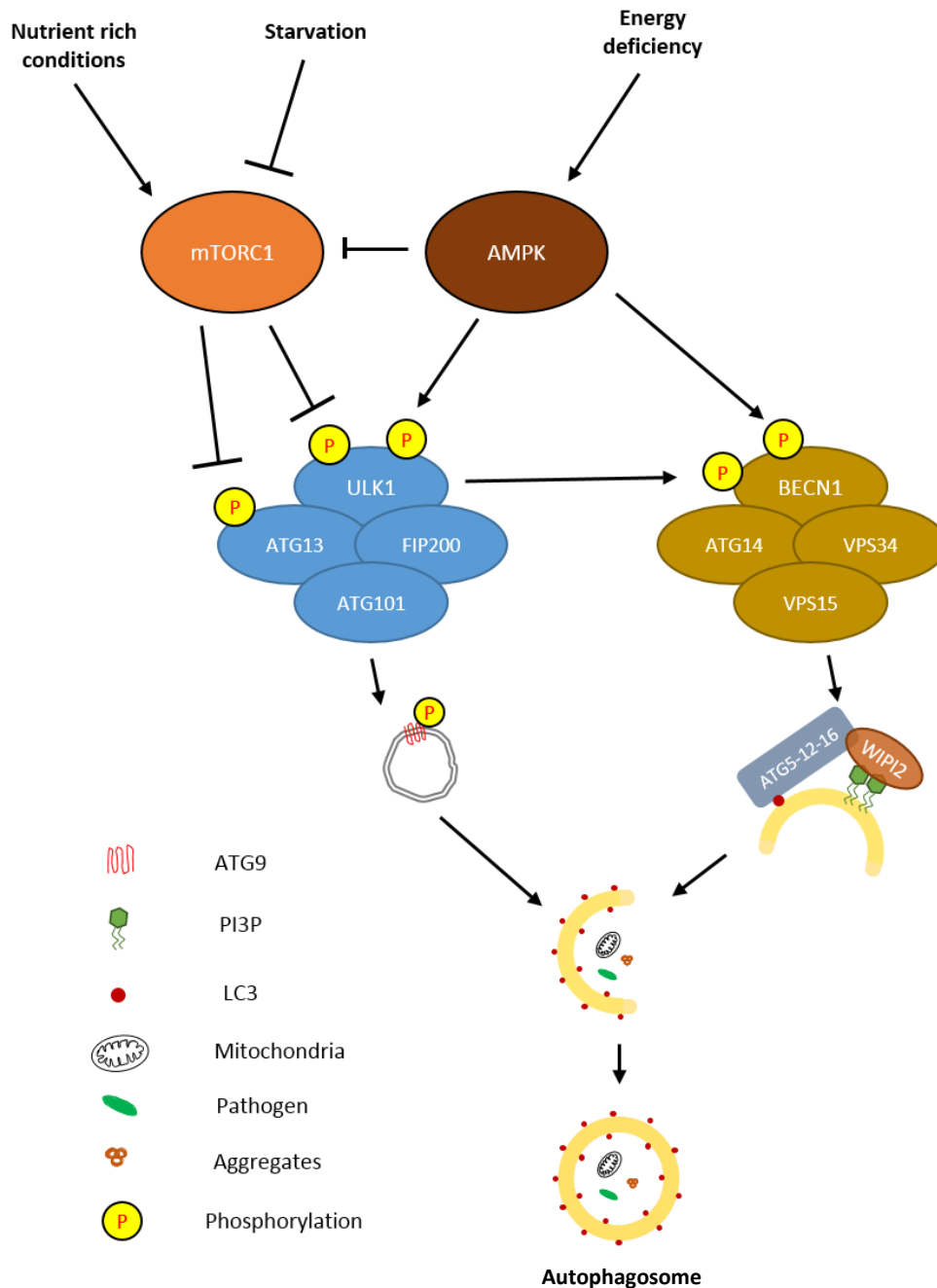
Fig 1.3. A brief schematic depicting the important early signalling processes that occur during autophagosome biogenesis. The stimulators and inhibitors of mTORC1, an important kinase complex responsible for regulation of autophagy, results in the activation/inactivation of downstream autophagy complexes mediated by the phosphorylation of their subunits. Activation of these downstream complexes eventually results in the synthesis of PI3P on the growing phagophore, which through a series of steps is responsible for the lipidation of LC3-I on to phosphatidylethanolamine to form LC3-II. The autophagosomes are therefore identified by the presence of lipidated LC3-II molecules on their surface. The phosphorylation of ATG9 (in yeast) by various kinases has been shown to assist in the growth of autophagosomes by facilitating membrane delivery to growing autophagosomes mediated by vesicles carrying phosphorylated ATG9. Please refer to the abbreviations and the figure legend for detailed description of the symbols and section 1.2 for detailed information about the autophagy complexes.

1.3. Transmembrane proteins in autophagy

1.3.1. ATG9

ATG9 is a multi-pass transmembrane protein involved in the process of autophagy. In mammalian cells, two isoforms of ATG9 are expressed namely ATG9A and ATG9B. Of these isoforms, ATG9A is the one that is ubiquitously expressed and hence widely studied and will now hereafter be referred to simply as ATG9. ATG9 consists of six-transmembrane segments with the N- and C-terminus of the protein facing the cytosolic side of the cell (Fig 1.4). Interestingly, it has been observed that the transmembrane domains of ATG9 are highly conserved whereas the cytosolic loops/domains are widely variant across different species. This suggests that the transmembrane domains might play a well-defined static function across species whereas the cytosolic domains play a dynamic function based on the evolutionary requirements of the organism (Tooze, 2010).

ATG9 has been shown to localise in several compartments in the cell, namely early endosomes, recycling endosomes, plasma membrane and the trans-Golgi network (Orsi et al., 2012; Puri et al., 2013; Young et al., 2006). More specifically, ATG9 has been identified to traffic through the plasma membrane to early endosomes to recycling endosomes where it was shown to meet ATG16. Also, the trafficking of ATG9 from the early to recycling endosomes was shown to be VAMP3-dependent (Puri et al., 2013). While the larger understanding about the ATG9 trafficking remains elusive, some of the regulators of ATG9 trafficking have been identified. I will now summarise some of the key regulators of ATG9 trafficking that have been studied.

The ULK1 kinase acting during the early stages of autophagy initiation was one of the first identified proteins regulating ATG9 trafficking. The knockdown of ULK1 was shown to result in the lack of redistribution of ATG9 from the juxta-nuclear trans-Golgi pool to the peripheral region (most likely recycling endosomes) in response to starvation (Young et al., 2006). In addition, the PI-3 kinase complex has also been shown to regulate ATG9 trafficking. Depletion of endogenous levels of the former was also shown to interfere with the redistribution of ATG9 (Young et al., 2006). Another regulator shown to affect ATG9 trafficking is Endophilin-B1 or BIF-1, a membrane-curvature driving protein. BIF-1 was shown to bind BECN1 via UVRAG and co-localised with the autophagy proteins LC3, ATG5 and ATG9. It was shown that ATG9

undergoes the process of continuous tubulation and fragmentation to form the observed cellular cytosolic puncta; this phenomenon, however, was shown to be abrogated when BIF1 levels were depleted from the cells (Takahashi, 2011; Takahashi et al., 2007). Another protein shown to regulate ATG9 trafficking was α-synuclein, a protein responsible for the pathogenesis of Parkinson's disease. It was seen that overexpression of this protein resulted in distribution of ATG9 away from the Golgi-network and a higher co-localisation of ATG9 with LC3 vesicles (Winslow, 2010). Consistent with this, it was seen that the D620N mutation in VPS35, which is associated with Parkinson's disease, was seen to impair autophagy and result in an accumulation of α-synuclein, which causes ATG9 redistribution. The VPS35 D620N mutation was shown to poorly associate with the WASH complex, which is responsible for actin-remodelling in the cells. This therefore was shown to result in the actin-dependent mistrafficking of ATG9 from the endosomal structures (Zavodszky et al., 2014). It was also seen that ATG9 is internalised from the plasma membrane via interaction with AP-2, clathrin and TBC1D5. This study also showed that the depletion of TBC1D5 resulted in the mislocalisation of ATG9 to late endosomes on autophagy activation (Noda, 2017; Popovic and Dikic, 2014). Furthermore, one more identified ATG9 trafficking regulator is the TRAPIII complex and depletion of its subunits have been shown to result in ATG9 mislocalisation (Noda, 2017). Additionally, a much recent study has identified SNX18 to regulate ATG9 trafficking from the recycling endosomes by binding to Dynamin-2. It was seen that cells lacking endogenous SNX18 resulted in the accumulation of ATG9 in recycling endosomes (Knævelsrud, 2013; Søreng et al., 2018). Finally, a recent study also identified AP-4, a new member of adaptor protein complexes family that are known to help in sorting transmembrane proteins, to regulate ATG9 trafficking. The study showed that depletion of AP-4 ε from the cells via CRISPR knockout resulted in the redistribution of ATG9 from the peri-nuclear region to the Golgi-complex and ATG9 was shown to interact with AP-4 complex via its N-terminal YXXØE motif. Deficiency of AP-4 has been shown to be associated with adulthood neurological problems and this therefore, could also potentially implicate the role of ATG9 localisation in the pathogenesis of some forms of complicated hereditary spastic paraplegias (Mattera et al., 2017). The studies mentioned above highlight the complexity of ATG9 trafficking and while the trafficking of ATG9 in mammalian cells has been studied to some extent, its function however remains elusive.

It is speculated that the primary function of mammalian ATG9, like its yeast homologue, is facilitating membrane delivery from various sources to the growing autophagosomes. The

studies identifying ATG9 trafficking pathways therefore play an important role towards strengthening the former hypothesis. As mentioned above, ATG9 meets ATG16 in recycling endosomes in a VAMP3-dependent fashion (Puri et al., 2013). In addition, subsequent studies also propose recycling endosomes as the primary compartment for autophagosome machinery assembly and autophagosome formation (Puri et al., 2018). Both of these studies thereby indicate the potential role of mammalian ATG9 in delivering membrane towards growing autophagosomes. Another study has shown ATG9, via its interaction with AP-1, to assist in the transport of lysosomal hydrolases like cathepsin D from the trans-Golgi network to endosomes. Depletion of ATG9 in these cells was shown to impair EGFR degradation and cathepsin D maturation, suggesting that ATG9 might act as a co-receptor for these hydrolases assisting in their export from the trans-Golgi network (Jia et al., 2017). A much recent study conducted in *Saccharomyces cerevisiae* has identified another function for Atg9. According to the study, Atg9 plays a vital role in the recruitment of Atg2 to the ends of the growing phagophore, which then assists Atg2 to recruit Atg18 leading to formation of a Atg9-Atg2-Atg18 complex. This complex in turn was shown to be necessary for the establishment and stabilisation of the ER-phagophore contact sites contributing towards autophagosome biogenesis in yeast (Gómez-Sánchez et al., 2018).

cD – cytosolic domain
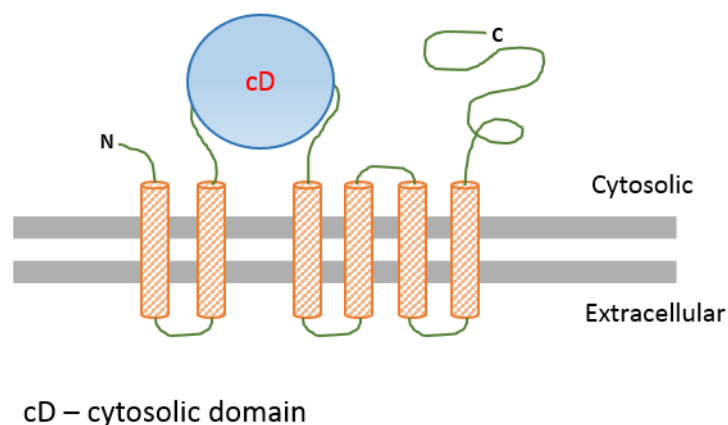
Fig 1.4. A schematic showing the known topology of human ATG9 on the plasma membrane. The cylindrical structures represent the transmembrane domains, grey lines represent a layer of the lipid bilayer and the green lines represent the protein sequence connecting the various domains. The N-terminal region of ATG9 has been seen to well-conserved across species whereas the long C-terminal tail, which has been characterised to possess an intrinsically disordered structure, has been shown to be less conserved across species and is predicted to adapt based on required function. Due to presence of even number (six) of transmembrane domains, both N- and C-terminus of ATG9 face the same side which is the cytosolic side of the plasma membrane. This figure was adapted from Rao et al. (2016).

1.3.2. VMP1

The other multi-pass transmembrane protein, VMP1, was recently identified as a protein involved in autophagy. The first study identifying the protein showed that the overexpression of VMP1 induced autophagy and this effect was reversed on autophagy inhibition by 3-methyladenine (3-MA). It also showed that silencing the expression of endogenous VMP1 resulted in the inhibition of autophagy (Ropolo et al., 2007). Further studies showed that VMP1 consists of a 20-amino acid hydrophilic C-terminus AtgD-domain which facilitates its binding to BECN1, a protein involved in autophagy initiation, possibly regulating early stages of autophagy and leading to a formation of a complex with VPS34/PI-3 kinase. The VMP1-BECN1-VPS34 complex was then shown to favour the association of ATG16 and LC3 with the autophagosome precursors, and was hence proposed to help in the recruitment of the autophagy initiation complexes to the autophagosome formation site (Molejon et al., 2013; Ropolo et al., 2007; Vaccaro et al., 2008). Interestingly, while most autophagy proteins in mammalian cells show respective homologous proteins in yeast, VMP1 has none, indicating that it might be responsible for an alternate pathway for autophagy initiation (Ropolo et al., 2007; Vaccaro et al., 2008).

However, studies on the VMP1 homologue in lower-order eukaryotic model system, *Dictyostelium discoideum*, has shown it be an ER-resident protein and the cells lacking VMP1 show multifaceted effects on organelle biogenesis, endocytic pathway and protein secretion. This effect was also shown to be rescued by the overexpression of mammalian VMP1 protein indicating that the protein function has been evolutionarily conserved (Calvo-Garrido et al., 2008). Indeed, recent studies in mammalian cells have shown that VMP1 associates with the endoplasmic reticulum subdomains that regulates the ER contact sites with other organelles. The study further shows that VMP1 localises with to ER-subdomains that are rich in enzymes responsible for phospholipid synthesis. Furthermore, depletion of VMP1 was shown to result in an irregular distribution of phosphoinositides in the cell affecting cellular trafficking events and organelle maturation (Tabara et al., 2018). Another study earlier showed the initiation of autophagosome biogenesis on the ER-subdomains that are rich in phospholipid synthesising enzymes (Nishimura et al., 2017). Therefore, both of the two independent studies consolidate the role of VMP1 in autophagy initiation.

Further studies on mice also showed the induction of VMP1 expression and autophagy during early cellular events, in pancreatic β-cells of these animals on treatment with streptozotocin, a drug known to induce experimental diabetes, indicating the potential role of VMP1 and autophagy in cellular defence mechanisms (Grasso et al., 2009). A follow-up study performed by the same research group also showed that treatment of pancreatic cancer (PANC-1) cells with gemcitabine, a standard chemotherapy drug for pancreatic cancer, induced VMP1 expression and autophagy during early stages of treatment, leading to autophagy-assisted apoptosis of the cancer cells (Pardo et al., 2010). In addition, VMP1 was also shown to be responsible for degradation of zymogen granules in pancreatic acinar cells during pancreatitis conditions. It was also shown that VMP1 interacts with USP9x, a ubiquitin protease, hinting towards an interplay between autophagy and ubiquitination machinery through VMP1 (Grasso et al., 2011). Moreover, VMP1 was also shown to modulate the ER-stress response independently of autophagy (Gilabert et al., 2013). While some of the above studies provide evidence of VMP1-dependent autophagy working towards apoptotic cell death of cancerous cells, there have been reports showing pro-survival and initiation role of VMP1 in colorectal and pancreatic cancer cells, helping cancer progression (Loncle et al., 2016; Qian et al., 2014). A more recent study has now shown that VMP1 together with VAPA and VAPB (VAPs) regulates ER-IM (endoplasmic reticulum-isolation membrane) contact sites. The ER-IM sites were observed to be stabilised, leading to a reduction in autophagosome formation, under VMP1-depleted conditions. Furthermore, depletion of VMP1 also resulted in stabilisation of the ER contacts with lipid droplets, mitochondria and endolysosomes, impairing autophagosome biogenesis. Similarly, under VAP-depleted conditions the autophagosome biogenesis was shown to be abrogated (Zhao et al., 2017; Zhao et al., 2018; Zhao and Zhang, 2018).

1.4. Membrane origin during autophagosome biogenesis

The origin of membrane of the growing autophagosomes has been one of the key unanswered questions in the field. Studies using high-resolution microscopy and biochemical analysis have shown various membrane sources to either be in contact with the growing autophagosome or be a part of the lipid content of the growing autophagosomes. A list of various organelles identified to date that contribute towards growing autophagosomes includes plasma membrane, recycling endosomes, endoplasmic reticulum (ER), ER-Golgi intermediate compartment

(ERGIC), mitochondria, Golgi complex and endosomes (Bento et al., 2016b; Lamb et al., 2013). However, an important point to be considered while evaluating whether an organelle is a membrane source during autophagosome biogenesis is whether the considered organelle is a known substrate for autophagy. This is since membranes of substrates would show association with autophagosomes regardless of whether they provide membrane to growing autophagosomes.

The first organelle to be proposed as a source of membrane for growing autophagosomes was the ER (Mari et al., 2011). Since then, multiple studies have expanded on the hypothesis stating ER membrane as a 'cradle' for autophagosome formation. The studies involved electron tomographic studies which showed the presence of isolation membrane, an early marker for autophagosomes, cradled within a subdomain of ER. The study also showed that PI3P, a phosphorylated lipid molecule that marks autophagosomes, marked subdomains of the ER which can be identified by DFCP1 staining (El et al., 2008; Hayashi-Nishino, 2009; Hayashi-Nishino et al., 2010).

The role of mitochondria as potential autophagosome formation site was shown by the co-localisation of ATG5 and LC3 puncta with outer-mitochondrial membrane markers. The observation was made during starvation, suggesting its role in starvation-induced autophagy. Some studies also show autophagosomes form at the ER-mitochondria sites, during starvation-induced autophagy, suggesting its role during autophagosome formation. Moreover, disruption of these sites resulted in impairment of starvation-induced autophagy (Hailey et al., 2010; Hamasaki, 2013).

In addition to the above compartments, the plasma membrane was proposed to contribute membrane to autophagosomes. The study involved labelling of the plasma membrane lipids and live-cell imaging of the cells. It was seen that the labelled lipids were incorporated into growing autophagosomes, suggesting that plasma membrane provides membrane to autophagosomes (Ravikumar et al., 2010). Subsequent studies identified autophagy proteins ATG9 and ATG16 trafficking from the plasma membrane to different endocytic compartments, which corroborate the prior observations. ATG9 was shown to traffic from the plasma membrane to early endosomes, while ATG16 was shown to traffic to recycling endosomes directly independent of early endosomes. ATG9 was then shown to be trafficked from early endosomes to recycling endosomes in a VAMP3-dependent manner, where it meets ATG16,

both of which then contribute to growing autophagosomes. Interestingly, ATG16 was shown to traffic directly to recycling endosomes from plasma membrane via clathrin-mediated endocytosis. This explains the probable mechanism of the membrane delivery from plasma membrane to growing autophagosomes (Moreau et al., 2011; Puri et al., 2013).

Furthermore, a recent study has shown that recycling endosomes contribute membrane towards growing autophagosomes and has suggested that this compartment acts as a primary platform for de novo autophagosome formation (Puri et al., 2018). This finding also presents a solid case for plasma membrane as membrane contributor since both ATG9 and ATG16, proteins known to play a role in early stages of autophagosome formation, meet each other in recycling endosomes after travelling through the plasma membrane (Puri et al., 2013).

To summarise, multiple organelles have been shown to be involved in the membrane delivery process during autophagosome formation so far. However, the overall understanding of the process still remains elusive and further investigation using high-resolution imaging and sophisticated biochemical techniques is required.

1.5. Cargo receptors and their role in autophagy

Autophagy, during the early years of discovery, was considered to be a non-selective process facilitating bulk degradation of cargo via its delivery to lysosomes. However, studies during recent years have witnessed a significant progress in helping understand the selectivity of the process and the proteins responsible for it. The process of selective autophagy can be identified based on the substrate being targeted for degradation. A few examples that have been described so far include mitochondria (mitophagy), aggregates (aggrephagy), peroxisomes (pexophagy), ribosomes (ribophagy), pathogens (xenophagy), etc. with newer processes being added to the list (Stolz et al., 2014).

The process of selective autophagy is mediated by autophagy receptors, a type of protein that binds to the cargo destined for degradation. These autophagy receptors act as bridging molecules recognising degradation signals on the cargo molecules on one hand and binding LC3 on the autophagosomal membrane using LIR (LC3-interacting regions) domain on the other, to facilitate the engulfment of the cargo. Over two dozen autophagy receptors have been

identified in mammalian cells using yeast two-hybrid systems and proteomic techniques (Stolz et al., 2014). Some of these autophagy receptors known to be involved in various forms of selective autophagy, such as mitophagy, zymophagy, pexophagy, aggrephagy, etc., are p62, NBR1, OPTN, BNIP3, FUNDC1, NIX, HDAC6, NDP52, and ALFY (Rogov et al., 2014). The most common form of signal for targeting a substrate for its degradation via autophagy, in mammalian cells, is ubiquitination. A common feature that the autophagy receptors share is the presence of both, a ubiquitin-binding domain (UBD) and LC3-interacting regions (LIR).

The first identified mammalian selective autophagy receptor shown to play an important role in autophagy was p62/SQSTM-1 (sequestosome-1) (Bjørkøy et al., 2005). p62 constitutes one of the most widely studied autophagy receptor and consists of an N-terminal PB1 domain shown to be necessary for self-oligomerisation of the protein, a C-terminal UBD that has the ability to bind ubiquitin conferring the specific cargo selection ability onto p62 and several other domains that mediate its binding to other proteins (Rogov et al., 2014; Zaffagnini et al., 2018). The LIR motif of p62 was identified to possess a core consensus sequence of Φ-X-X-ψ, where Φ corresponds to aromatic amino acids (W/F/Y), ψ corresponds to hydrophobic amino acids (L/I/V) and X corresponds to any amino acid (Pankiv et al., 2007; Rogov et al., 2014). p62 accumulates into inclusion bodies in autophagy-deficient mice and these structures were also shown to be positive for ubiquitin (Komatsu et al., 2007). A different study has also shown that the p62 aggregates sequestered the E1-like ATG7 enzyme into these aggregates. It also showed that this sequestration is mediated via the interaction of LC3-I with ATG7 and that while p62 shows preferential binding towards LC3-II, it is indeed capable of binding to the lipidation defective LC3-G120A mutant (Gao et al., 2013). Furthermore, misregulation of p62 was shown to have significant implications towards the progression of various neurodegenerative diseases due to defective autophagy (Moscat and Diaz-Meco, 2009).

1.6. Post-translational modifications in autophagy

Autophagy is tightly regulated at several stages by post-translational modification of proteins involved during the process. The most commonly studied post-translational modification in cells is phosphorylation, which involves transfer of a phosphate group to the side chain of an amino acid. In eukaryotes, phosphorylation primarily occurs on the side chains of three amino acids namely serine, threonine and tyrosine. The phosphorylation of protein results in the either

inhibition or activation of the activity of the protein. Usually the phosphorylation status of a protein is tightly regulated by a pair of specific kinase and phosphatase, indicating that phosphorylation is a reversible process (Xie et al., 2015). The early stages of autophagy are finely regulated by phosphorylation of key proteins like mTOR and ULK1 kinase involved in the autophagic signalling pathway. A cascade of the phosphorylation events taking place during glucose deprivation and nutrient rich conditions that modulate autophagy has been described in the section 1.2.1 of this thesis. The example involves phosphorylation of ULK1 kinase, an early stage regulator of autophagy, by AMPK in response to the nutrient stimuli around the cells. This example provides great insight into the complexity of the process and also highlights the level of regulation involved during autophagy modulation (Feng et al., 2014; McEwan and Dikic, 2011).

Another common form of post-translational modification includes addition of the small molecule, ubiquitin, to proteins. Ubiquitin is a 76-amino acid polypeptide with a molecular weight of approximately 8-kDa. The ubiquitination usually occurs on the side chain of the amino acid residue, lysine, via a sequence of enzymatic reactions. This form of post-translational modification governs the degradation of proteins in the cell via its recognition by the 26S proteasomal subunit. In addition to the two ubiquitin-like reactions described in above sections 1.2.3 and 1.2.4, ubiquitination regulates the activity of proteins like BECN1 and ULK1. A well-studied example of ubiquitination is the ubiquitination of BECN1 by TRAF6 (TNF receptor-associated factor 6, E3 ubiquitin protein ligase) or AMBRA1 at distinct lysine residues. This modification was shown to regulate the binding of BECN1 with BCL2, which in-turn modulates autophagic regulation (Shi and Kehrl, 2010; Xia et al., 2013). Interestingly, TRAF6 and AMBRA1 were also shown to ubiquitinate ULK1 increasing its stability and activity during autophagy induction (Nazio, 2013; Xie et al., 2015). In addition to the regulatory functions described above, ubiquitination also serves a much more fundamental role in autophagy and is required for cargo recognition during selective autophagy. Similar to phosphorylation, ubiquitination is tightly regulated by a pair of ubiquitinating and deubiquitinating enzymes. For example, BECN1 has been shown to be deubiquitinated by the enzymes USP13, USP10 and ataxin-3 leading to autophagy induction (Ashkenazi et al., 2017; McEwan and Dikic, 2011; Xie et al., 2015). The above examples, therefore, highlight the importance of ubiquitination in the process of autophagy.

Another important post-translational modification regulating autophagy is acetylation. The process usually involves the transfer of an acetyl group onto the ε-amino group of lysine side chain. The donor of the acetyl group is a metabolite produced during cellular processes called acetyl-coenzyme A. The transfer of the acetyl group is catalysed by the class of enzymes named lysine acetyltransferases. Like phosphorylation and ubiquitination, acetylation too is a reversible modification and the dynamic between protein acetylation and deacetylation tightly regulates numerous important cellular processes. Various ATG proteins have been shown to undergo acetylation/deacetylation resulting in the modulation of autophagy. A notable example of the role of acetylation in the regulation of autophagy has been shown in yeast and involves the post-translational modification of Atg3. Under conditions where Atg3 is acetylated, on lysine residues 19 and 48, by Esa1 acetyltransferase its affinity for LC3 binding increases. In contrast, when Atg3 undergoes deacetylation on the same sites as mentioned above by a histone deacetylase Rpd3, it results in an inhibition of the autophagic process (Xie et al., 2015; Yi et al., 2012). Extending the observation in the mammalian system, in HeLa cells it was seen that the knock-down of the EP300 acetyltransferase resulted in an induction of autophagy and the mechanism of autophagy inhibition under normal conditions was identified to be via the acetylation of core autophagy proteins namely ATG5, ATG7, ATG8 and ATG12 (Lee and Finkel, 2009). Similarly, forced deacetylation of these proteins in cells by the overexpression of the deacetylase SIRT1 (sirutin-1), resulted in autophagy induction under starvation conditions. Moreover, this effect was not observed in SIRT1-null cells as they showed a lack of functional autophagy (Lee et al., 2008; Xie et al., 2015). These examples exhibit the level of control that acetylation of key proteins can exert on the process of autophagy.

1.7. Signalling pathways involved in autophagy

Autophagy is a complex process that is regulated at several steps via multitude signalling processes. These signalling pathways can be broadly classified into mTOR-dependent and mTOR-independent pathways. This classification is based on the involvement of the mTORC1 complex in the regulation of autophagy. It is worth noting that the mTOR-dependent pathways were the first to be identified and hence have been studied in more depth compared to mTOR-independent pathways, both of which will be covered in the section below.

1.7.1. mTOR-dependent signalling

The mammalian target of rapamycin (mTOR) is a 289-kDa serine-threonine kinase that responds to several environmental cues and belongs to the PI3K- related kinase (PIKK) family of proteins. It was named mTOR based on its homology with the yeast TOR gene and its ability to bind the peptidyl-prolyl isomerase FKBP12-rapamycin complex. Furthermore, as the name suggests it is inhibited by rapamycin (sirolimus), which is an anti-fungal macrolide produced by the bacterial species *Streptomyces hygroscopicus* named after the site of its discovery (Saxton and Sabatini, 2017). The kinase mTOR is at the catalytic core of two complexes mTOR complex1 (mTORC1) and complex 2 (mTORC2). The components of mTORC1 complex include mTOR, Raptor (regulatory protein associated with mTOR) and mLST8 (mammalian lethal with Sec13 protein 8). mTORC2 consists of mTOR, mLST8 and Rictor (rapamycin insensitive companion of mTOR), however, unlike mTORC1, mTORC2 is known to be resistant to inhibition by rapamycin. However, longer treatments of rapamycin inhibits the activity of the mTORC2 complex by preventing the incorporation of rapamycin-bound mTOR into the newly formed complexes (Ballou and Lin, 2008; Saxton and Sabatini, 2017).

mTORC1 was identified as a key regulator for autophagy and inhibition of its activity results in an upregulation of the autophagic process. As mentioned in the above sections, ULK1 is an important kinase that initiates and regulates the early stages of autophagy induction. Under nutrient-rich conditions, mTORC1 phosphorylates ULK1 at serine-757 which causes it to be resistant to activation via AMPK phosphorylation. Under starvation however, mTORC1 is inactivated resulting in AMPK-mediated activation of ULK1 and autophagy (Kim et al., 2011; Saxton and Sabatini, 2017). In addition, mTORC1 also regulates the phosphorylation status of TFEB (transcription factor EB), which in-turn regulates its localisation. It was shown that the phosphorylation of TFEB inhibits its translocation to the nucleus and prevents the activation of transcription of genes responsible for autophagy and lysosome biogenesis (Roczniak-Ferguson et al., 2012; Settembre et al., 2012).

The role of mTORC2 on the other hand still remains elusive and possibly works opposite to the effect mTORC1 on autophagy, partly because the effects of mTORC2 on autophagy are indirect. For instance, it was shown that inhibition of autophagy under the IGF-1 depleted conditions was a result of inhibition of mTORC2. The inhibition of mTORC2, then results in

reduction of the protein kinase C (PKCα/β), which results in perturbation of actin rearrangement dynamics leading to impaired clathrin-mediated endocytosis, resulting in impaired autophagosome precursor formation (Bento et al., 2016b; Renna et al., 2013). In addition it also was shown that mTORC2 regulates cell survival, metabolism and cytoskeleton via phosphorylating multiple kinases like Akt, PKCα, etc. with the overall mechanism still unknown (Laplante and Sabatini, 2012a, b).

1.7.2. mTOR-independent signalling

In addition to the mTOR-dependent pathways, several recent studies have described autophagy regulation through mTOR-independent routes. The first pathway to be identified involved in the mTOR-independent autophagic regulation was the inositol pathway. The presence of higher levels of inositol or IP_3 (myo-inositol-1,4,5-triphosphate) was shown to inhibit the autophagosome biogenesis. Furthermore, inositol-lowering drugs, that are also known to act as mood-stabilising drugs, such as lithium, carbamazepine or valproic acid, induced autophagy without inhibiting the mTOR activity. The induction of autophagy by lithium was shown to work via the inhibition of IMPase leading to an abrogation of inositol recycling causing its intracellular depletion (Sarkar, 2013; Sarkar et al., 2005).

Another stimulus shown to affect autophagy independent of mTOR has been the levels of calcium inside the cell. Elevated levels of intracellular Ca^{2+} was shown to inhibit autophagy specifically at the stages of formation and fusion of autophagosomes with lysosomes. Drugs acting as Ca^{+2} channel antagonists like verapamil, loperamide, etc. were shown to be inducers of autophagy (Williams et al., 2008). The identified mechanism for autophagy inhibition by elevated Ca^{2+} levels was via the Ca^{2+}-dependent cysteine proteases, calpain 1 and calpain 2. Inhibition or genetic depletion of these proteases was shown to induce autophagic flux without affecting mTORC1 activity. On the other hand, overexpression of a constitutively active form of calpain 2 or activation of the calpains was shown to inhibit autophagy (Sarkar, 2013; Williams et al., 2008).

As described in section 1.2.2, the PI-3 kinase complex consists of VPS34 and BECN1. The activity of this complex is essential for the initiation of autophagosome biogenesis. The binding of BECN1 to BCL-2 and BCL-X$_L$ via the BH3 domain of BECN1, was shown to inhibit

autophagy. Furthermore, BH3 domain mimics compete for the binding of BECN1 to BCL-2, leading to activation of autophagy (Maiuri et al., 2007; Malik et al., 2011; Sarkar, 2013). This is another example of autophagy regulation in an mTOR-independent fashion.

Autophagy has been shown to be regulated via small molecules like trehalose. Trehalose is a disaccharide found in non-mammalian cells species and protects cells from environmental stress. It was shown to enhance the clearance of the known autophagy substrates and proteins implicated in neurodegenerative diseases like mutant huntingtin and the A30P and A53T mutants of α-synuclein (Sarkar, 2013; Sarkar et al., 2007a). Consistent with these observations, a bulk of the existing literature reports trehalose to be a potent inducer of autophagy. A recent study identified the mechanism of autophagy induction by trehalose via inhibition of glucose transporters. Specifically, the study highlighted an inhibition in the activity of glucose transporters such as GLUT1, GLUT2, GLUT3, GLUT4 and GLUT8 at the plasma membrane upon treating the cells with trehalose. This was then seen to activate AMPK resulting in the phosphorylation and activation of ULK1, finally leading to potent autophagy induction (DeBosch et al., 2016). A couple of recent studies, however, have shown that trehalose might also act as potent blocker of autophagic flux under certain conditions. These studies therefore question the effects of trehalose on autophagy and potentially indicate towards a complex mechanism of regulation of autophagy (Lee et al., 2018; Yoon et al., 2017).

A selected list of small molecules/compounds that affect autophagy and could act as potential therapeutic modulators of the process can be found in Table 1.1. A brief description of the proposed site and mechanism of action for each of these compounds has been mentioned in the corresponding row. It is worth noting that most of the identified therapeutic modulators of the process of autophagy act along the mTOR-independent signalling axis and result in the induction of the autophagic response that assists towards clearance of toxic protein aggregates.

Potential therapeutic modulators of autophagy	Proposed site and mechanism of action	Selected references
Rapamycin and rapalogs	Autophagic induction via mTORC1 inhibition	(Ravikumar et al., 2004; Williams et al., 2008)
Lithium	Autophagic induction by lowering inositol and IP_3 levels	(Sarkar et al., 2005)
Trehalose	Autophagic induction via unknown mechanism	(Sarkar et al., 2007a)
Rilmenidine	Autophagic induction by decreasing cAMP levels	(Williams et al., 2008)
Verapamil	Autophagic induction by lowering intracellular calcium levels	(Williams et al., 2008)
Valproate	Autophagic induction by lowering inositol and IP_3 levels	(Williams et al., 2008)
Clonidine	Autophagic induction by lowering intracellular calcium levels	(Williams et al., 2008)
Carbamazepine	Autophagic induction by lowering inositol and IP_3 level	(Williams et al., 2008)
SMER28	Autophagic induction via unknown mechanism	(Sarkar et al., 2007b)
Bafilomycin A1	Autophagic inhibition by inhibition of V-type ATPase	(Ebrahimi-Fakhari et al., 2011; Shacka et al., 2006)
Chloroquine	Autophagic inhibition by alkalisation of the lysosomal pH	(Ebrahimi-Fakhari et al., 2011)

Table 1.1 A table enlisting a selected list of chemical compounds that could act as potential therapeutic modulators of autophagy. The proposed site of action and mechanism have also been briefly mentioned for these compounds. It is worth noting that most of these compounds work towards autophagic induction and in an mTOR-independent fashion. Additional details regarding the mechanistic action of these compounds and the corresponding signalling pathways they regulate can be found in the selected references as stated in the table above.

1.8.   Role of autophagy in diseases

Autophagy, as described above, is an important pathway for cell survival and is activated under conditions like starvation, stress, infection, protein aggregation, etc. This makes autophagy an important housekeeping pathway for normal cellular function. Therefore, autophagy has been shown to be affected under many diseased conditions like neurodegeneration, cancer, metabolic diseases, autoimmune diseases, etc (Bento et al., 2016b; Rubinsztein, 2006). I will now briefly summarise some of these disease links in the context of autophagy.

1.8.1. Autophagy and neurodegeneration

Autophagy was identified as one of the key pathways disrupted in several neurodegenerative disease conditions making it an enticing target for developing therapeutic interventions. It has been observed that autophagy deficiency leads to an accumulation of protein aggregates which is the hallmark for neurodegenerative diseases like Alzheimer's, Parkinson's and Huntington's diseases (Rubinsztein, 2006). A selected list of genes, mutations in which are known to impair the autophagic process, can be found in Table 1.2 of this thesis together with corresponding references describing the pathogenesis of the disease due to the associated mutation. I will now describe the most common forms of neurodegenerative diseases and the identified role of autophagy in the disease pathogenesis.

Alzheimer's disease (AD) is characterised by the accumulation of intracellular tau neurofibrillary tangles and extracellular amyloid-β (Aβ) aggregates called plaques. It constitutes the most common form of neurodegeneration with patients showing progressive dementia. The Aβ peptide responsible for formation of plaques is a product of cleavage of the amyloid precursor protein (APP). Studies have shown that impaired autophagic process enhances the pathogenesis of AD in animal models and cells. In addition, induction of autophagy in these models have also shown to lower the Aβ levels (Ravikumar et al., 2008; Rubinsztein, 2006). It was seen that neurons from AD patients showed an accumulation of autolysosomes/lysosomes (Nixon et al., 2005). In addition, some of the core autophagy proteins like LC3, ATG5 and ATG12 were shown to co-localise with the intracellular tau aggregates and surprisingly, the extracellular Aβ plaques indicating that autophagy might play a role in Aβ secretion and plaque formation (Ma et al., 2010; Nilsson et al., 2013).

Parkinson's disease (PD) constitutes the second most common neurodegenerative disease. The patients display bradykinesia, rigidity of muscles and resting tremor. It is characterised by progressive loss of dopaminergic neurons in substantia nigra and displays accumulation of cytoplasmic aggregates known as Lewy bodies, which are made up of the protein α-synuclein. Increased levels of α-synuclein in the cells have been shown to be sufficient to cause PD, and overexpression of α-synuclein in cells was shown to impair autophagy and cause ATG9 mislocalisation (Winslow, 2010). On the contrary, BECN1 overexpression leading to autophagic induction reduced α-synuclein accumulation and cell death, indicating that the relationship between autophagy and α-synuclein is multifaceted (Spencer et al., 2009; Webb et al., 2003). In addition, several other mutations have been described to affect the levels of α-synuclein leading to PD. For instance, mutations in the ATP13A2, which encodes a lysosomal P5-type ATPase that facilitates cation transport, causes autosomal recessive early-onset PD. Decrease in the levels of ATP13A2 via decrease in synaptotagmin 11 levels results in an impaired lysosomal function and autophagosome degradation, which as a result causes an accumulation of α-synuclein (Bento et al., 2016a).

Huntington's disease is characterised by mutation at the N-terminus polyglutamine (polyQ) domain of the huntingtin gene, resulting in increase in the number of repeats and expansion of the polyQ tract. The result of an expanded polyQ tract is the formation of mutant oligomers which combine to form disruptive aggregates in different parts of the brain (Rubinsztein, 2006). It has been shown that autophagy is affected in Huntington's disease via different mechanisms. An example would be the impairment of autophagy by polyQ proteins through Ras homolog enriched in striatum (Rhes). Rhes was shown to competitively bind to BECN1, inhibiting BECN1 binding with BCL-2, leading to autophagy induction. The polyQ proteins were shown to interact with Rhes and causing a reduction in its binding to BECN1, which leads to increased binding between BECN1 and BCL-2 resulting in decreased autophagy (Mealer et al., 2014). A recent study has shown that ataxin-3 is a positive regulator of autophagy by acting as a deubiquitinase for BECN1, thereby preventing its degradation. The ataxin-3-BECN1 interaction is mediated via the normal polyQ stretch in ataxin-3. In diseased conditions like Huntington's, the polyQ tract expansion of the soluble protein leads to a competition between it and ataxin-3 for their binding to BECN1. This causes a reduction in starvation-induced autophagy in these model systems, contributing towards disease progression (Ashkenazi et al., 2017).

Gene implicated in autophagic impairment	Identified neurological disorder association	Selected references
ATG5	Form of ataxia	(Ebrahimi-Fakhari, 2018; Zhu et al., 2018)
AP4	Rare form of hereditary spastic paraplegia	(Mattera et al., 2017)
SPG11, ZFYVE26 (SPG15)	Hereditary spastic paraplegia	(Ebrahimi-Fakhari, 2018; Ebrahimi-Fakhari et al., 2016)
p62	Amyotrophic lateral sclerosis (ALS), Fronto-temporal dementia (FTD), p62-associated childhood-onset ataxia	(Du et al., 2009; van Beek et al., 2018; Zhu et al., 2018)
WIPI4	Beta-propeller protein associated neurodegeneration (BPAN)	(Ebrahimi-Fakhari et al., 2016)
EPG5	Vici Syndrome	(Zhao et al., 2013)
ATG12, ATG7	Parkinson's disease	(van Beek et al., 2018)
ATP13A2, SYT11	Parkinson's disease	(Bento et al., 2016a)
SNX14	Cerebellar ataxia	(Ebrahimi-Fakhari, 2018)

Table 1.2 A table enlisting selected autophagy genes that have been implicated in the pathogenesis of several neurological disorders. The mutations associated with these genes, known to cause defective autophagy, have been observed to be associated with a spectrum of neurological disorders, a brief list of which has been mentioned above with selected references citing the first studies for each gene. Additional information about the mechanisms of pathogenesis of the disease as a result of mutation in the corresponding autophagic gene can be found in the corresponding references.

1.8.2. Autophagy and cancer

The role of autophagy in various forms of cancer has been studied and shown to act as a double-edged sword. While autophagy helps stop the cancer disease progression during early stages, it has also been shown to assist cancer cell proliferation during the later stages (Jiang and Mizushima, 2014).

Autophagy was initially thought to play a protective role acting as a tumor-suppressor. This was based on the observation that 40-75% of the reported cases for human prostate, breast and ovarian cancers showed monoallelic deletion of the gene encoding core autophagy protein BECN1. It was also seen that suppression of autophagy in cells and mouse models with single allele deletion of BECN1 (heterozygous mutation) promoted tumor growth, supporting the hypothesis. While the exact mechanism of how loss of autophagy promotes tumor growth is unclear, it has been shown that loss of autophagy results in higher oxidative stress, activation of DNA damage response and genomic instability. The higher oxidative stress then activates nuclear factor, erythroid-2-like 2 (NRF2) which promotes tumor growth (Kimmelman and White, 2017; White, 2015).

On the other hand, it has been seen that cancer cells show much higher levels of autophagy than normal cells and tissues. This has been attributed to the higher metabolic requirements of the cancer cells and the hypoxic environment at the core of tumors. It was also shown that in RAS-transformed cancer cells autophagy is upregulated to promote their growth and survival. It was shown that tumor-specific deletion of ATG7 in mice led to accumulation of dysfunctional mitochondria, arrest of cell growth and cell death. More importantly, this also led to change in the fate of the tumors from being malignant to benign characterised only by the accumulation of dysfunctional mitochondria. This led to development of the concept of cancer cells being 'autophagy addicted' and RAS-driven cancer cells together with many other forms of cancer today are considered as 'autophagy addicted' (White, 2015).

1.8.3. Autophagy and immunity

Autophagy plays an important role in the functioning of the immune system. Clearance of pathogens, presentation of antigens, control of inflammatory processes and secretion of

immune mediators are some of the primary functions of autophagy in regulating the immune system (Deretic et al., 2013).

The process of clearance of pathogens by autophagy is a form of selective autophagy known as 'xenophagy'. The general mechanism of this process has been described in the section 1.4 of this thesis. This form of selective autophagy also plays a significant role in antigen presentation. The MHC class II mediated antigen presentation to $CD4^+$ T cells is mediated by autophagy. The extracellular antigens can be processed by phagocytosis and subsequent fusion with endolysosomal compartments. The processed peptides can then be loaded on to the MHC class II molecules for presentation. In addition, autophagy also helps with the presentation of intracellular antigens where the autophagosomes directly fuse with MHC class II compartment instead of lysosomes (Deretic et al., 2013; Yang et al., 2015). Furthermore, autophagy has been shown to be an important contributor towards Crohn's disease, an autoinflammatory bowel disease. Polymorphisms in the gene encoding the core autophagy protein ATG16 was shown to be associated with a high risk of Crohn's disease development in Caucasian population. Lower levels of ATG16 have been hypothesised to be unable to inhibit inflammasome activation leading to increased cytokine production and repeated inflammation of the gut. However, the precise role of ATG16 in the pathogenesis of Crohn's disease remains unclear (Yang et al., 2015).

1.9. Objectives

The transmembrane autophagic protein, ATG9, was identified closely after the identification of some of the other core autophagy proteins. However, its function and regulation of trafficking remain elusive. Therefore, I decided to work towards understanding the biology of the trafficking and regulation of ATG9 function via its post-translational modifications. My first results chapter (Chapter 3) of this thesis, therefore, primarily describes the identified phosphorylation sites on ATG9 that might potentially affect its trafficking and function in cells. To test this, I generated a range of phospho-mimetic and non-phosphorylatable mutants of identified phosphorylation sites on ATG9 using site-directed mutagenesis. To aid me towards identifying the role of these phosphorylation sites, I also needed to develop a cellular system with no endogenous protein expression. Therefore, I generated a ATG9 CRISPR-knockout cell line which has been characterised in detail in my second results chapter (Chapter number 4) of

this thesis. Furthermore, the mass spectrometric analysis of the ATG9 IP sample also helped me identify a putative Ser/Thr kinase, known as DNA-PKcs/PRKDC, which could phosphorylate one or few serine residue(s) of ATG9. The interaction of PRKDC with ATG9 was confirmed using various experimental approaches. However, since the expression levels of various phospho-mutants of ATG9 could not be normalised as a result of varying protein stability; and since the reduction in the levels of PRKDC also could not be related to the perturbations in autophagic flux using multiple strategies, the results were considered to be inconclusive.

In my third results chapter (Chapter 5), I've studied and described a new role for p62 in autophagy-impaired cells that was revealed when I was characterising the ATG9 knockout cells that I made. Under autophagy-impaired conditions especially when the lipidation of LC3 is affected, the role of p62 remains unknown. In this chapter, I show that p62 forms aggregates in autophagy-impaired conditions that can force cells to form LC3-I positive structures. These LC3-positive structures on close examination look similar to LC3-II puncta, with a slight difference in size that could be potentially misleading. Therefore, I confirm that in cells with defective autophagy, p62 aggregate formation leads to the formation of LC3-I puncta like structures, thereby making LC3 immunofluorescence studies under these conditions unsuitable. My results also identify a novel homeostatic function of p62 in autophagy-impaired cells.

Finally, my last results chapter (Chapter number 6) focuses on the trafficking of ATG9 and VMP1. VMP1, as described above, is a newly identified transmembrane protein involved in autophagy besides ATG9. However, the trafficking of VMP1 and its relation to the only other transmembrane autophagy protein hasn't been identified yet. Therefore, I was interested to check if VMP1 shared some biology with ATG9, its importance for the process of autophagy and its trafficking. In this chapter, I describe that VMP1 shares the trafficking route and interacts with ATG9 inside the cell. Interestingly, I also show that VMP1 overexpression induces autophagy and that this induction is dependent on the ATG9 expression in the cells. Furthermore, I show that ATG9 traffics via an additional novel trafficking route that is dynamin-independent, and that this trafficking route is also shared by VMP1. Moreover, VMP1 also potentially traffics via a different dynamin-independent route in addition to the one formerly mentioned for ATG9.

2. Materials and methods

2.1. Cell culture

The cell lines were cultured in Dulbecco's Modified Eagle Medium (DMEM) supplemented with 10% fetal bovine serum, 100 U/ml penicillin-streptomycin and 2 mM L-glutamine, all obtained from Sigma, UK. The cell line was maintained by passaging the cells, using Trypsin-EDTA solution (Sigma), after they are confluent to around 75-90% in T75 (75 cm^2 area) flasks (Falcon).

The cell line used for the most part of the study was HeLa (Human cervical cancer cells) cell line. Once confluent, the media was aspirated with the help of a vacuum pump and the flask was washed once with 10 ml Phosphate Buffered Saline (PBS). This step was followed by trypsinisation of the cells using 3 ml Trypsin-EDTA solution for 5 minutes at 37°C. The trypsin was then inactivated by adding 7 ml of complete DMEM medium. The number of cells per ml was calculated using the countess slides from Invitrogen and the cells were seeded, in 6-well plates or coverslips, as per experimental requirement. The CRISPR KO cells were cultured and passaged in a similar manner mentioned above.

2.2. Plasmid constructs

The human ATG9-MycDDK plasmid, cloned in a pCMV6-entry vector, together with the corresponding empty vector were purchased from Origene, US. The GFP-tagged VMP1 construct and the corresponding empty vector was also purchased from Origene, US. ATG16-pEGFP was a kind gift from Dr Y. Takahashi and pEGFP-LC3 and mRFP-GFP-LC3 were kind gifts from Dr. T. Yoshimori. The pEGFP-ARF6- wild type, T27N and Q67L inserted into an EGFP background vector and the corresponding HA-tagged variants of ARF6 cloned into a pcDNA3.1 background vector, were obtained from J.G. Donaldson, National Institutes of Health, Bethesda, MD. The pEGFP-Atg16L1 (the cDNA corresponding to the open reading frame of mouse Apg16L1 cloned into pEGFP-C1) was obtained from T. Yoshimori, Research Institute for Microbial Diseases, Osaka University, Osaka, Japan. The GFP-tagged RavZ construct was a kind gift from the Dr. Craig Roy, Yale university school of medicine.

2.3. Transformation of bacteria

The plasmids were propagated and purified from bacterial cultures. High-efficiency *E.coli* DH5α competent cells, obtained from Bioline US Inc, were used for the transformation of plasmids.

The transformation was performed by adding 10-100 ng of purified plasmid DNA to 50 µl of competent cells and incubating this mixture on ice for 30 minutes. Next, the cells were subjected to a heat shock for 30 seconds at 42°C in a water bath, followed by 2 minutes of incubation on ice. This was followed by the addition of 950 µl of Luria Broth (LB) medium to the tubes and the cells were allowed to grow at 37°C for 60 minutes. A 100 µl volume of the cell suspension was then plated on a LB-agar plate containing an appropriate selection marker (antibiotic) for the plasmid. These plates were then incubated at 37°C for 16-20 hours and checked for colonies the next day.

2.4. Plasmid isolation

The plasmids were isolated from the bacteria using a PureLink™ HiPure Plasmid Filter Maxiprep Kit from Invitrogen, US. The colonies obtained after transformation were inoculated in 200 ml of LB with appropriate antibiotic and incubated at 37°C for 16-20 hours. The cells were then harvested by spinning them down at 10000 rpm for 10 minutes in a centrifuge. The pellet was then subjected to a series of steps, mentioned in the manufacturer's protocol, to obtain purified plasmid DNA. The protocol is based on the principle of alkaline-lysis method of purification of plasmid DNA. The quantification of the plasmid DNA was performed using a spectrophotometer (Nanodrop1000, Thermo Scientific) using water or TE buffer (as appropriate) as blank.

2.5. Transfection

The HeLa cells were transfected with the purified plasmid using the Mirus TransIT-2020 transfection reagent. The transfection was performed using optiMEM medium, as per the manufacturer's protocol.

A mixture of 100 µl of optiMEM with 1 µg of DNA was prepared and incubated at room temperature for 5 minutes. Another mixture containing 100 µl optiMEM with 5 µl of Mirus was prepared and incubated for 5 minutes. Both the solutions were then mixed together and incubated for approximately 20-25 minutes. The total volume was then added to one well of a 6-well plate, already containing 1 ml of optiMEM. The amount of DNA generally used for transfection was 1 µg.

2.6. siRNA knockdown

The cells for siRNA knockdown were transfected using lipofectamine 2000 transfection reagent. The transfection was performed using optiMEM medium, as per the manufacturer's protocol.

A mixture of 100 µl of optiMEM with 3 µl of 20 µM or 1 µl of 100 µM siRNA was prepared and incubated at room temperature for 5 minutes. Simultaneously, another mixture containing 100 µl optiMEM with 5 µl of Lipofectamine 2000 was prepared and incubated for 5 minutes. Both the solutions were then mixed together and incubated for approximately 20-25 minutes. The total volume was then added to one well of a 6-well plate, already containing 1 ml of optiMEM for 4 hours at 37°C. After the incubation, the media was changed and replaced with full media. The cells were then harvested after 24 hours of incubation if a single KD was desired. For double KD studies, next round of siRNA transfection, following the same protocol as mentioned above, was performed 48 hours from the first round. The cells were then split and seeded to respective plates or coverslips for further experiments.

siRNA	Type/ Sequence
scrambled	ON-TARGETplus Non-targeting siRNA #1 (Dharmacon)
p62	ON-TARGETplus Human SQSTM1 siRNA Smartpool (Dharmacon)
PRKDC	ON-TARGETplus Human PRKDC siRNA Smartpool (Dharmacon)

2.7. Cell-surface biotinylation

The cell-surface biotinylation assay was used to check the presence of VMP1 on the plasma membrane. The technique exploits the interaction between the side chains of the accessible lysine residues exposed on the cell membrane and the highly active form of biotin [NHS-LC-Biotin: (succinimidyl-6-(biotinamido)hexanoate)]. These NHS-activated biotin molecules are known to react with the exposed primary amine ($-NH_2$) groups to form stable amide bonds in basic environment (Thermo Scientific instructions manual for EZ-Link® NHS-Biotin reagents). The side chains of the amino acid lysine or N-terminus of proteins that are exposed on the surface of the cell provide free primary amine groups and are therefore good targets of labelling by NHS-LC-biotin. The technique then exploits the high affinity interaction between biotin and streptavidin to isolate the biotinylated proteins exposed at cell-surface using Streptavidin-immobilised agarose/magnetic beads. Variants of this biotin that are membrane impermeable are also available to simplify the process of labelling (Thermo Scientific instructions manual for EZ-Link® NHS-Biotin reagents).

The cells were washed twice with 1x PBS and incubated in a buffer (1 mM $MgCl_2$, 2 mM $CaCl_2$, 150 mM NaCl) supplemented with 0.5 – 1 mg/ml NHS-LC-Biotin for 60-90 minutes at 4°C. Next, the cells were washed with quenching buffer (1 mM $MgCl_2$, 0.1 mM $CaCl_2$, 100 mM glycine) twice, to stop the biotinylation of the proteins on the surface, for 10 minutes at 4°C. Finally, the cells were washed twice with 1x PBS and lysed in RIPA buffer (150 mM NaCl, 50 mM Tris-HCl (pH 7.4), 5 mM EDTA, 1% Triton X-100, 0.5% deoxycholate, and 0.1% SDS, cocktail of protease and phosphatase inhibitors) on ice for 30 minutes. The cell lysates were then centrifuged at 13000 rpm for 10 minutes at 4°C and the supernatant was collected. The protein concentration was estimated using the Biorad protein assay kit and the samples were normalised in protein concentration. 10 µl of the lysate was then collected and mixed with 10 µl of the 2X Laemmli buffer to be used as an input control. Meanwhile, 50 µl of the Streptavidin-magnetic beads, washed twice with RIPA buffer, were added to the cell lysates and the mixture was tumbled at 4°C for 2 hours. The beads were then magnetically separated and washed twice with RIPA buffer. Finally, the beads were resuspended in 30 µl of 2X Laemmli buffer and the streptavidin-biotin complex was denatured by heating the resuspended beads at 95°C for 5 minutes.

2.8. Immunocytochemistry

The immunocytochemistry analysis was performed on cells grown on 22 x 22 mm coverslips. The cells were grown at a confluency of 70-80%, washed once with PBS and then fixed using 4% PFA for 5-7 minutes. The PFA was discarded in accordance with the safety regulations and the cells were washed thrice with PBS. The cells were then permeabilised using 0.5% TritonX-100 for 5-7 minutes and washed thrice with PBS to remove any residual detergent. A solution containing 1% BSA was then added onto the coverslips, as a blocking solution, for reducing the non-specific binding of the primary and secondary antibodies and kept for 1 hour at room temperature. The blocking solution was then tapped off the slides and the primary antibodies at appropriate dilutions were added on the coverslips. The coverslips with primary antibodies were incubated at 4°C for 16-20 hours in a moist and humid chamber. The coverslips were next washed thrice with PBS and incubated with secondary antibodies containing solution for 1 hour at room temperature. (Note that the primary and secondary antibody solutions were made in the blocking buffer.) The usual dilution of the secondary antibody in 1% BSA was 1:400. In the final step, the coverslips were washed twice with PBS and high purity sterile water, and mounted on glass slides using Pro-Long gold anti-fade DAPI mounting medium (Invitrogen, US).

The coverslips were then imaged using the Zeiss LSM880 or LSM780 confocal microscope using the 63x oil immersion objective.

2.9. Super-resolution microscopy

Samples were seeded onto Zeiss High precision No 1.5 170 + or − 5µm, 18mm X 18mm coverslips. Following staining the samples were mounted in Prolong Gold (Life Technologies) and left to harden for 3 days to reach a constant Refractive Index (RI) of 1.46. Samples were imaged using Structured Illumination on the Elyra PS1 (Carl Zeiss Microscopy). Following stage alignment, laser lines of 405,488 and 561nm were used to image a bead stack in order to correct for chromatic aberration using the channel alignment algorithm. Z stacks were acquired at 5 phases and 5 rotations of the illumination grid and subsequently processed and aligned using the ZEN Black Elyra edition software (Carl Zeiss Microscopy).

2.10. PI3P staining

PI3P molecules constitute an integral part of the autophagy signalling pathway and are synthesised on the growing phagophore by the PI3K-VPS34 kinase complex (Bento et al., 2016b). Since PI3P molecules, in general, form an important of the cellular signalling process, levels of PI3P puncta in a cell therefore represent the signalling activity of the cell at a given time. Thus, to stain for the PI3P puncta in ATG9 wild-type and knockout HeLa cells, they were fixed in 2% paraformaldehyde and permeabilised with 20µM digitonin in buffer A (20 mM PIPES pH 6.8, 137 mM NaCl, 2.7 mM KCl). Then cells were blocked with buffer A supplemented with 5% (v/v) FBS and 50 mM NH_4Cl. Anti-PI3P antibodies from Echelon (for 1 h, 1:300) and secondary antibodies were applied in buffer A with 5% FBS. Cells that underwent post-fixation for 5 min in 2% paraformaldehyde, were washed with PBS containing 50 mM NH_4Cl, then were washed once with water and then mounted with Mowiol (Hammond et al., 2009).

2.11. Western Blot

The levels of proteins of interest in cells were determined using western blots. The technique involves separation of protein samples based on their molecular weight (M.W.) using SDS-PAGE and transferring them on a PVDF membrane. The membrane is then incubated with primary, secondary antibodies and developed to detect the levels of protein of interest.

The sample preparation for the western blots required cell lysis and the buffer used to lyse the cells was chosen based on the downstream processing required. For instance, 1X Laemmli Buffer was generally used to lyse the cells, but in a case where protein quantitation using Bradford's method was essential, RIPA buffer had to be used. Therefore, the optimum buffer for the cell lysis was tested and selected based on the application. After the cells were lysed, 20-30 µl of samples were loaded onto a 10-well, 12-15% SDS-PAGE and run at 100-120 V. A standard M.W. ladder was loaded along with the samples to keep a track of the movement of the proteins in the gel. Meanwhile, a PVDF membrane (Immobilon-FL membrane, Millipore) of appropriate size was cut and activated by soaking it in pure methanol for 5 seconds. The membrane was then equilibrated by soaking it in 1X transfer buffer for a few minutes. After the desired separation of the proteins was achieved, the proteins were transferred onto the

activated PVDF membrane in a tank containing 1X transfer buffer run at 100 V for 60 minutes. The transfer unit was also surrounded by ice, since lower temperatures increase the efficiency of transfer. Furthermore, care was taken about the methanol percentage in the transfer buffer based on the protein to be transferred. The transfer for small M.W. proteins required higher percentage of methanol in the transfer buffer as compared to large M.W. proteins; since, methanol interferes with SDS-binding to the protein and a higher percentage could lead to precipitation of large M.W. protein. The membrane was removed on completion of the transfer and was soaked in 5% skimmed milk for blocking the non-specific binding sites, for 1 hour at room temperature and the solution was then discarded. Next, a solution containing specific primary antibody (prepared in 5% skimmed milk or in 10% BSA based on the manufacturer's instructions) at an appropriate dilution was added on to the membrane for overnight incubation at 4°C. Next day, the primary antibody was collected and stored at -20° until further use. The membranes were then washed thrice with PBST (Phosphate buffer saline + 0.1% Tween-20) before the addition of secondary antibody. The secondary antibody, also prepared in 5% skimmed milk, was incubated with the membrane for 1 hour at room temperature. The dilution of the secondary antibody was generally kept at 1:4000 for enhanced chemiluminescence (ECL) HRP-conjugated antibodies and 1:5000 for LICOR fluorophore-conjugated antibodies. The membranes were then washed again with PBST multiple times and developed using a mixture of equal volumes of developing solutions 1 and 2 for ECL or imaged directly for fluorescence signal detection using LICOR Image Studio software (LICOR, US).

2.12. Proximity ligation assay

This assay helps identify the interacting protein partners inside the cell. The technique was published in 2006 (Söderberg et al., 2006) and utilises the binding proximity of antibodies raised in two different species to target proteins. The primary antibodies are recognised by secondary antibodies that have been tagged with oligonucleotides. A linker DNA solution then links and ligates the two oligonucleotides, when present in close proximity, with the help of a DNA ligase. The ligated dsDNA is used as a template for rolling circle replication by the polymerase and the replicated DNA is recognised by a red fluorescent ssDNA probe.

The experiments were performed as per the manufacturer's instructions (Duolink). The reaction volume used was 80μl and the reaction was performed on coverslips. The blocking

36

buffer and antibody diluent provided with the kit were used, whereas PBS was used instead of wash buffers A and B. The primary antibody dilution used was 1:200 for ATG9 (Abcam), 1:100 for PRKDC/DNA-PKcs (Thermo) and 1:200 for GFP (Living colors, Clontech) to detect overexpressed VMP1-GFP. The coverslips were finally mounted on glass slides using Pro-Long gold anti-fade DAPI mounting medium (Invitrogen).

2.13. Immunoprecipitation

This technique exploits the binding affinity of proteins, like Protein A, G and L, for the antibody heavy chains (Fc region). The Fc-binding proteins are immobilised onto magnetic beads and are used for purifying/isolating the protein of interest. This technique is also useful to identify interactions between protein pairs, a modified technique, termed as co-immunoprecipitation.

The immunoprecipitation was performed using a confluent 10 cm dish of cells. The cells were scraped and lysed in 1ml of IP buffer, which is specific for the protein to be immunoprecipitated. The solution was then transferred to a 1.5 ml eppendorf tube and was incubated on ice for 30 minutes. The cell debris was separated by centrifuging the lysate at 10000 rpm for 10 minutes. 100 µl of the supernatant was then collected in an eppendorf tube to be used as input control. The remaining supernatant was distributed equally in 3 tubes. The antibody against the protein to be isolated was added to the first vial, while a non-specific antibody like anti-FLAG/GFP/IgG was added to the second vial; the dilutions of the antibodies was always kept 1:100 or as mentioned on the MSDS. No antibody was added to the third vial and the eppendorf tubes were tumbled for overnight at 4°C. Meanwhile, 30 µl of Protein A/G (chosen based on the antibody isotype) magnetic beads were washed with 100 µl IP buffer thrice. The lysates in the sample and control tubes were then added to the washed beads and tumbled for 2 hours at 4°C. After the incubation period, beads were collected at the side of the tube using a magnetic stand and the solution was discarded. These beads were then washed with 100 µl IP buffer thrice and were finally resuspended in 50µl of 1X Laemmli buffer. The tubes were vortexed to make sure that all the beads are resuspended in the buffer and the tubes were then heated at 100°C for 5 minutes to detach the antibody complexes from the beads. Finally, the buffer was separated from the beads using a magnetic stand and the IP samples were immediately loaded onto SDS-PAGE for separation or stored at -20°C until further use.

2.14. Click-IT® chemical assay

The protein synthesis rates in cells were determined using the Click-IT® reaction kit. The protocol was followed as per the manufacturer's instructions.

Briefly, the cells were grown in a methionine-free media for $1 - 2$ hours to deplete the methionine reserves in the cells. Next, media containing L-AHA (L-azidohomoalanine), an azido moiety containing biomolecule which serves as a replacement for methionine, was added to the cells for 4 hours to label newly synthesised proteins. The cells were then collected, lysed and the lysates were processed through different solutions provided in the Click-IT® protein reaction buffer kit resulting in isolation of the labelled newly synthesised proteins. The protein samples were then loaded on to the gel (SDS-PAGE) and immunoblotted for the proteins of interest.

2.15. Membrane fractionation

The membrane fraction was isolated and purified based on the subcellular fractionation protocol provided by Abcam®.

Briefly, cells grown on a 10cm dish were lysed using 500µl of the fractionation buffer the composition of which is as follows:

Fractionation buffer	Stocks	50ml 1x solution
250 mM Sucrose	-	4.28 g
20 mM HEPES (pH7.4)	1 M	1 ml
10 mM KCl	-	0.0373g
1.5 mM MgCl$_2$	0.1 M	750 µl
1 mM EDTA	0.5 M	100 µl
1 mM EGTA	0.1 M	500 µl

At the time of use, the fractionation buffer was supplemented with 10 µl of 1M DTT stock and 50 µl of protease inhibitor cocktail (III). The cells were scraped and the suspension was transferred into a 1.5 ml Eppendorf tube. The cells were then lysed by passing the suspension

through a 25 Ga needle 10 times using a 1 ml syringe. The lysate was allowed to sit on ice for 20 minutes. The nuclear fraction was then removed by centrifuging the samples at 3000 rpm at 4°C for 5 minutes. The pellet was discarded, and the supernatant was transferred to a fresh Eppendorf tube. This lysate was then centrifuged at 8000 rpm at 4°C for 5-10 minutes. The pellet constitutes the mitochondrial fraction and the supernatant is the cytosol + membrane fraction of the cell. The pellet was then discarded, and the supernatant was transferred to an ultracentrifuge tube. The membrane fraction was then separated by centrifuging the supernatant at 40000 rpm (100000g) at 4°C for 1 hour. After centrifugation, the supernatant was collected and stored as the cytosolic fraction. The pellet was washed by adding 400 µl of fractionation buffer and resuspended with pipetting. The solution was then passed through the 25Ga needle as used earlier. The samples were then re-centrifuged for 45 minutes and the supernatant was discarded. The pellet was then resuspended in 25-50 µl of 2X Laemmli buffer to load onto the gel.

2.16. Plasma membrane protein purification

The proteins from the plasma membrane were purified using the 'plasma membrane protein extraction kit' from Abcam®. The kit helps in the extraction of all the cellular proteins which can be further used to purify proteins that reside at the plasma membrane. The kit claims to purify proteins with high yield and purity (over 90%) and the protocol was performed according to manufacturer's instructions.

2.17. CRISPR knock-out cell line generation

Generating the CRISPR knock-out requires a guide RNA targeting an exonic region of the gene to be deleted (Ran et al., 2013). This designing was performed using the online tool developed by the Zhang Lab (Hsu et al., 2013). The top three single guide RNA (sgRNA) hits were modified manually to add BbsI restriction sites and were ordered from Invitrogen. The restriction site was added by addition of the overhang CACC to the forward sgRNA and a 'G' nucleotide if the guide does not contain one.

sgRNA-Fw: 5' *CACC(G).....*3'

The addition of the 'G' nucleotide is known to increase the specificity and the efficiency of the system (Ran et al., 2013). Similarly, the reverse sgRNA was obtained by reverse complementing the top strand and an overhang of AAAC was added to the 5' end.

sgRNA-Rv: 5' *AAAC*….3'

The sgRNA of desalted purity were then ordered from Invitrogen. The sequences used for ATG9 CRISPR knockout were as follows:

	Sequences (5' to 3')
Guide1	CACCGCTGTTGGTGCACGTCGCCGA
	AAACTCGGCGACGTGCACCAACAGC
Guide2	CACCGTGTTGGTGCACGTCGCCGAG
	AAACCTCGGCGACGTGCACCAACAC
Guide3	CACCGCGCGGATCTCCGGAGGATAT
	AAACATATCCTCCGGAGATCCGCGC

The highlighted nucleotides indicate the added overhangs as per the requirements mentioned above. The sgRNAs were then ligated in the psCas9-2A-puromycin backbone obtained from Addgene plasmid repository. The forward and reverse sgRNAs were first allowed to anneal in a temperature-controlled PCR reaction as follows:

Annealing
8.5 µl oligo1 (100 µM)
8.5 µl oligo2 (100 µM)
2 µl 10X T4 DNA Ligase buffer (NEB) [NOTE: Aliquot the T4 DNA ligase buffer before using. Multiple freeze-thaw cycles render the buffer non-functional)
1 µl ddH2O
(The final concentration of oligos comes to approx.45 µM of each primer in mix)

PCR program

Lid heated

37°C 1 hour

95°C 5 minutes

ramp down to 25°C at 5°C/minute (= 0.1°C per second)

This reaction mixture was then kept at 4°C until further use.

The backbone and the annealed sgRNAs were then digested using BbsI restriction enzyme, creating a symmetric cleavage site in the backbone and the sgRNAs. After completion of digestion, a ligation reaction was setup to generate a construct containing sgRNAs. It is to be noted that an empty vector digestion was also set up in parallel to the test samples to check the efficiency of digestion and ligation steps. The volumes of different components of the reaction mixture are mentioned below:

Cas9 digestion

2 µl 10x Buffer NEB 2.1

1 µl BbsI

X µl pX335 1(µg)

make volume up to 20 µl H$_2$O

37°C 1 hour

Ligation

To all of the above digestion reactions add:

2.5 µl 10x T4 Ligase buffer

1 µl annealed oligo (1:5 dilution in ddH2O from 45 µM stock) to get approx. 0.4 µM final concentration

1.5 µl T4 DNA ligase

37°C 1 hour

The ligated product (2 µl) was then transformed in gold efficiency *E.coli* competent cells purchased from Bioline, US. The transformants were grown in 10ml of LB and the plasmid was isolated using the miniprep kit (Qiagen,DS) the next day.

The insertion of sgRNA in the plasmid backbone was then checked by digestion of the isolated plasmid with two restriction enzymes BbsI and BglII and the digestion product was loaded on 1.5 % agarose gel, containing Midori green nucleic acid stain, together with Cas9 empty vector control. The insertion of the sgRNA into the backbone causes the disruption of BbsI restriction site leading to visualisation of just one band on the gel of size 8.5 kb, caused due to digestion with BglII. However, an unsuccessful ligation reaction would result in two bands on digestion of sizes 1.4 and 7.1 kb respectively. The digestion reaction was set up as follows:

Digestion with BglII+BbsI
1 µl Buffer 2 by NEB
2 µl DNA (from miniprep)
0.3 µl BbsI
0.6 µl BglII
6 µl water
37°C for 2 hours

The successfully ligated plasmids together with empty Cas9 vector control were then transfected in HeLa cells and the expression was allowed for 24 hours. The transfected cells were then selected by adding puromycin to the cells at a final concentration of 2-4 µg/ml. The cells were allowed to grow until all the non-transfected cells are dead. The positive cells were then trypsinised and the cell number was counted using Invitrogen Countess slides (10 µl homogenous cell suspension + 10 µl Trypan blue). Based on the live cell population, 0.2×10^4 cells were aspirated and serially diluted in a 96-well plate to obtain single cell colonies. The serial dilution was always 1:1 and the final volume in each well at the end of dilution was kept to 200 µl. The dilution was first performed horizontally by adding 200 µl of fresh complete medium in rows A2-A11. Next, the cell suspension containing 0.2×10^4 cells was added in the A1 well and the volume was made up to 400 µl using fresh complete medium. Next, 200 µl of the diluted cell suspension was added from A1 to A2 and was mixed well with pipetting. In the next step, 200 µl of the suspension from A2 was then added to A3 and so on, until A12 contains 200 µl of medium. Now using a multi-channel pipette, 100 µl of diluted cell suspension from A1-A12 was aspirated and added to the wells B1-B12 already containing 100 µl of media. Similarly, the dilution was performed until the wells H1-H12 contained 100 µl of diluted cell suspension.

These cells were allowed to attach to the substrate and grow for 24-48 hours. The wells were seen under the microscope using a low magnification objective and the wells containing colonies growing from single cells were marked.

When these colonies grow big, the cells were trypsinised and transferred to a 12-well plate for increasing the number of cells for analysis. When the wells get approximately 80% confluent, the cells were trypsinised using 100 µl of Trypsin-EDTA solution and a fresh 12-well plate is seeded using 20 µl of the cell suspension. The remaining 80 µl of the suspension was lysed using 100 µl of 2X LB and the samples are loaded on SDS-PAGE, transferred to a membrane to check for the knock-out of the protein of interest.

The identified knockout clonal pairs for ATG9 were not tested for off-target effects, however, both the ATG9 knockout cell lines generated showed similar level of the LC3-I and LC3-II protein in the cell lysates when visualised using western blotting, increasing my confidence in the data generated from the knockout cells.

2.18. Statistical analysis

The statistical significance levels for comparisons between two groups were estimated using two-tailed t-test. The conventions used to depict the results across the thesis are as follows: $*p \leq 0.05$; $**p \leq 0.01$; $***p \leq 0.001$ and the error bars represent standard deviation or standard deviation of the mean based on the experiment.

2.19. Antibodies

The antibodies used in this work are listed in the table below:

Primary Antibodies	Proteins/organelles detected	Host species	Dilution	Source
LC3	LC3-I and LC3-II	Mouse	1:200 (IF)	Nanotools, Germany
LC3	LC3-I and LC3-II	Mouse	1:1000 (WB)	Novus Biologicals, UK

LC3	LC3-I and LC3-II	Rabbit	1:200 (IF)	Abcam, UK
DNA-PKcs/PRKDC	DNA-dependent protein kinase catalytic subunit	Mouse	1:100 (IF) 1:100 (PLA) 1:1000 (WB)	Thermo Scientific, US
Actin	Actin	Rabbit	1:1000 (WB)	Sigma, US
ATG9	ATG9	Rabbit	1:200 (IF) 1:100 (IP) 1:1000 (WB) 1:200 (PLA)	Abcam, UK
EEA1	Early endosome marker	Mouse	1:200 (IF)	Abcam, UK
RAB11A	Recycling endosome marker	Rabbit	1:200 (IF)	Abcam, UK
CD63	Lysosomal marker	Mouse	1:200 (IF)	-
GFP	Green fluorescent protein	Mouse	1:200 (IF)	ClonTech, US
ULK1	ULK1	Rabbit	1:100 (IF)	Novus Biologicals, UK
ATG16	ATG16	Rabbit	1:200 (IF)	MBL International corporation, US
VPS26	VPS26	Rabbit	1:200 (PLA)	Abcam, UK
VPS35	VPS35	Mouse	1:200 (PLA)	Abcam, UK
WIPI2	WIPI2	Mouse	1:200 (IF)	Abcam, UK
VMP1	VMP1/TMEM49	Rabbit	1:100 (IF)	Novus Biologicals, UK
BECN1	BECN1	Rabbit	1:200 (IF)	Invitrogen, US
MHC-I	MHC class I – pan-conformational (W6/32)	Mouse	1:50 (IF)	Kind gift from Prof. Paul Lehner, CIMR

ARF6	ADP-ribosylation factor 6	Mouse	1:50 (IF)	Santa Cruz biotechnology, Inc.
p62	p62	Mouse	1:100 (IF) 1:1000 (WB)	BD Biosciences
Calnexin	ER, MAM	Mouse	1:200 (IF) 1:1000 (WB)	BD Biosciences
GAPDH	GAPDH	Mouse	1:1000 (WB)	Abcam, UK
Tubulin	α-Tubulin	Mouse	1:1000 (WB)	Sigma, US

Secondary antibodies	Antigen	Host species generated	Dilution	Source
ECL-IgG-HRP Rabbit (ECL)	Rabbit primary antibody	Donkey	1:4000	GE Healthcare UK Limited
ECL-IgG-HRP Mouse (ECL)	Mouse primary antibody	Donkey	1:4000	GE Healthcare UK Limited
Alexa goat anti-rabbit 488 (IF)	Rabbit primary antibody	Goat	1:400	Invitrogen, US
Alexa goat anti-mouse 488 (IF)	Mouse primary antibody	Goat	1:400	Invitrogen US
Alexa goat anti-rabbit 555 (IF)	Rabbit primary antibody	Goat	1:400	Invitrogen, US
Alexa goat anti-mouse 555 (IF)	Mouse primary antibody	Goat	1:400	Invitrogen, US
Alexa goat anti-rabbit 647 (IF)	Rabbit primary antibody	Goat	1:400	Invitrogen, US
Alexa goat anti-mouse 647 (IF)	Mouse primary antibody	Goat	1:400	Invitrogen, US

Goat anti-rabbit IR Dye 680 (LI-COR)	Rabbit primary antibody	Goat	1:5000	Odyssey, LI-COR Biosciences, US
Goat anti-mouse IR Dye 680 (LI-COR)	Mouse primary antibody	Goat	1:5000	Odyssey, LI-COR Biosciences, US
Goat anti-rabbit IR Dye 800 (LI-COR)	Rabbit primary antibody	Goat	1:5000	Odyssey, LI-COR Biosciences, US
Goat anti-mouse IR Dye 800 (LI-COR)	Mouse primary antibody	Goat	1:5000	Odyssey, LI-COR Biosciences, US

3. Studying ATG9 phosphorylation in HeLa cells

3.1. ATG9 is phosphorylated on multiple serine residues under different conditions

Recent studies have shown the importance of post-translational modifications in autophagy. The post-translational modifications like phosphorylation, glycosylation, ubiquitination, acetylation, etc. have been shown to modulate the interaction between various proteins regulating autophagy (Xie et al., 2015). Of these modifications, phosphorylation constitutes the most common method employed by the cells for regulation of protein trafficking, in which one or more phosphate group(s) is added to the protein. The existing literature consists little information on how ATG9 trafficking is being regulated inside the cell. This led me to think that the trafficking of ATG9 could possibly be regulated by its phosphorylation.

Therefore, I checked the phosphorylation status of ATG9 under various conditions via mass spectrometry. I performed immunoprecipitation of endogenous ATG9 protein from HeLa cells grown in either full media, EBSS (starvation medium) for 4 hours or 100 mM trehalose for 16 hours. The samples were then digested with trypsin and subjected to mass spectrometric analysis to identify ATG9 residues that are phosphorylated under these conditions. The condensed raw results showing at least 1 unique peptide detected for each phosphorylation site has been summarised in Table 3.1 a. The results showed the presence of 4 phosphorylated serine residues common to all the three conditions. When compared to the phosphorylation status in starved condition, basal condition showed phosphorylation of 1, while the trehalose treatment showed presence of 3 exclusively phosphorylated serine residues (Table 3.1 b). Interestingly, all of the identified phosphorylation sites were located in long C-terminal cytosolic tail of ATG9, with the exception of 2 sites located in the short N-terminal cytosolic fragment (Table 3.1 b).

	Sequence	Modifications	Start	Stop	Position identified
Basal	(R)LEAsYSDSPPGEEDLLVHVAEGSK(S)	Phospho (+80)	11	34	S14
	(R)SFsPLQPGQAPTGR(A)	Phospho (+80)	654	667	S656
	(R)REsDESGESAPDEGGEGAR(A)	Phospho (+80)	733	751	S735
	(R)ESDESGEsAPDEGGEGAR(A)	Phospho (+80)	734	751	S741
	(R)HPEPVPEEGsEDELPPQVHKV(-)	Phospho (+80)	819	839	S828

	Sequence	Modifications	Start	Stop	Position identified
Starvation	(R)LEAsYSDSPPGEEDLLVHVAEGSK(S)	Phospho (+80)	11	34	S14
	(R)SFsPLQPGQAPTGR(A)	Phospho (+80)	654	667	S656
	(R)REsDESGESAPDEGGEGAR(A)	Phospho (+80)	733	751	S735
	(R)HPEPVPEEGsEDELPPQVHKV(-)	Phospho (+80)	819	839	S828

	Sequence	Modifications	Start	Stop	Position identified
Trehalose	(R)LEAsYSDsPPGEEDLLVHVAEGSK(S)	Phospho (+80), Phospho (+80)	11	34	S14, S18
	(R)RESDEsGEsAPDEGGEGAR(A)	Phospho (+80), Phospho (+80)	733	751	S738, S741
	(R)SFsPLQPGQqAPTGR(A)	Phospho (+80)	654	667	S656
	(R)LEASYSDsPPGEEDLLVHVAEGSK(S)	Phospho (+80)	11	34	S18
	(R)SFsPLQPGQAPTGR(A)	Phospho (+80)	654	667	S656
	(R)REsDESGESAPDEGGEGAR(A)	Phospho (+80)	733	751	S735
	(R)HPEPVPEEGsEDELPPQVHKV(-)	Phospho (+80)	819	839	S828

b)

	Residues Identified						
Basal	S14	-	S656	S735	-	S741	S828
Starved	S14	-	S656	S735	-	-	S828
Trehalose	S14	S18	S656	S735	S738	S741	S828

Table 3.1: a) Table showing the summary for at least 1 unique peptide identified per phosphorylation residue of ATG9. The protein IP sample was digested with trypsin and the digest was subjected to mass spectrometry to identify phosphorylated sites. The identified phosphorylation sites in the sequence are shown in lower case letters. **b)** Table depicting the various phosphorylation sites on ATG9 identified under various conditions using mass spectrometry.

To test the role of these phosphorylation sites, I generated phospho-mimetic and non-phosphorylatable mutants by site-directed mutagenesis of the human WT ATG9-MycDDK (purchased from Origene, US). The parental construct was tested for its expression and distribution in the cell together with calnexin, an ER resident protein. ATG9-MycDDK showed no co-localisation with calnexin and displayed peri-nuclear localisation similar to the endogenous ATG9 staining, confirming that the protein is not stuck in the ER and is being synthesised and trafficked normally (Fig 3.1 a). The phospho-mimetic mutants were generated by substituting the serine residue with a glutamate, since the side chain of glutamate resembles a phosphate group and is negatively charged. Similarly, the non-phosphorylatable mutants were generated by substituting the serine residue with alanine, eliminating the side chain and the ability of the kinase to phosphorylate the protein. All of the mutants generated were confirmed using DNA sequencing. The mutants were then tested for their expression levels in the cells by transfecting the same amount of DNA in the cells. The cells were then harvested and probed for the transfected protein expression using an antibody against the DDK tag. All of the mutants showed varying expression levels (Fig 3.1 b). To normalise the expression levels of the mutants the approximate amount of DNA to be transfected was calculated based on the expression levels of the WT construct, however, it did not result in any change in the variance of expression. This might be due to a change in the protein stability or turnover rate caused by the introduced mutations making the screening of the mutants difficult.

In order to test the mutants effectively, I generated ATG9 knockout cell lines using the CRISPR technique. The results of the cell line characterisation and studies are described in detail in chapter 4 of this thesis. To perform a mutant screen with the normalised amount of DNA, ATG9 mutants were transfected into ATG9 CRISPR knockout cells and the levels of LC3-II were assessed. Unfortunately, the levels of LC3-II did not correspond to the levels of ATG9 mutant expression (Fig 3.2 a and b).
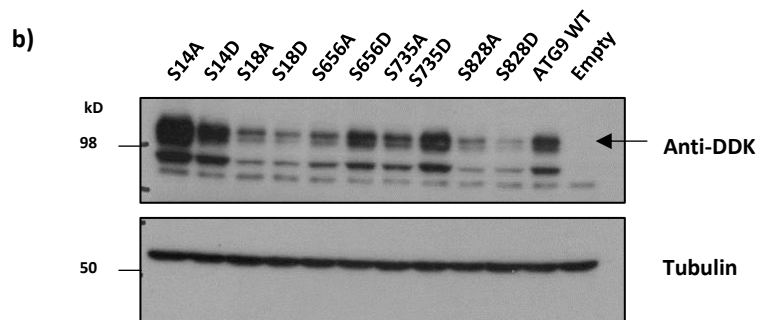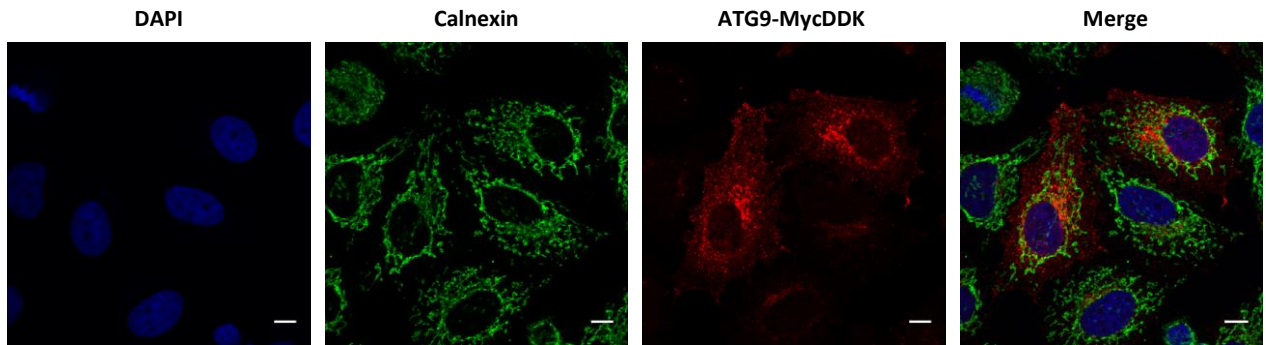
Fig 3.1: a) Representative images of HeLa cells grown in full media that were transfected with ATG9-MycDDK construct. Cells were fixed and stained using an antibody against calnexin and FLAG (DDK-tag) to detect the transfected protein. The scale bars represent a distance of 10 µm. **b)** Representative western blot showing the expression levels of the ATG9 mutants generated using site-directed mutagenesis. The cells were transfected with 1 µg of DNA of each mutant and the cell lysates were probed with an antibody against the DDK tag. The arrow marks the band corresponding to the correct molecular weight of ATG9.
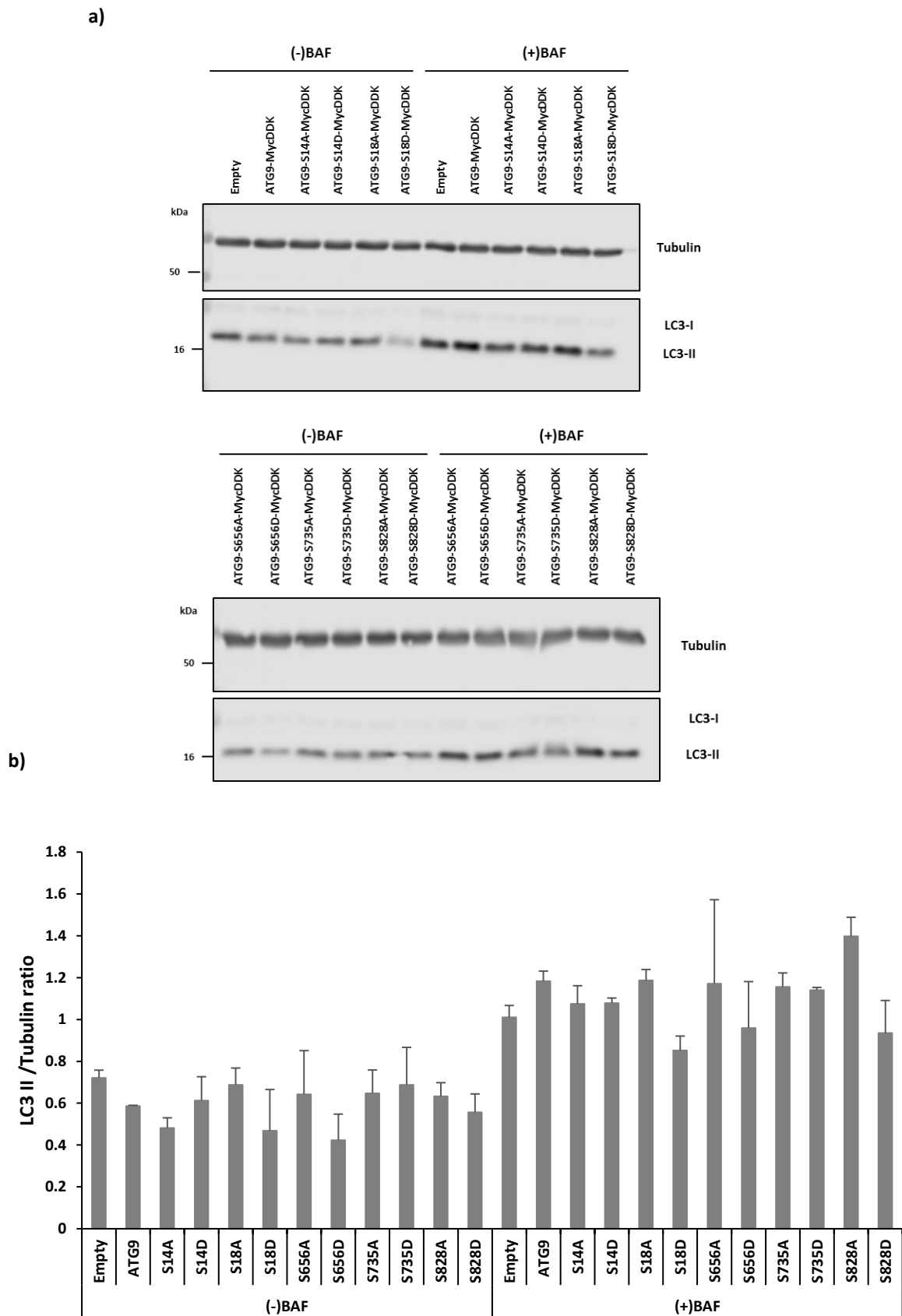
Fig 3.2: a) Representative western blot to assess LC3-II levels on transfection of ATG9 mutants in ATG9 CRISPR KO cells. ATG9 knockout cells were transfected with normalised amount of ATG9 mutants and were harvested 16-24 hours after transfection. **b)** The western blots were quantified for LC3-II and tubulin levels the using LICOR-imaging software and using tubulin as loading control, the ratio of LC3-II to tubulin was plotted.

3.2. ATG9 interacts with DNA-dependent protein kinase (PRKDC)

The mammalian ATG9 sequence was checked for motifs known to be phosphorylated by specific kinases using the Scansite 4.0 algorithm (Obenauer et al., 2003). This algorithm searches the protein sequence for conserved motifs, using a reference proteome and lists the putative kinases with their corresponding phosphorylation sites. It also takes into account the surface accessibility of the site to solvents while calculating the percentile score of the kinase. Interestingly, a recent study showing ATG9 phosphorylation under hypoxic conditions by 14-3-3ζ kinase was predicted by this algorithm with a strong percentile score (Weerasekara et al., 2014). The results obtained using Scansite have been summarised in a table below (Table 3.2). Interestingly, all the sites that were found to be phosphorylated using mass spectrometry (Table 3.1 b) were listed, in addition to serine-761 that was shown to be phosphorylated specifically under hypoxic conditions (Weerasekara et al., 2014).

Meanwhile, I performed mass spectrometry of the ATG9 IP samples to check for its binding partners. The list of proteins was sorted and checked for the proteins with highest iBAQ value, which corresponds to the sum of all peptide intensities divided by the number of observable peptides of a protein (Fabre et al., 2014), between ATG9 IP and non-specific IP sample. Interestingly, DNA-dependent protein kinase (PRKDC) was found to be a hit with highest iBAQ value and specificity. PRKDC is a serine/threonine kinase that acts as a sensor for DNA damage and plays a role in DNA repair. It is involved in non-homologous end joining (NHEJ) of the double-stranded DNA breaks (Meek et al., 2007).

I confirmed the interaction between ATG9 and PRKDC using co-immunoprecipitation and proximity ligation assay, showing the interaction between ATG9 and PRKDC to be highly specific (Fig 3.3 a and b). The interaction between VPS26 and VPS35, components of the retromer complex, was used as a positive control for the proximity ligation assay (Zavodszky et al., 2014).

3.3.   PRKDC knockdown blocks autophagy

The effect of the putative identified kinase PRKDC on autophagy was checked by knocking it down using siRNA SMARTpool. The knockdown of PRKDC resulted in reduction of approximately 60% of the protein accompanied by cell death of approximately 30% of the cells. The PRKDC knockdown samples showed approximately 12% higher levels of LC3-II in conditions without BAF compared to control. Under BAF conditions however, the levels of LC3-II were the same as control, indicating that PRKDC knockdown causes a block in LC3-II degradation (Fig 3.4 a, b and c). This could be caused due to defective transport of autophagosomes to lysosomes or defective degradation of the autophagosomes. The statistical analysis of the repeats, however, indicates that the observed difference was non-significant. This was most likely a result of cell death of the population that had effective PRKDC depletion and survival of the cells that had insufficient knockdown of PRKDC.

Therefore, an alternative strategy was used to suppress PRKDC activity in the cells. A chemical inhibitor, NU7026, was used as a selective small-molecule inhibitor of PRKDC in a study that implicated PRKDC as a potential therapeutic target for leukaemia (Veuger et al., 2003; Willmore et al., 2004). The molecule was shown to be specific and effective at a concentration of 10 µM in the study. Therefore, HeLa cells were treated with 10 µM of NU7026 for 1 hour and the effect on LC3 levels were checked. Surprisingly, no effect on the levels of LC3 were observed on treatment. Hence, a dose response experiment, with a higher starting concentration, was setup to find the optimal inhibitory concentration of NU7026 in HeLa cells. As seen from Fig 3.5 a and b, NU7026 has almost no effect at 25 µM, a mild effect at 50 µM and a strong effect at 100 µM on LC3-II levels. However, a concentration of NU7026 this high is known to non-specifically inhibit other PI-3 kinases, ATM and ATR. Therefore, the approach of using the inhibitor to specifically suppress PRKDC activity in the cells failed. Moreover, when the cells were treated with 100 µM NU7026 for 1 hour it resulted in mislocalisation of EEA1, an early endosomal marker protein, indicating a defect in endocytic pathway. Interestingly, ATG9 was also found to be mislocalised in cells treated with the NU7026 inhibitor, however, due to lack of specificity of the inhibitor nothing can be concluded from the observations (Fig 3.5 c). In addition, a PRKDC-GFP overexpression construct was obtained from the lab of Prof. Katheryn Meek, however, since the molecular weight of PRKDC

is 450 kDa, the overexpression construct was approximately 17 kb. As a result of unusually large size of the plasmid, the purification of the plasmid resulted in fragmentation of the DNA.

Identified serine residue	Score	Percentile	Sequence	SA	Enzyme	Gene card
S656	0.5819	2.942%	ASALRSFSPLQPGQA	0.787	14-3-3 Mode 1	YWHAZ
S656	0.5759	2.800%	ASALRSFSPLQPGQA	0.787	Protein Kinase A	PRKACG
S14	0.4601	1.111%	EYQRLEASYSDSPPG	1.884	PKC epsilon	PRKCE
S14	0.6012	4.276%	EYQRLEASYSDSPPG	1.884	Casein Kinase 2	CSNK2B
S18	0.6045	4.511%	LEASYSDSPPGEEDL	1.626	Casein Kinase 2	CSNK2B
S18	0.6148	2.254%	LEASYSDSPPGEEDL	1.626	GSK3 Kinase	GSK3A
S18	0.5369	0.879%	LEASYSDSPPGEEDL	1.626	Erk1 Kinase	MAPK3
S18	0.6192	3.502%	LEASYSDSPPGEEDL	1.626	Cdk5 Kinase	CDK5
S735	0.4633	0.791%	HVWHRRESDESGESA	4.037	Protein Kinase A	PRKACG
S828	0.5434	1.051%	EPVPEEGSEDELPPQ	2.636	DNA PK	PRKDC
S828	0.6213	4.009%	EPVPEEGSEDELPPQ	2.636	ATM Kinase	ATM
S828	0.3944	0.154%	EPVPEEGSEDELPPQ	2.636	Casein Kinase 2	CSNK2B
S761	0.2096	0.013%	QSIPRSASYPCAAPR	0.54	14-3-3 Mode 1	YWHAZ
S761	0.5446	1.886%	QSIPRSASYPCAAPR	0.54	Protein Kinase A	PRKACG
S761	0.5724	0.712%	QSIPRSASYPCAAPR	0.54	Akt Kinase	AKT1
S761	0.6224	0.793%	QSIPRSASYPCAAPR	0.54	AMP_Kinase	PRKAA1
S738	0.4767	0.353%	HRRESDESGESAPDE	2.04	DNA PK	PRKDC

Table 3.2: Table depicting the predicted kinases and the corresponding phosphorylation sites on ATG9 as identified by Scansite. The percentile score indicates the confidence of the hit based on all the results obtained from the proteome database. Highlighted rows indicate the putative kinase of interest that was pursued for further studies.
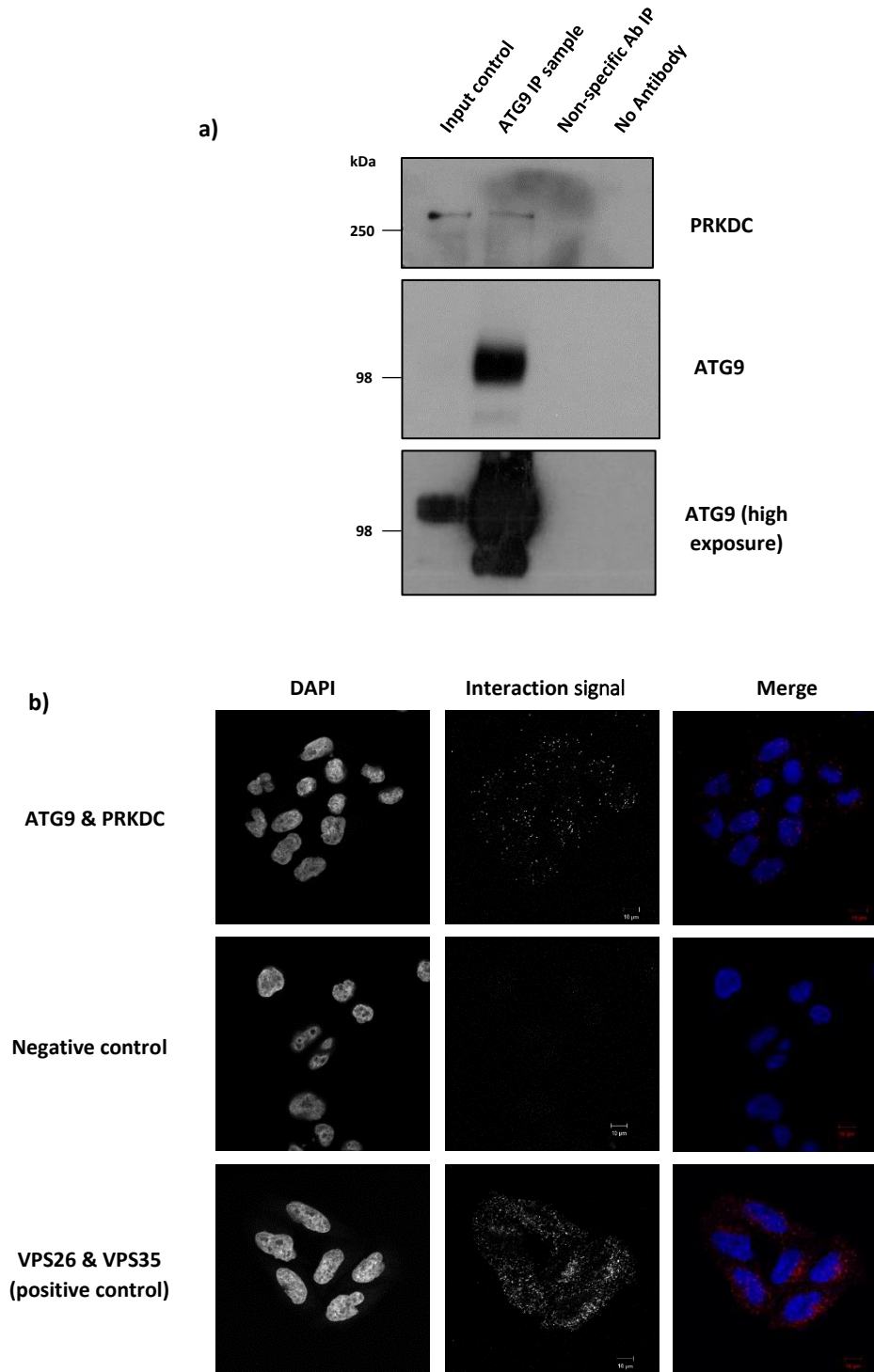
Fig 3.3: a) Representative western blot of the immunoprecipitation experiment showing the interaction of endogenous ATG9 with endogenous PRKDC. ATG9 was immunoprecipitated from HeLa cells grown in full media and the samples were separated using SDS-PAGE. **b)** Representative images of the proximity ligation assay to confirm the interaction between endogenous ATG9 and PRKDC. The proteins VPS26 and VPS35 are components of the retromer complex and were used as a positive control for the assay (Zavodszky et al., 2014). The scale bars represent a distance of 10 µm.
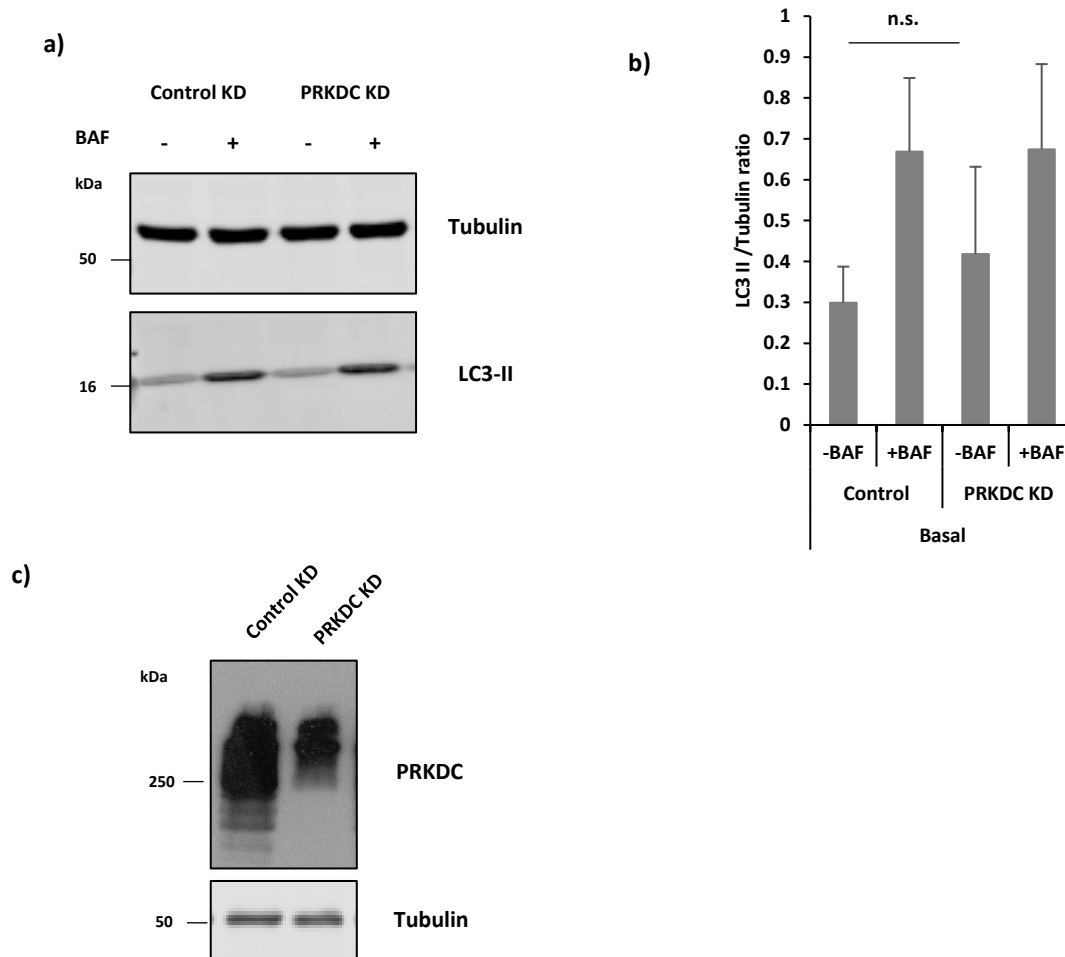
Fig 3.4: a) Representative western blot showing the effect of PRKDC knockdown on LC3-II levels. HeLa cells were transfected with the scrambled/PRKDC siRNA using lipofectamine-2000 and the proteins in the lysates were separated using SDS-PAGE and probed for antibodies against tubulin and LC3-II. **b)** The levels of protein were quantified with tubulin as loading control using the LICOR-imaging software and the ratio of LC3-II to tubulin was plotted (n.s. = non-significant). **c)** Representative western blot showing the efficiency of PRKDC knockdown upon transfection of PRKDC SMARTpool siRNA using lipofectamine-2000. The levels of tubulin were used as a loading control.

c)
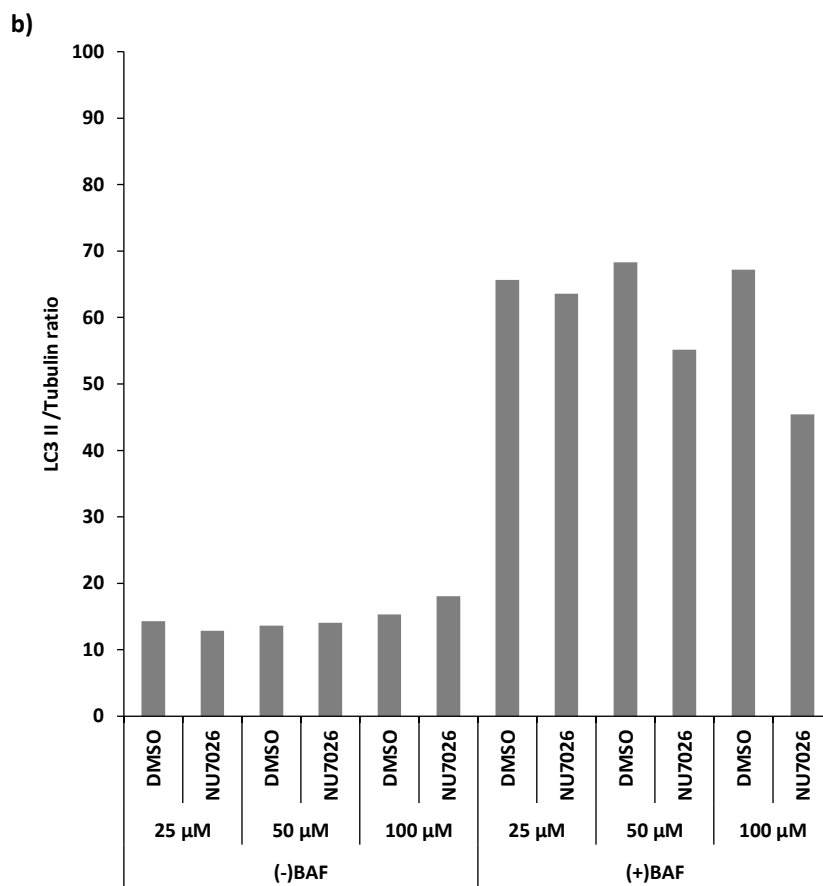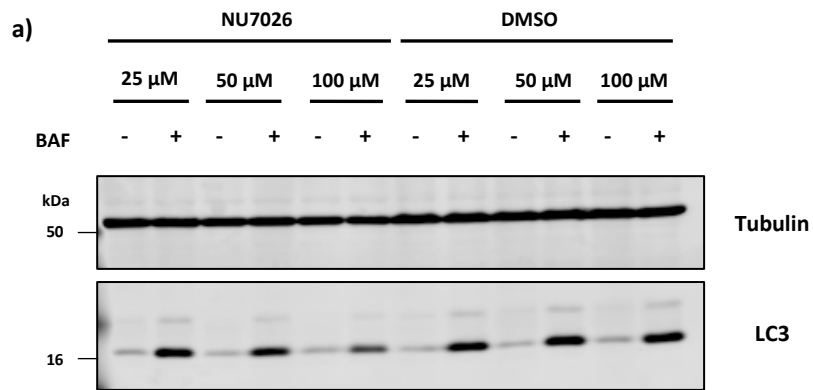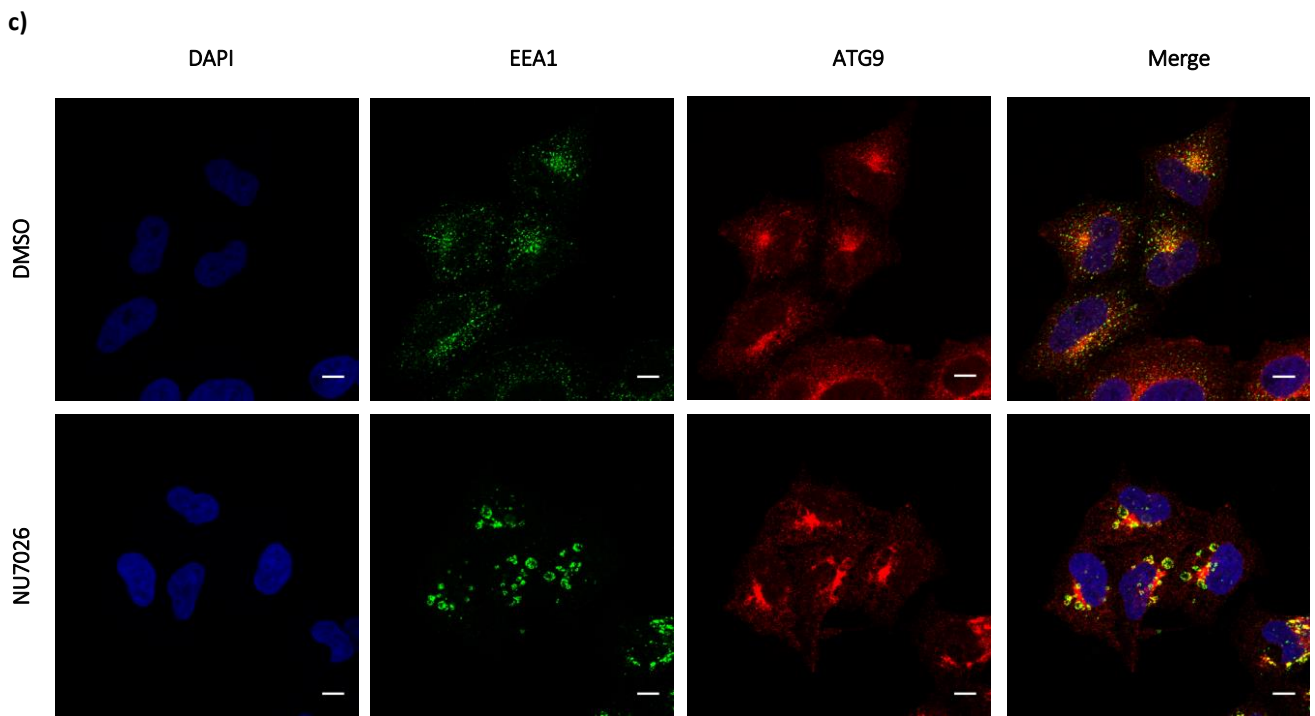
Fig 3.5: a) Representative western blot showing the dose dependent effect of the PRKDC inhibitor, NU7026, on LC3-II levels. HeLa cells were treated with either 25, 50 or 100 µM of NU7026 for 1 hour with DMSO as control. The cell lysates were collected and the proteins were separated using SDS-PAGE. **b)** Levels of protein were quantified with tubulin as loading control using the LICOR-imaging software and the ratio of LC3-II to tubulin was plotted. The graph lacks error bars since the experiment was only performed once due to the non-specific inhibition of PRKDC by the NU7026 inhibitor at higher concentrations. **c)** Representative immunofluorescence images showing the effect of NU7026 on EEA1 and ATG9 localisation in HeLa cells. HeLa cells were treated with 100 µM NU7026 and DMSO as control for 1 hour and labelled with antibodies against endogenous EEA1 and ATG9. The scale bar represents a distance of 10 µm.

This led me to try generating a PRKDC CRISPR knockout cell line. However, the knockout of the gene was lethal and no knockouts survived. This is consistent with the observation of high cell death on PRKDC knockdown indicating that the cell death was probably a result of higher knockdown levels of PRKDC, since it's an essential kinase for cell survival. Owing to the lack of viable strategies for PRKDC depletion and mutant screening, the project was not pursued any further.

To summarise, the results in this chapter show that mammalian ATG9 is phosphorylated on multiple serine residues. A few of these sites were found to be specifically phosphorylated upon starvation and trehalose treatment. It was also observed that mutating the sites to generate phospho-mimetic and non-phosphorylatable mutants resulted in affecting the stability/turn-over rate of the mutant ATG9 in the cells, indicating a potential regulatory role for some of these sites on protein stability. The Scansite and mass spectrometry results hinted towards PRKDC as a putative kinase and an interacting partner of ATG9. This interaction was then confirmed using immunoprecipitation and proximity ligation experiments. Furthermore, PRKDC knockdown showed a small non-significant increase in LC3-II level compared to control, potentially indicating that it might be a blocker of autophagy. This however could not be confirmed, since higher levels of PRKDC knockdown resulted in cell death, also resulting in the generation of PRKDC CRISPR cell line strategy non-viable. Moreover, the working PRKDC inhibitor concentration in HeLa cells was found to be in a range where its effects were non-specific and therefore, as mentioned above, this project was not pursue any further. However, this project led me to generate ATG9 CRISPR knockout cell line, which as a result helped me identify an important phenotypic anomaly in autophagy-impaired cells. The detailed characterisation of the ATG9 knockout cell line together with the observed phenotype has been described in depth the next two chapters of this thesis.

4. Characterisation of the ATG9 CRISPR knockout cell line

To study the role of site-specific ATG9 phosphorylation in its trafficking and function (as described in chapter 3 of this thesis), I needed to test the generated phospho-mimetic and non-phosphorylatable mutants of ATG9 in an endogenous ATG9-null background. Therefore, I aimed towards generating a ATG9 knockout cell line using the CRISPR gene editing technique.

The CRISPR-mediated gene editing has been established as a powerful and precise genome-engineering technique in the recent years. The technique, originally identified as a part of the microbial adaptive immune system, was modified and adapted to edit mammalian genomes using target sequence-specific RNA (Hsu et al., 2013). The CRISPR gene-knockout strategy involves the recognition of target sequence by a single-guide RNA (sgRNA) molecule, which results in the cleavage of target sequence. This process is mediated by the RNA-guided nuclease Cas9 which introduces a double-stranded break (DSB) in the target genome-sequence. The introduction of a DSB results in the activation of the DNA-damage repair pathways that introduce mutations such as insertion-deletion(s), frameshift or insertion of premature stop codons, thereby facilitating a desired genetic-knockout (Hsu et al., 2013; Ran et al., 2013). To obtain a genetic knockout of the endogenous ATG9 gene in HeLa cells, I therefore, transfected the wild-type cells with a construct designed to express sgRNA against the ATG9 gene. I then selected the transfected cells by adding puromycin to the growth medium. I further trypsinised the antibiotic-selected cells and serially diluted them in a 96-well plate in a fashion that maximises the likelihood of each well of the plate to consist of a single cell at the end of serial dilution procedure. These cells were then allowed to attach to the substrate and grow for 24-48 hours to form a distinct colony. The wells with a single colony, which arose from a single cell were marked and the selected colonies were then tested for the knockout of ATG9. Following this protocol, I was able to obtain 2 pairs of ATG9 wild-type and knockout single-cell derived clonal populations that were negative for endogenous ATG9 expression amongst the total of 25 pairs of colonies that were screened for ATG9 knockout. A detailed protocol of the process of the CRISPR-mediated ATG9 knockout cell line generation has been described in the Materials and methods - section 2.17 of this thesis for more information.

This chapter will now describe the observed results of the characterisation of the generated ATG9 wild-type and knockout HeLa cells.

4.1. ATG9 knockout cells show impaired autophagy and abnormally large LC3 puncta

The 2 clonal pairs of ATG9 wild-type and knockout cells amongst the total of 25 clonal pair of cells were selected by checking for the expression of ATG9 on a western blot using an antibody developed against the human endogenous ATG9 protein. The selected clonal pairs were then tested for autophagic function, using a standard autophagy assay which relies on checking the levels of LC3-I and LC3-II in the presence and absence of the lysosomal pH inhibitor, BafilomycinA1 (BAF) (that blocks LC3-II clearance by blocking autophagosome-lysosome fusion, Fig 1.1 b). The LC3-I and LC3-II levels for each pair were then quantified separately relative to the levels of the loading control, tubulin and the data was plotted in the form of a histogram to visualise the difference in the levels of LC3-I and LC3-II. Both ATG9 knockout cell lines, which were a part of the two identified ATG9 wild-type and knockout cells clonal pairs, were seen to behave in a similar fashion and showed an impaired autophagic response compared to their respective wild-type control cells (Fig 4.1 b, c, e and f). Interestingly, both of these ATG9-knockout cell lines did not respond to BAF treatment, which was seen as the levels of LC3-II remained unchanged upon treating the cells with BAF for 4 hours (Fig 4.1 b, c, e and f). It is worth noting at this point that the two ATG9 knockout cells of each clonal pair also show significantly higher levels of LC3-I compared to their respective controls, the significance of which has been explored in further details in chapter 5 of this thesis (Fig 4.1 d and g). Upon closer examination, it was seen that the clonal pair 2 of the ATG9 wild-type and knockout cells showed a relatively lower difference in LC3-levels accompanied with an unclear response related to autophagic impairment compared to the clonal pair 1. Therefore, to maximise the chances of seeing a real difference in phenotype and the effects of ATG9 knockout, all the experiments from this point henceforth were exclusively performed using the clonal pair 1 of the ATG9 wild-type and knockout cells. Interestingly, upon further investigation it was seen that these ATG9 knockout cells not only show an impaired autophagic response and higher levels of LC3-I, but also showed the presence of fewer but larger LC3 puncta compared to control cells, which were identified upon immunostaining of these cells using an antibody against LC3 which recognises both LC3-I and LC3-II forms of the protein (Fig 4.1 h, i and j).

To confirm that the effects seen on the LC3-I and LC3-II levels on a western blot were specifically a result of the lack of ATG9 expression in the knockout cells, I tried to rescue the observed phenotype using ATG9-GFP. Therefore, I overexpressed empty-pEGFP and ATG9-GFP in ATG9 knockout cells and showed that the LC3-I and LC3-II levels can be successfully rescued in cells upon ATG9-GFP but not empty-pEGFP overexpression (Fig 4.2 a and b). To further confirm impaired autophagy in these cells, clearance of overexpressed GFP-tagged exon-1 of huntingtin with 72 CAG repeats (EGFP-Q74) (a mutant form of huntingtin associated with Huntington's disease and an accepted autophagic cargo) was tested in clonal pair of control and ATG9 knockout cells. It was observed that there was excessive aggregate accumulation in ATG9 KO cells compared to control cells (Fig 4.2 c).
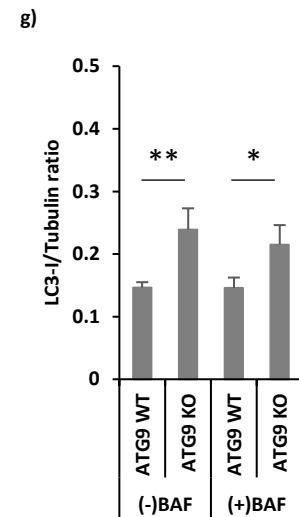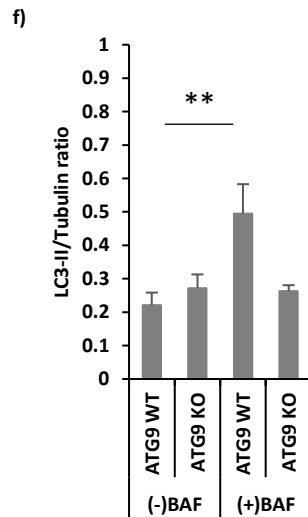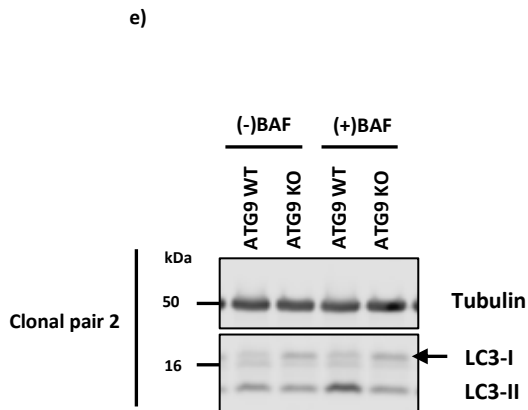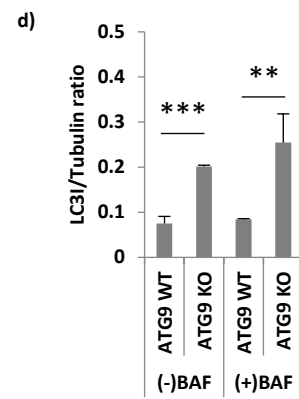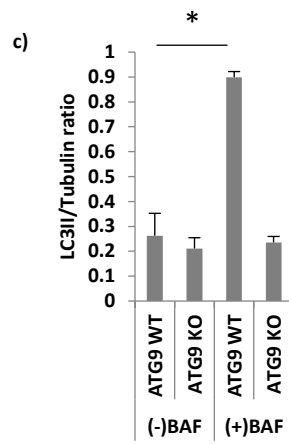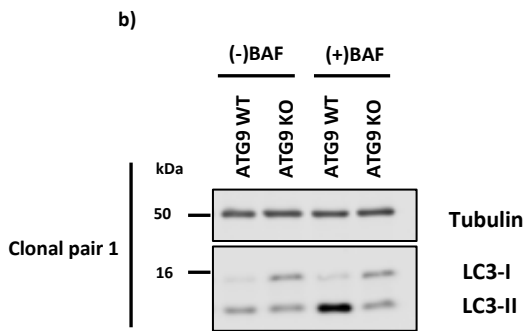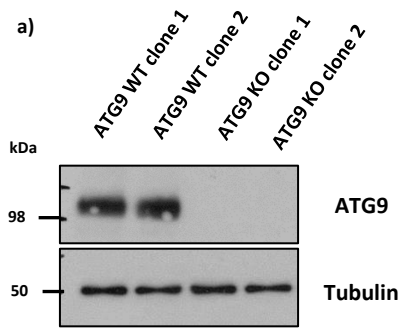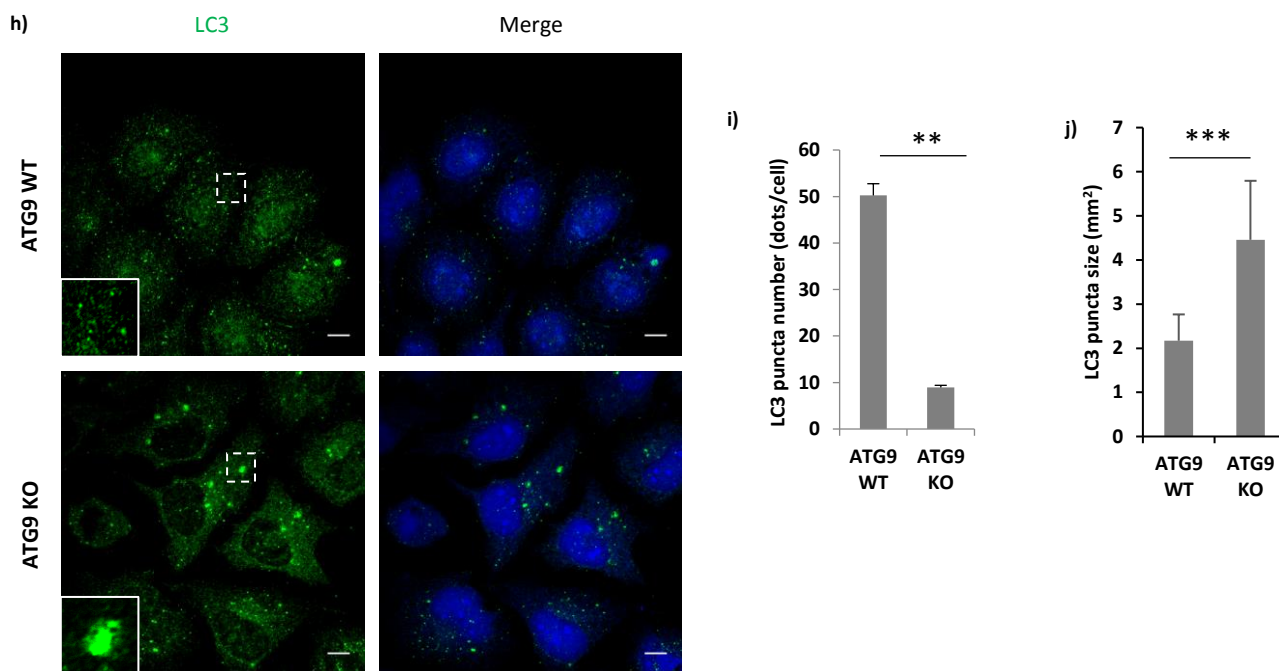
Fig 4.1 a) Representative western blot showing the efficiency of the CRISPR knockout cells by immunoblotting for the levels of endogenous ATG9 in the CRISPR knockout clones and their corresponding wild-type (control) cells (clonal pairs). 2 out of 25 screened cell lines lacking endogenous ATG9 expression were successfully generated using the CRISPR technique and these knockout cell lines together with their respective wild-type (control) cells have been labelled as clonal pair 1 and clonal pair 2. **b)** A representative western blot showing the levels of the two LC3 isoforms in ATG9 wild-type (control) and knockout cells of the clonal pair 1. **c)** Quantification of the intensities of the LC3-II bands for the clonal pair 1, observed in panel b) of this figure, was performed using the LICOR-imaging software. The LC3-II values were then plotted against the values of the loading control, tubulin. The data is from the quantification of three experiments performed in triplicates and the error bars represent the standard error of the mean (SEM). **d)** Quantification of the intensities of LC3-I bands for the clonal pair 1, observed in panel b) of this figure, was also performed using the LICOR-imaging software. The LC3-I values were then plotted against the values of the loading control, tubulin. The data represents the quantification of three experiments performed in triplicates and the error bars represent SEM (* = $p < 0.05$, ** = $p < 0.01$, *** = $p < 0.001$). **e)** A representative western blot showing the levels of the two LC3 isoforms in ATG9 wild-type (control) and knockout cells of clonal pair 2. **f)** Quantification of the intensities of the LC3-II bands for the clonal pair 2, observed in panel e) of this figure, was performed using the LICOR-imaging software. The LC3-II values were then plotted against the values of the loading control, tubulin. The data is from the quantification of three experiments performed in triplicates and the error bars represent the standard error of the mean (SEM). **g)** Quantification of the intensities of LC3-I bands for the clonal pair 2, observed in panel e) of this figure, was also performed using the LICOR-imaging software. The LC3-I values were then plotted against the values of the loading control, tubulin. The data represents the quantification of three experiments performed in triplicates and the error bars represent SEM (* = $p < 0.05$, ** = $p < 0.01$, *** = $p < 0.001$). It is worth noting that both clonal pairs of ATG9 wild-type and knockout cells i.e. 1 and 2, show similar effects on the levels of LC3-I and LC3-II

on the western blots, however, since the effect of ATG9 knockout in the clonal pair 1 was much clearer, it was selected for all the future experiments. **h)** Representative immunofluorescence images showing LC3 puncta staining in ATG9 control and knockout cells (clonal pair 1). ATG9 control and knockout cells were fixed and labelled for endogenous LC3 with an antibody that recognises both the forms of LC3. **i), j)** The quantification of the LC3 puncta size and number of the images shown in h) was performed using ImageJ quantification tool (** = $p < 0.01$, *** = $p < 0.001$). The quantification data represents the puncta size and number generated from the population after excluding the background (very small puncta) by setting a threshold value of 0.0009 as a cut-off size for puncta recognition. Quantification was performed based on the results from 3 experiments with more than 25 cells quantified per experiment per condition. The error bars represent standard deviation (SD).
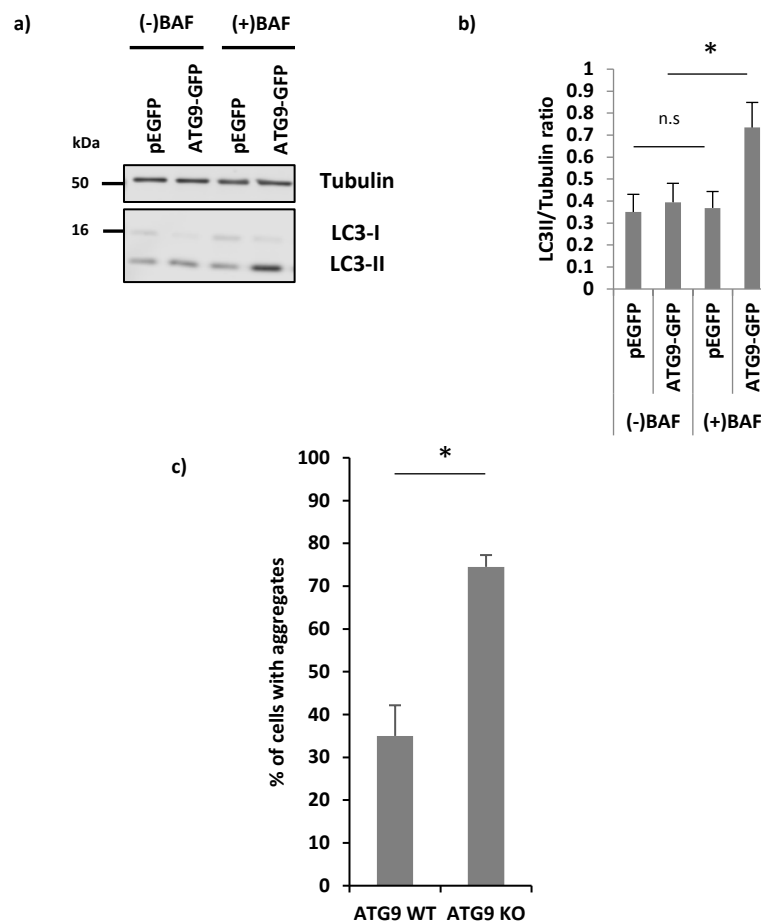
Fig 4.2 a) A representative western blot depicting the levels of LC3-I and LC3-II upon rescue of the selected ATG9 knockout cells using ATG9-GFP construct in the absence and presence of BAF. **b)** Quantification of the LC3-II levels of the control and knockout cells, as seen in panel a) of this figure, was performed using the LICOR-imaging software (* = $p < 0.05$, n.s. = non-significant). The data represents the quantification performed from three independent experiments performed in triplicates and the error bars represent SEM. **c)** Graph showing the difference in the percentage of cells with Q74-GFP aggregates between ATG9 wild-type and knockout cells (* = $p < 0.05$). The data has been obtained from the quantification of two experiments performed in triplicates and the error bars represent SEM.

4.2. ATG9 knockout cells show lower number of PI3P and WIPI2 puncta

As described in the last section, ATG9 knockout cells show impaired autophagy as observed using the standard LC3-II western blot assay. However, another way of confirming the autophagic response in cells relies on the quantification of the PI3P puncta formation in response to starvation conditions, as increased PI3P synthesis correlates with autophagosome formation and is an important marker of growing autophagosomes. It is known that PI3P generation leads to recruitment of WIPI-family of proteins like WIPI2 and further studies have shown that WIPI2 assists in the recruitment of the ATG5-ATG12-ATG16 complex. This complex was then shown to dictate the site of LC3 lipidation (Bento et al., 2016b; Dooley et al., 2014; Vicinanza et al., 2015).

My results show that the ATG9 knockout cells of the clonal pair show less generation of PI3P-positive structures compared to the respective control cells under both basal and starvation conditions (Fig 4.3 a and b). However, an observed increase in the starvation induced PI3P puncta formation in ATG9 knockout cells possibly hints that the general population of PI3P-positive puncta do not represent a population of functional autophagosomes and hence, this might not be an autophagy-specific assay. It could also indicate that contrary to the existing hypothesis in the field, ATG9 perhaps does not play a very important role in starvation-induced autophagy in HeLa cells. To therefore consolidate the relevance of decrease in PI3P puncta formation on functional autophagy levels in the ATG9 knockout cells, the effect of starvation on WIPI2 puncta formation was tested. While changes in the levels of PI3P synthesis could be an effect of perturbations of various cellular processes, reduction in the levels of WIPI2 puncta formation is a direct indicator of LC3 lipidation and therefore, autophagy. Interestingly, the WIPI2 puncta formation in ATG9 knockout cells upon autophagic stimulation by starvation was also seen to be significantly impaired compared to the control cells of the pair (Fig 4.3 c and d).

4.3. The LC3 puncta in ATG9 knockout cells co-localise with p62

To test whether the abnormally large LC3-positive puncta were a result of defective trafficking or increased binding affinity of LC3 with proteins/organelles involved in endocytic trafficking, I checked the co-localisation of these LC3-positive puncta with the endosomal markers known

to play a role in the trafficking of important autophagy proteins. For instance, the co-localisation of LC3 puncta with RAB5 and RAB11 was checked, since ATG9 and ATG16 were shown to meet at recycling endosomes (Puri et al., 2013); and recycling endosomes have been also proposed to be a primary platform for autophagosome formation (Puri et al., 2018). The co-localisation of these LC3 puncta was also checked with syntaxin-17, since perturbations in the levels of SNX17 was shown to result in accumulation of LC3-positive structures (Hegedűs et al., 2013). In addition, the co-localisation of these puncta was also checked with p62 to understand if these puncta were simply aggregates. The co-localisation between 2 markers was confirmed by visualising the pixels that co-localise in two different fluorescence signal channels. These co-localisation pixels were identified and a profile was generated and visualised using an unsupervised ImageJ plugin algorithm called 'colocalization', which was developed by Pierre Bourdoncle (Institut Jacques Monod, Service Imagerie, Paris; 2003-2004). The algorithm allows manual thresholding of the acquired images, facilitating the elimination of background noise based on pixel intensities of different channels. The threshold for the pixel intensities can be adjusted within range of 0-255 and two pixels above threshold value are considered to be co-localised if their ratio of intensity is higher than the set value, which was set to the default value of 50%. The algorithm finally generates a profile with grey pixels representing exclusive co-localisation between the two markers. It was observed that while the LC3-positive puncta show no specific co-localisation with any endosomal markers or STX17, these puncta however showed a near complete co-localisation with p62 (Fig 4.4). This was a very interesting observation and its significance will be described in further details in chapter 5 of this thesis.
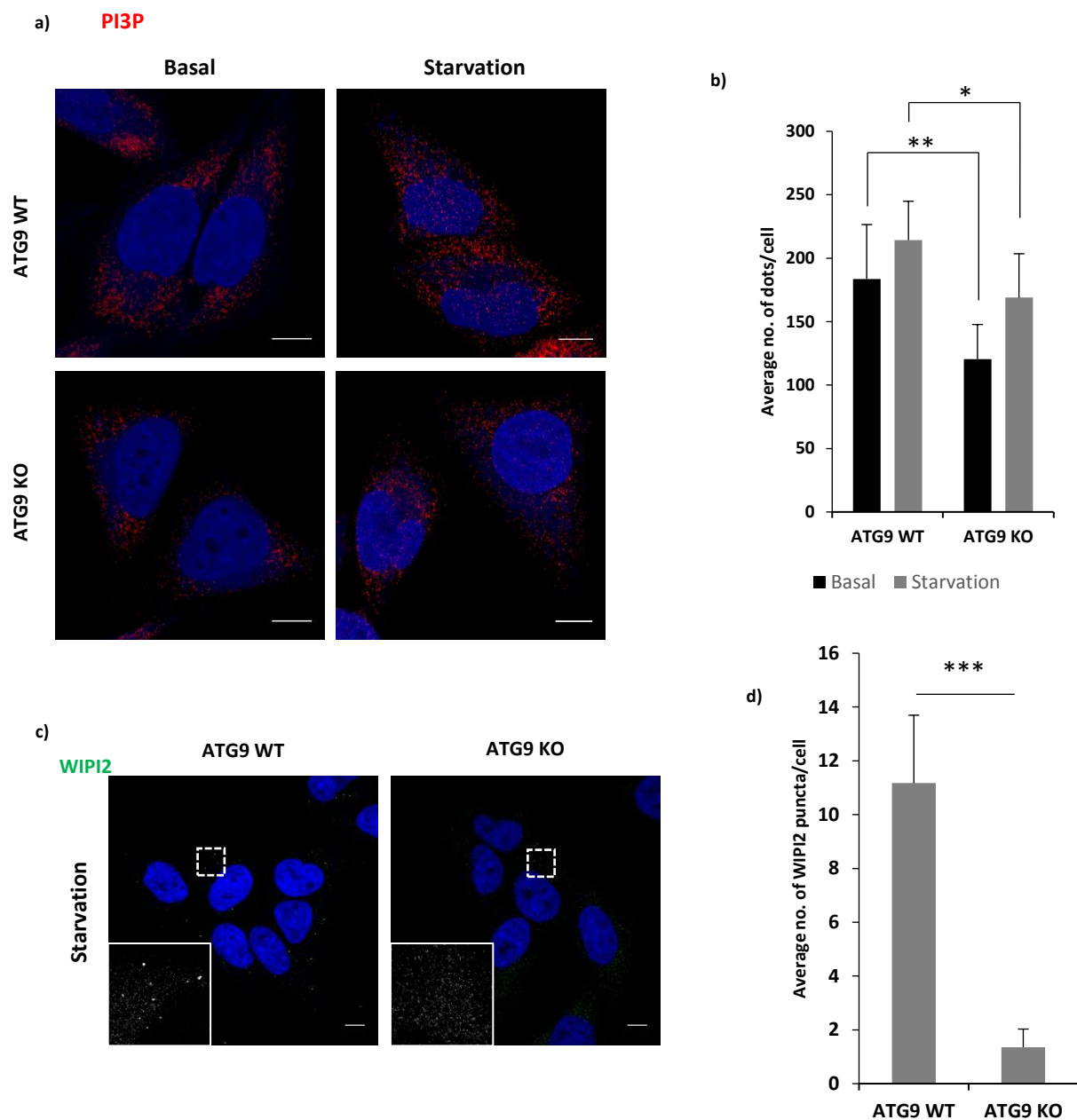
Fig 4**.3 a)** Representative immunofluorescence images showing PI3P staining in representative ATG9 wild-type and knockout cells under basal and starvation conditions. **b)** Quantification of the number of PI3P puncta from the images shown in panel a) performed using the ImageJ quantification tool software (* = p < 0.05, ** = p < 0.01). The quantification was performed on the data from 3 independent experiments with at least 25 cells quantified for per experiment per condition. The error bars represent the standard deviation (SD). **c)** Representative immunofluorescence images showing WIPI2 staining in representative ATG9 wild-type and knockout cells under starvation conditions. It is important to consider that the WIPI2 puncta are only visible upon starvation. **d)** The quantification of the number of WIPI2 puncta from the images shown in panel c) was performed using the ImageJ quantification tool software (*** = p < 0.001). Quantification performed from the data from 3 independent experiments with at least 25 cells quantified for each condition. The error bars represent standard deviation (SD) and the scale bars represent a distance of 10µm.

4.4.   ATG9 knockout cells show lower protein synthesis and RavZ mimics the LC3 phenotype in wild-type cells

To identify whether the decrease in the observed levels of LC3 due to defective autophagy was also being affected due to an overall reduction in protein synthesis, I performed a Click-IT® chemical assay to check the levels of newly synthesised proteins in the ATG9 wild-type and knockout cells. The Click-IT® assay is a non-radioactive assay based on the principle of a pulse-chase assay, therefore capable of labelling freshly synthesised proteins. These proteins can then be isolated and detected using SDS-PAGE. I observed that the ATG9 knockout cells showed a massive reduction in the protein synthesis levels of LC3-I and LC3-II compared to control cells (Fig 4.5 a and b).

To further understand whether the observed phenotype in ATG9 null cells (as previously shown in Fig 4.1) is a result of LC3-I accumulation together with impaired autophagy, I tried to mimic this effect in control cells using RavZ overexpression. RavZ is a bacterial effector protein, produced by *Legionella pneumophila*, which was shown to inhibit autophagy. More specifically, this protein was shown to catalyse the hydrolysation of the amide bond between C-terminal glycine and an adjacent aromatic amino acid residue in LC3, producing a version that is non-conjugatable thereby inhibiting autophagy (Choy et al., 2012). On overexpression of GFP-RavZ in HeLa cells, I observed that the LC3 puncta staining resembled the phenotype observed in ATG9 knockout cells (Fig 4.5 c). Consistent with the identified mechanism of RavZ activity, it was observed that cells expressing RavZ-GFP showed impairment of autophagy together with a distinct increase in the levels of LC3-I on western blot (Fig 4.5 d).

ATG9 knockout cells
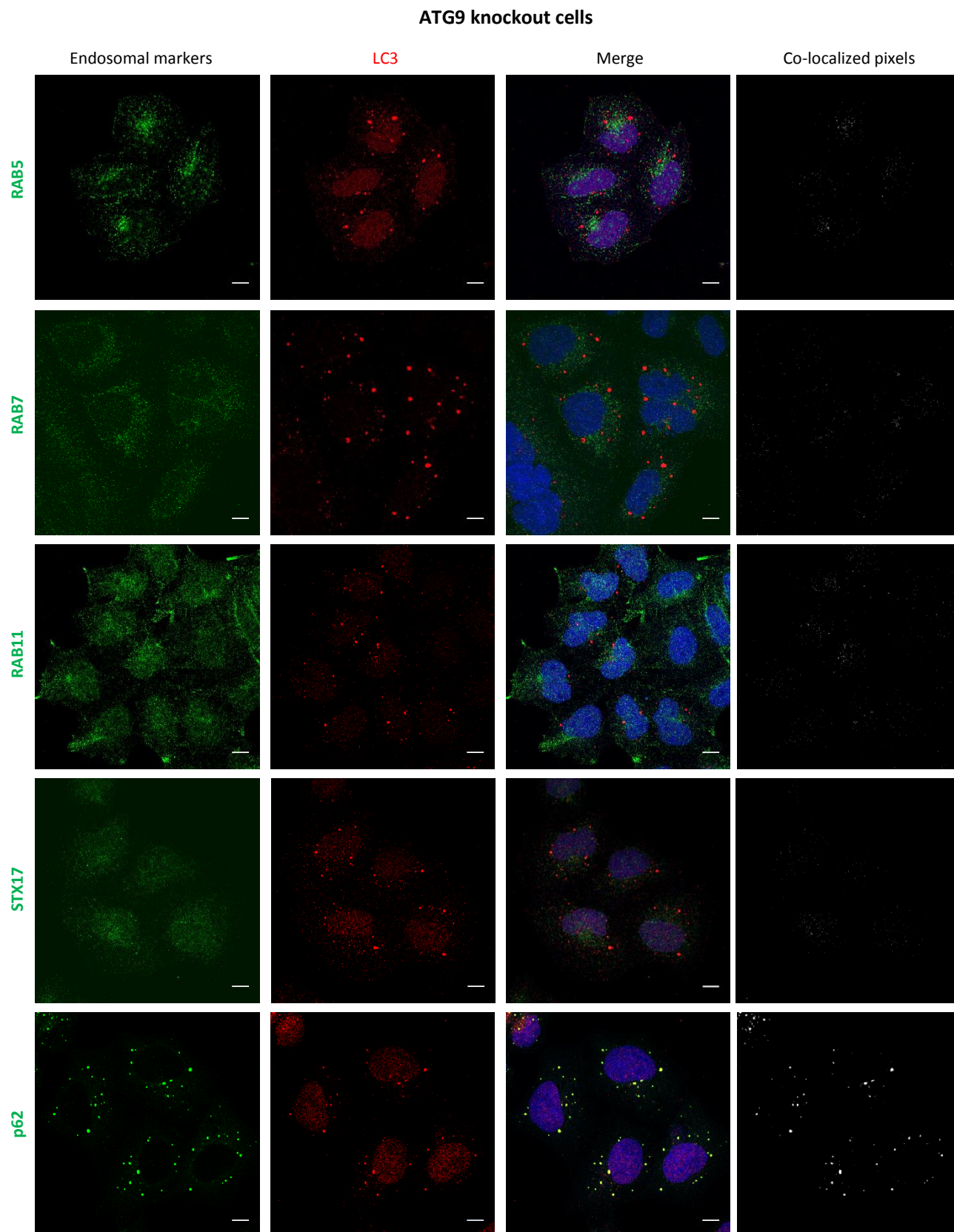
Fig 4.4 Representative immunofluorescence images showing the co-localisation of LC3 puncta with various endosomal markers, syntaxin-17 and p62 in representative ATG9 knockout cells using co-localisation profile generation. The co-localisation pixels were identified and a profile was generated using an unsupervised ImageJ

70

plugin algorithm called colocalization, which was developed by Pierre Bourdoncle (Institut Jacques Monod, Service Imagerie, Paris; 2003-2004). The algorithm allows manual thresholding of the acquired images that facilitates the elimination of background noise based on pixel intensities of different channels to generate a profile with grey pixels representing co-localisation of the markers. Briefly, the cells were fixed with PFA and labelled for endogenous LC3 which recognises both forms of LC3 viz. LC3-I and LC3-II together with antibodies against small molecule GTPase effectors which act as conventional markers for respective endosomal compartments such as RAB5 for early endosomes, RAB7 for late endosomes and RAB11 for recycling endosomes. The co-localisation between the LC3 puncta was also tested against the SNARE-protein STX17, that was identified to play a role in autophagosome-lysosome fusion. Finally, the co-localisation was tested between LC3 and the common autophagy receptor, p62 in the knockout cells which show impaired autophagy. The co-localisation between the different marker pairs was then visualised by looking at the grey pixels in the co-localisation pixels panel. As mentioned above, the grey pixels represent the identified pixels above threshold that are present in both green and red channels and therefore, represents co-localisation between the used markers. The scale bars in the images represent a distance of 10µm.
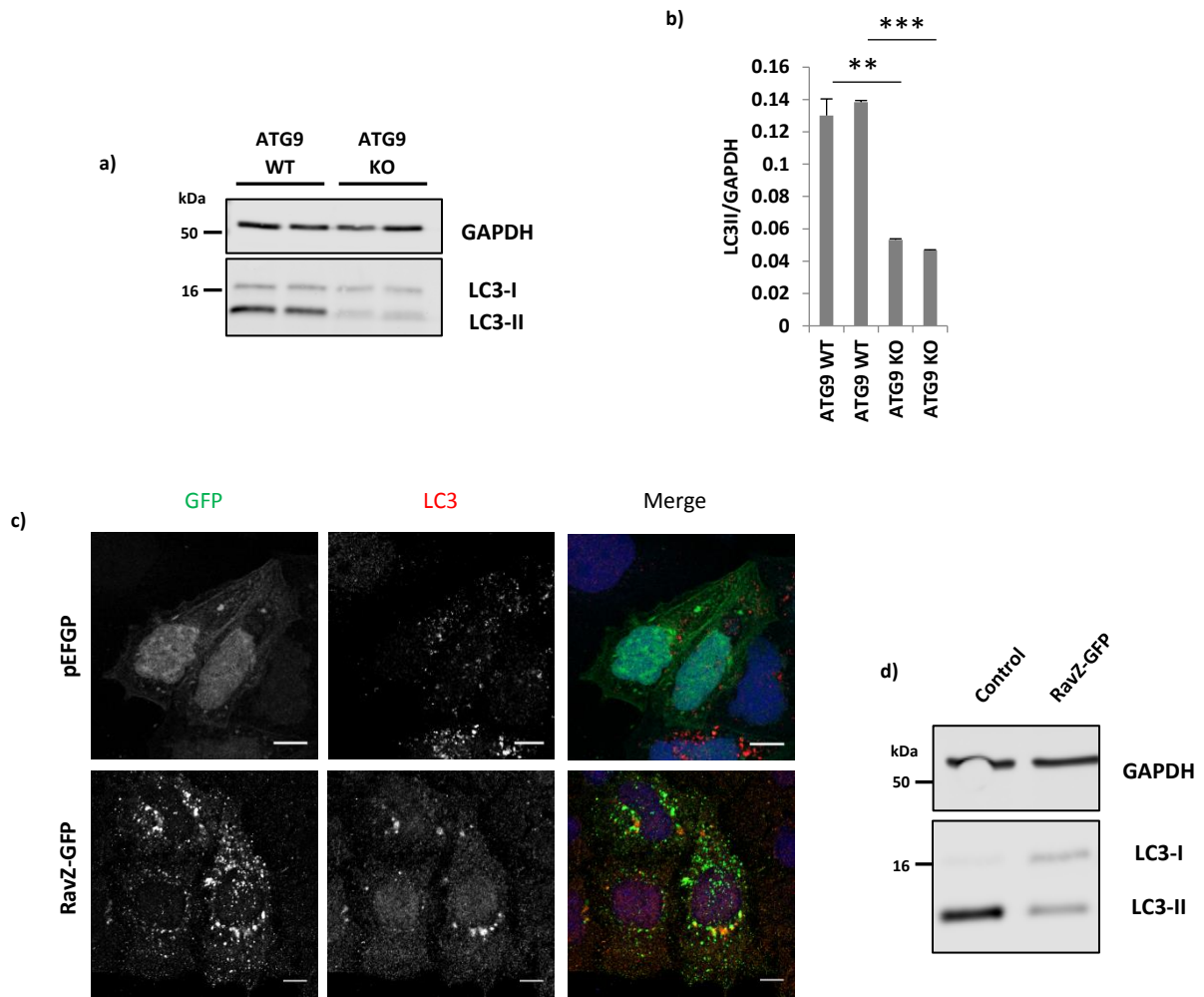
Fig 4.5 a) A representative western blot depicting the levels of LC3-I and LC3-II protein synthesis in ATG9 wild-type and knockout cells. GAPDH was immunoblotted to be used as a loading marker for quantification. **b)** The quantification of the blot was then performed using the LICOR-imaging software. The data represents the quantification from two experiments performed in duplicates and the error bars represent SEM (** = p < 0.01, *** = p < 0.001). **c)** Representative immunofluorescence images showing the effect of overexpression of empty-pEGFP or GFP-RavZ on LC3 staining in representative wild-type HeLa cells. **d)** A representative western blot showing the effect of empty-pEGFP or GFP-RavZ overexpression on LC3-I and LC3-II levels in HeLa cells. GAPDH was immunoblotted to be used as a loading control. RavZ was shown to inhibit autophagy via the hydrolysation of the amide bond between C-terminal glycine and an adjacent aromatic amino acid residue in LC3 producing non-conjugatable LC3-I molecules. The experiment was performed twice in duplicates. The scale bars represent a distance of 10µm.

To summarise, the ATG9 knockout cells showed an impaired autophagic process corresponding to their wild-type partners. Moreover, these ATG9 knockout cells also showed a distinct lack of an autophagic response upon BAF treatment, which is known to result in an accumulation of LC3-II in the wild-type cells. Furthermore, these knockout cells showed much higher levels of LC3-I compared to control cells. More interestingly, the lower levels of LC3 in the knockout cells corresponded to an increase in the LC3 puncta size and a decrease in the number of LC3 puncta, upon visualisation using immunofluorescence, compared to wild-type cells. This phenotype was then seen to be mimicked in wild-type HeLa cells by overexpression of the *Legionella* protein RavZ, which results in generation of non-conjugatable form of LC3 similar to LC3-I. This, therefore, indicates that the abnormal LC3-puncta phenotype observed in ATG9 knockout cells using immunofluorescence is related to the corresponding higher levels of LC3-I in knockout cells upon western blotting of the cell-lysates. Moreover, the abnormal levels of LC3 and lack of BAF response observed in ATG9 knockout cells was seen to be rescued by overexpression of ATG9-GFP and not empty-pEGFP. Consistent with the observation of impaired autophagy in ATG9 knockout cells, these cells also showed lower levels of PI3P and much lower levels of WIPI2 puncta formation upon starvation. Finally, the aberrant LC3 puncta observed in the ATG9 knockout cells were seen to not co-localise with any conventional endosomal markers such as RAB5, RAB7 and RAB11 but were seen to co-localise almost completely with p62.

5. LC3-I associates with p62 in autophagy-impaired cells

The ubiquitinated cargoes destined for degradation by autophagy have been shown to bind to p62 cargo receptor via the UBA-domain. p62 also binds to both forms of LC3, with a preference for LC3-II upon autophagic stimulation, using the LIR domain to help the engulfment of the cargo into the growing autophagosomes and its subsequent degradation (Ciuffa et al., 2015; Gao et al., 2013; Ichimura, 2008; Moscat and Diaz-Meco, 2009; Pankiv et al., 2007; Zaffagnini et al., 2018). The completed autophagosomes appear as punctate structures in cells when visualised using LC3-II as the marker. However, my results in this chapter show that ATG9-null and ATG16-null cells (i.e. autophagy-impaired cells) are capable of forming LC3-positive structures. Interestingly, these structures are also p62 and ubiquitin positive. It has been shown that p62 forms inclusion bodies in autophagy-deficient mice and these structures were also shown to be positive for ubiquitin (Komatsu et al., 2007). A different study has also shown that the p62 aggregates sequestered the E1-like ATG7 enzyme into these aggregates. It also showed that this sequestration is mediated via the interaction of LC3-I with ATG7 and that while p62 shows preferential binding towards LC3-II, it is indeed capable of binding to the lipidation defective LC3-G120A mutant (Gao et al., 2013). My results thereby confirm this observation that LC3-I can form a complex with p62 under autophagy-impaired conditions such as those that exist in ATG9- and ATG16-knockout cells. Therefore, results from experiments involving autophagy-impaired cells should be carefully assessed to avoid confusion of considering LC3-I positive structures as mature autophagosomes.

5.1. Autophagy-impaired cells show aberrant LC3-positive puncta

As mentioned in the ATG9 knockout cells characterisation chapter of this thesis, the ATG9 knockout cells showed lower levels of LC3-II compared to control cells (Fig 4.1 b and c). This led me to check the morphology and number of the LC3-II puncta in these cells. Interestingly, the LC3-II puncta formed in these cells were much bigger and fewer in number compared to control cells (Fig 5.1 a, b and c). However, more interestingly, the ATG9 knockout cells also showed very high levels of LC3-I compared to control cells (Fig 4.1 b and d). I tried to confirm this observation using immunofluorescence, however, the overall cytosolic staining representing LC3-I did not change in ATG9 knockout cells (Fig 5.1 a). This, therefore, hints towards LC3-I existing in a form other than the conventional cytosolic form.

To confirm this hypothesis, I checked the LC3 staining pattern in ATG16 knockout cells, which were generated, validated and published in a study from the Rubinsztein laboratory (Fig 5.1 e) (Bento et al., 2016a). These cells only possess LC3-I and completely lack the presence of LC3-II, due to a defect in the common lipidation process that requires ATG16 expression and are therefore autophagy-impaired. Based on the conventional view, I expected to observe no puncta formation due to defective LC3 lipidation and only cytosolic staining for LC3-I. However, contrary to my expectations the ATG16 knockout cells showed presence of rather large and distinct LC3-positive structures (that are LC3-I). These LC3-I structures did not seem to accumulate or change when the cells were treated with compounds that inhibit autophagic flux like BAF and ammonium chloride (NH_4Cl) (Fig 5.1 d).

To confirm that this observation was not an artefactual, the LC3 staining in these cells was tested using 2 different antibodies obtained from Abcam® and NanoTools. These antibodies require different fixation of the samples. The rabbit Abcam® antibody requires 4% PFA fixation while the mouse NanoTools antibody requires the cold-methanol fixation of the cells. Regardless of the antibody however, the observation of large LC3-positive structures in the autophagy-impaired cells was found to be consistent (Fig 5.1 f). However, since PFA fixation was more suitable for the staining of the other antibodies used in various experiments throughout the study, the rabbit Abcam® antibody was the primarily used antibody across this thesis unless mentioned otherwise.

f)

LC3 (Nanotools) **LC3 (Abcam®)**

ATG16 control

ATG16 KO

Methanol fixation Paraformaldehyde fixation
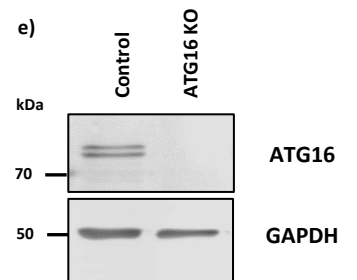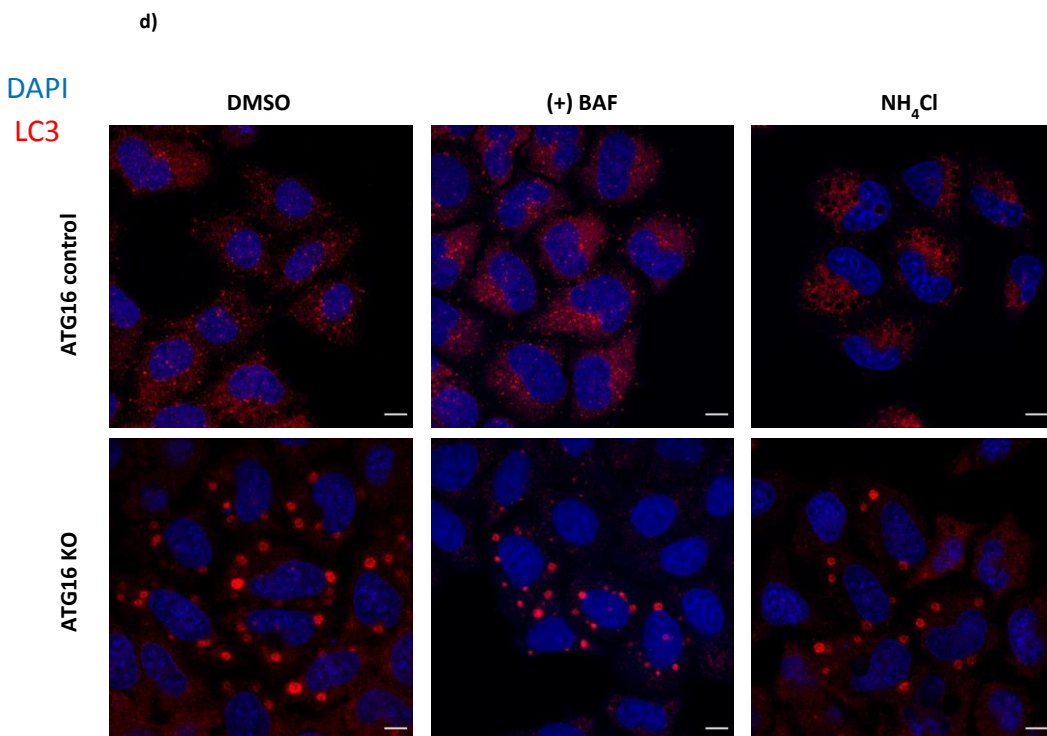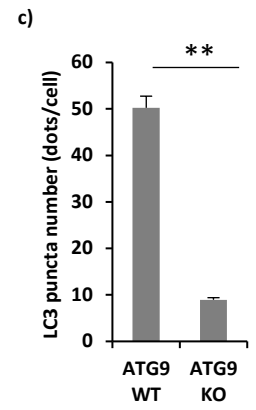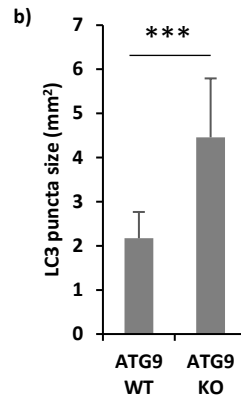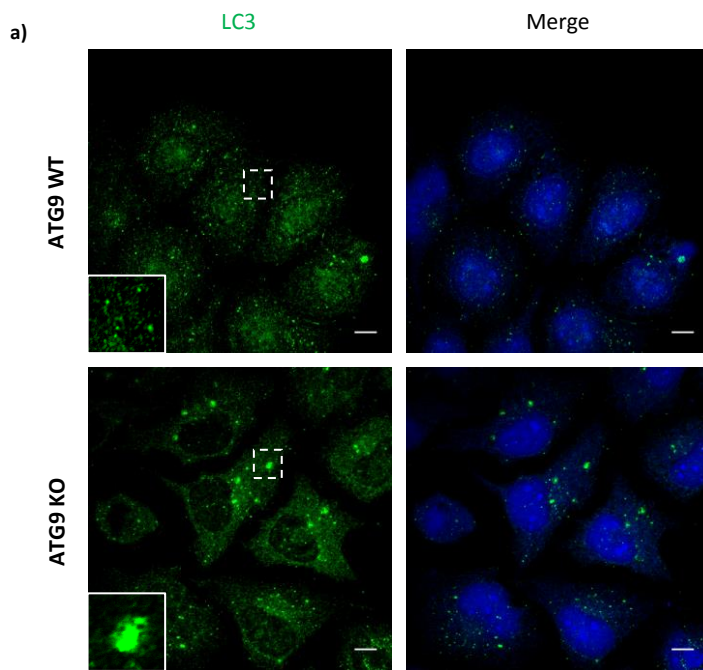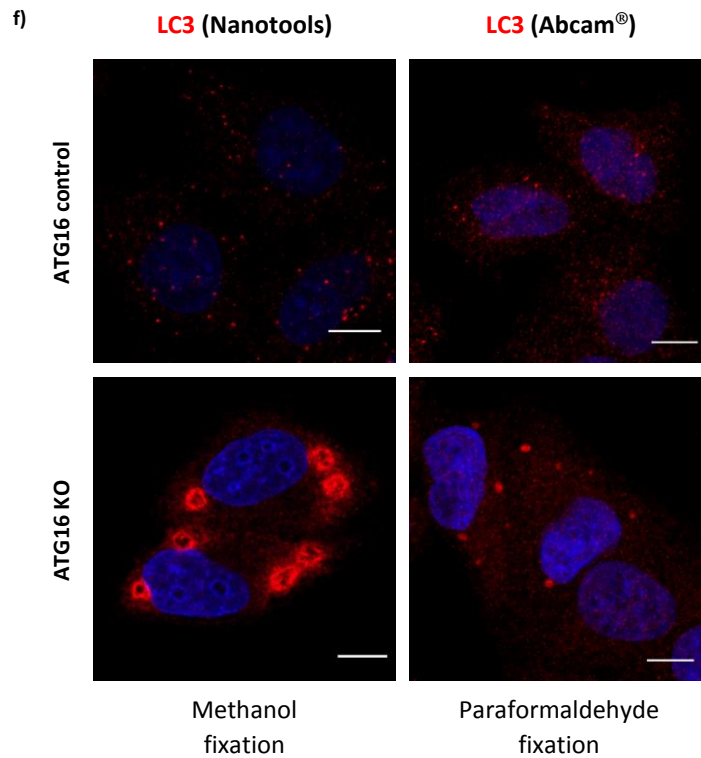
Fig 5.1: a) Representative immunofluorescence images showing LC3 staining in representative ATG9 control and knockout cells. ATG9 control and knockout cells were fixed and labelled for endogenous LC3. **b), c)** Quantification of the LC3 puncta size and number of the images in a) performed using ImageJ quantification tool (** = $p < 0.01$, *** = $p < 0.001$). Quantification performed from 3 experiments with at least 25 cells quantified for each condition. The error bars represent standard deviation (SD). **d)** Representative immunofluorescence images showing LC3 staining in representative ATG16 control and knockout cells. Cells were fixed with methanol and labelled for endogenous LC3. Please note that the antibody against LC3 used here is a mouse monoclonal antibody from Novus Biologicals and needs methanol fixation of the samples. **e)** Representative western blot showing the ATG16 expression levels in ATG16 CRISPR knockout cells used for throughout the studies in this thesis. **f)** Representative immunofluorescence images showing LC3 staining in representative ATG16 control and knockout cells using two different antibodies requiring different fixation conditions. The cells were fixed with either 4% PFA or cold-methanol (as per manufacturer's instructions) and labelled for endogenous LC3. The scale bar represents a distance of 10 µm.

5.2. Overexpression of mutant non-conjugatable forms of LC3 results in formation of distinct LC3 structures in autophagy-impaired cells

To confirm whether the observed endogenous-LC3 positive structures in autophagy-impaired cells were LC3-I structures, I overexpressed mutant non-conjugatable forms of LC3 such as GFP-LC3G120A and myc-LC3G120A-ΔC22 in control and autophagy-impaired cells. These mutants cannot be lipidated since the glycine residue located at 120th position has been mutated to alanine, hence the protein cannot be cleaved, activated and conjugated (Wang et al., 2013). After transfection, the cells were allowed to express mutant protein for 24 hours and the cells were then visualised for LC3 structures using the GFP signal or an antibody against the myc-tag (Fig 5.2 a, b and d). It was observed that these non-conjugatable forms of mutant LC3 forms structures that resemble the LC3 phenotype observed in autophagy-impaired cells as seen in Figs 5.1 a and d. It is worth noting that the staining of the LC3-positive structures formed in control cells is much lighter than ATG9 and ATG16 knockout cells is due to the lack of functional autophagy in the knockout cells. This also further confirms the hypothesis that LC3-I exists not simply in a cytosolic form. In addition, while these structures were observed to not co-localise with any of the conventional endosomal markers or lipid droplets, upon overexpression of RAB5-Q69L-GFP dominant-negative mutant in ATG16 knockout cells, the size of LC3-positive structures was observed to decrease (Fig 5.2 a, b, c, e and f and Fig 4.4).

5.3. LC3-I accumulates in autophagy-impaired cells and is associated with the membranous fraction

Since the observations seen above indicate towards a sub-population of LC3-I that exists in non-cytosolic form, I performed a membrane fractionation experiment to check if LC3-I is associated with the membranous fraction within the autophagy-impaired ATG9 and ATG16 knockout cells (Fig 5.3). The membrane fraction obtained using the protocol consists of the total membrane constituent of the cells excluding the nuclear membrane fraction. The purified membranous fraction was checked for purity using calnexin as a marker while tubulin was used as a marker to assess the purity of the cytosolic fraction. Interestingly, LC3-I was seen to be associated with the membranous fraction in both ATG16 knockout and ATG9 knockout cells. Furthermore, quantification of the normalised ratio of LC3-I/Calnexin, which indicates the association of LC3-I with the membrane fraction, in the ATG9 and ATG16 knockout cells

showed a statistically significant increase in the knockout cells compared to their respective control cells. In addition, the ATG16 knockout cells showed much lower LC3-II/Calnexin ratio compared to control cells and is consistent with the fact that these cells only consist of LC3-I (Fig 5.3). This result potentially indicates that LC3-I is being recruited to the membrane prior to its lipidation to LC3-II. It is also worth noting that the ATG9 knockout cells showed much higher overall LC3 levels than ATG9 control cells. But, the statistics for LC3-II/Calnexin for ATG9 knockout cells show the difference in the ratios to be non-significant due to high variance between repeats. A possible reason that might explain this is that ATG9 knockout cells possess a residual level of autophagy and therefore the LC3-II levels in these cells on a western blot represents a snapshot of the LC3-II association with membrane. This can be confusing and highly variable based on the stimuli that cells receive prior to lysis and/or the phase of the cell cycle the cells are in.

a)

| | GFP-LC3G120A | EEA1 | Merge |

ATG9 WT

ATG9 KO

b)

| | GFP-LC3G120A | EEA1 | Merge |

ATG16 WT

ATG16 KO

c)

| | Rab5Q79L-GFP | LC3 | Merge |

ATG16 WT
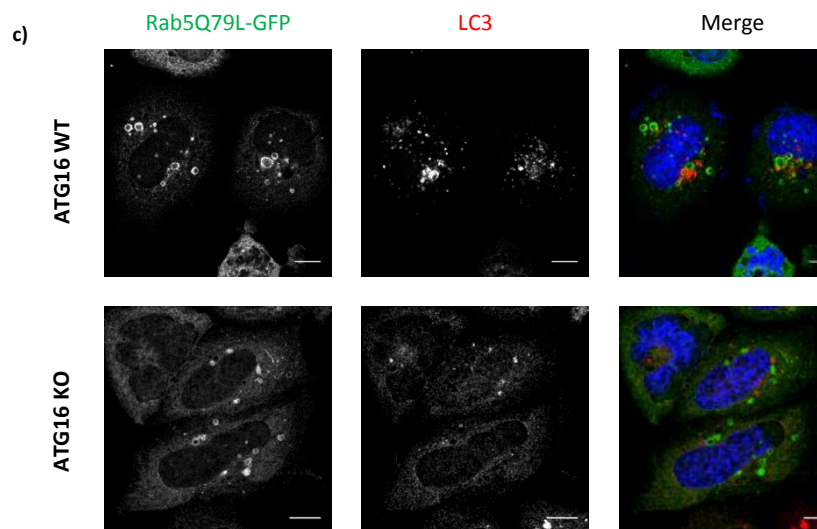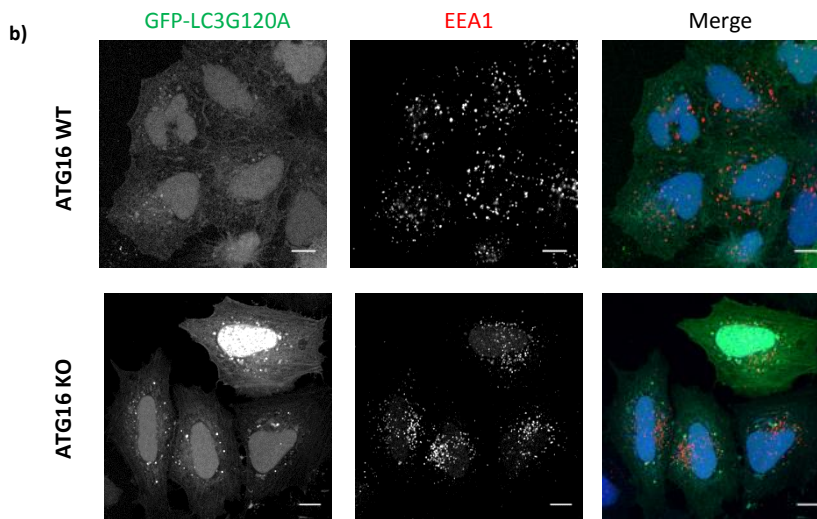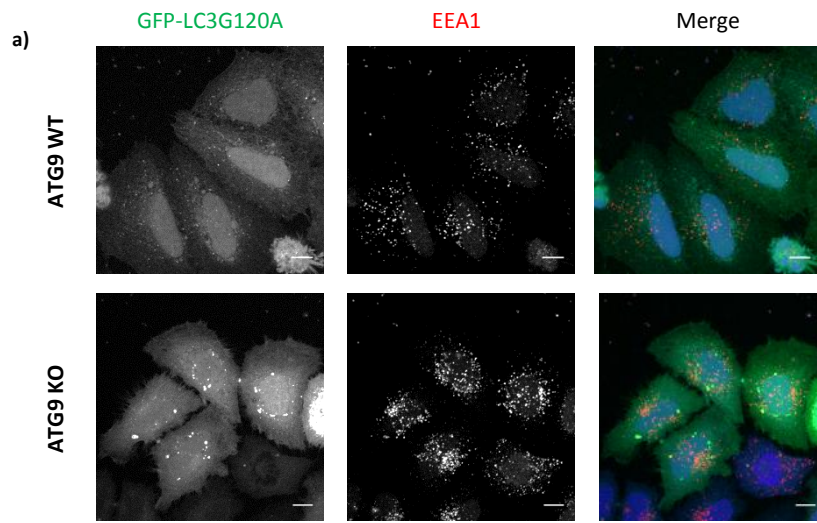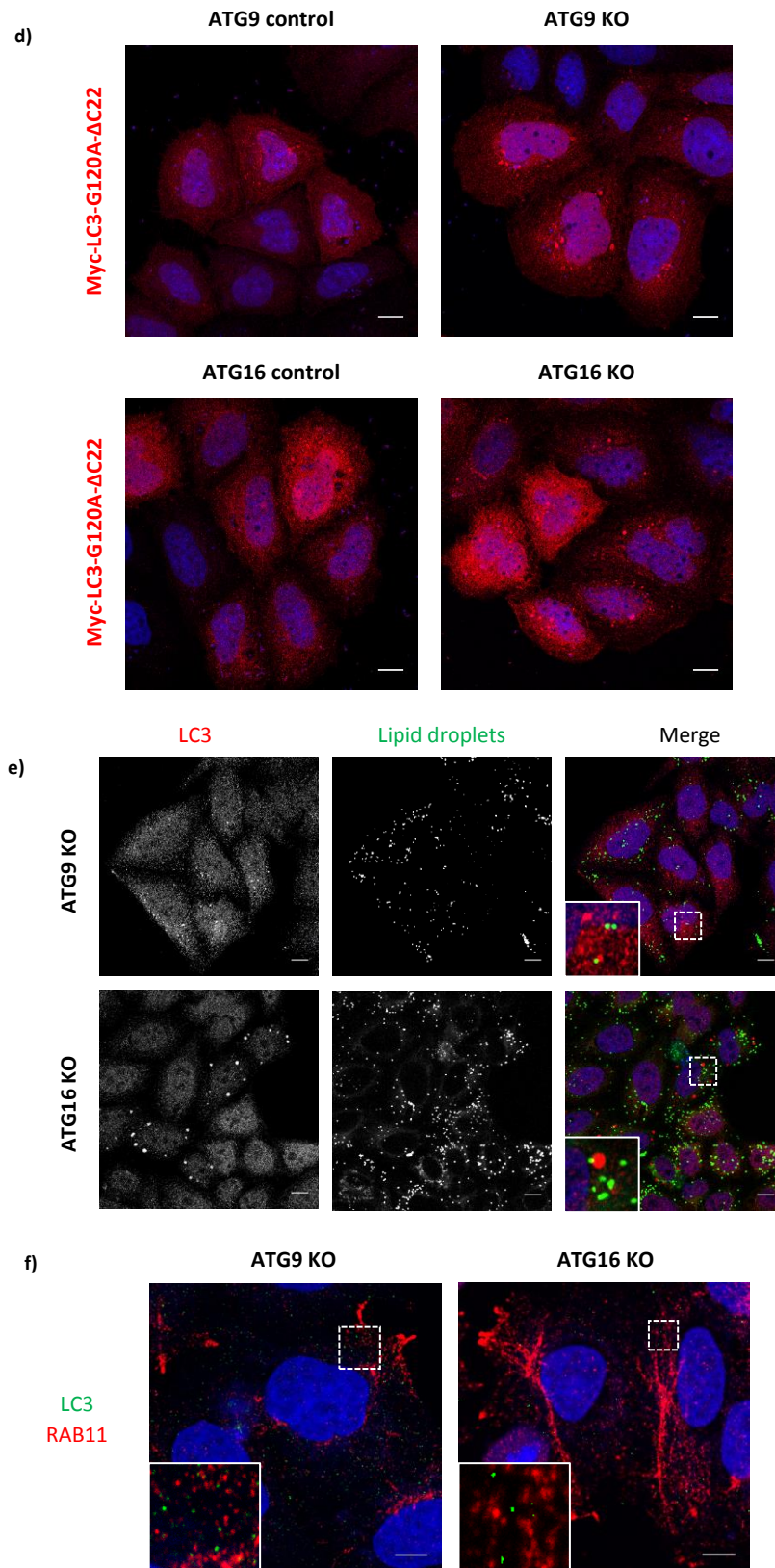
ATG16 KO

Fig 5.2: a), b) Representative immunofluorescence images showing the GFP-LC3G120A and early endosomal marker, EEA1 staining in representative ATG9 and ATG16 knockout cells with their respective controls. Cells were fixed with PFA and stained with antibodies against endogenous EEA1 and GFP signal. **c)** Representative

81

immunofluorescence images showing constitutively active Rab5Q79L-GFP and endogenous LC3 staining in representative ATG16 control and knockout cells. Cells were fixed with PFA and stained with antibodies against endogenous LC3 (Abcam®). **d)** Representative immunofluorescence images showing Myc-LC3G120A-ΔC22 staining in autophagy impaired ATG9 and ATG16 knockout cells. Cells were fixed with PFA and stained with antibody against the myc-tag. The scale bar represents a distance of 10 µm. **e)** Representative immunofluorescence images showing LC3 and lipid droplets stained using BODIPY stain in representative ATG9 and ATG16 knockout cells. Cells were fixed with PFA and stained with antibodies against endogenous LC3 and BODIPY. **f)** Representative immunofluorescence images showing LC3 and the recycling endosome marker, RAB11 staining in representative ATG9 and ATG16 knockout cells. Cells were fixed with PFA and stained with antibodies against endogenous LC3 and RAB11. It is worth noting that the mouse monoclonal antibody for endogenous LC3 staining works well only under methanol fixed conditions however, the endogenous RAB11 antibody does not work under methanol fixed conditions. Therefore, the cells had to be fixed with PFA, which made the LC3 puncta less visible. The scale bar represents a distance of 10 µm.
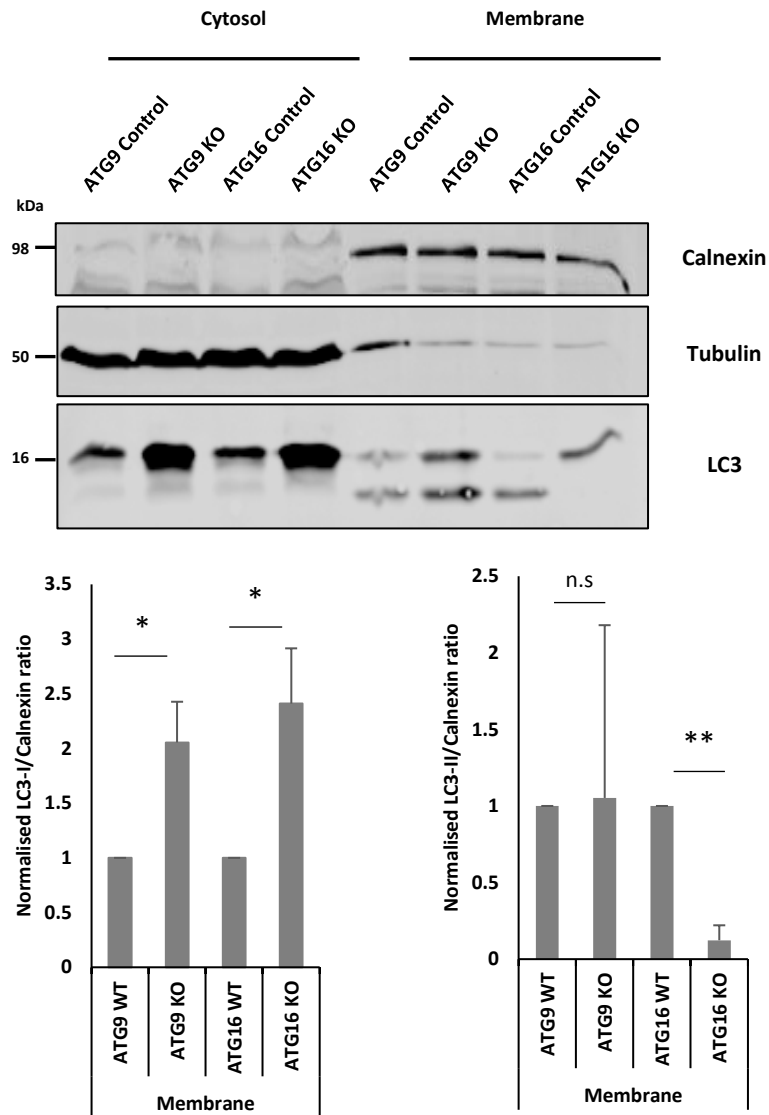
Fig 5.3: Representative western blot to check the association of LC3-I with membranous fraction in the autophagy-impaired cells viz. ATG9 and ATG16 knockout cells using a membrane fractionation protocol. The membrane fraction here represents total membrane constituent of the cells except the nuclear fraction. To confirm the purity of these fractions, tubulin was used as a purity marker for the cytosolic fraction while calnexin was used as a purity marker for the membrane bound fraction. The graphs represent the quantification and plots of the normalised ratios of LC3-I/Calnexin and LC3-II/Calnexin for the membrane fraction. It is worth noting that the levels of LC3-I associated with the membrane fraction are consistently higher in the knockout cells compared to control cells and are statistically significant. Also, the ATG16 knockout cells show no presence of LC3-II in soluble or membrane fractions with statistically significant quantification values. The statistics for LC3-II/Calnexin, however, show the difference in the ratios to be non-significant due to high variance between repeats. A possible reason that might explain the variance between the repeats is that since the ATG9 knockout cells possess a residual basal level of autophagy, the LC3-II levels in these cells on a western blot represents a snapshot of the LC3-II association with membrane. This can be confusing and highly variable based on the stimuli that cells receive prior to lysis and/or the phase of the cell cycle the cells are in.

83

5.4. The LC3-I structures are p62 positive

Since the observed structures did not co-localise with most of the conventional endosomal markers, I checked whether these LC3-I positive structures co-localise with p62. Since the cells are autophagy-impaired, I expected LC3 to be not associated with p62 in ATG16 knockout cells due to the lack of LC3 lipidation and hence, functional autophagy (Bento et al., 2016b). However, immunofluorescence studies showed that these structures showed high co-localisation with p62 in both ATG9 knockout and ATG16 knockout cells (Fig 5.4 a). These p62 structures looked like p62 aggregates which have formed as a result of defective autophagy. Recent studies have shown that p62 aggregate formation is accelerated under the presence of ubiquitinated substrates (Ciuffa et al., 2015; Zaffagnini et al., 2018), therefore I checked whether these p62 structures are positive for ubiquitin. Indeed, the immunofluorescence imaging showed that these p62 aggregates formed in ATG9 knockout and ATG16 knockout cells were positive for ubiquitin (Fig 5.4 b).

To further understand the morphology of the p62 aggregates and the localisation of LC3 within the aggregates, I performed super-resolution microscopy on the ATG9 and ATG16 knockout cells stained for endogenous LC3 and p62 (Fig 5.5 a, b and c). The images showed the presence of LC3 in association with the p62 aggregates. The aggregates were much smaller in ATG9 knockout cells compared to ATG16 knockout cells. Moreover, some ATG16 knockout cells showed much larger aggregates but the number of these cells in the population was few. It could also be seen that smaller p62 aggregates are associated with more LC3 compared to larger p62 aggregates, which had fewer LC3 molecules associated with them. This is consistent with the observations from a recent study, that showed that the p62 aggregates need ubiquitinated-substrates to oligomerise and higher levels of LC3 inhibit the growth of the p62 aggregates (Zaffagnini et al., 2018).
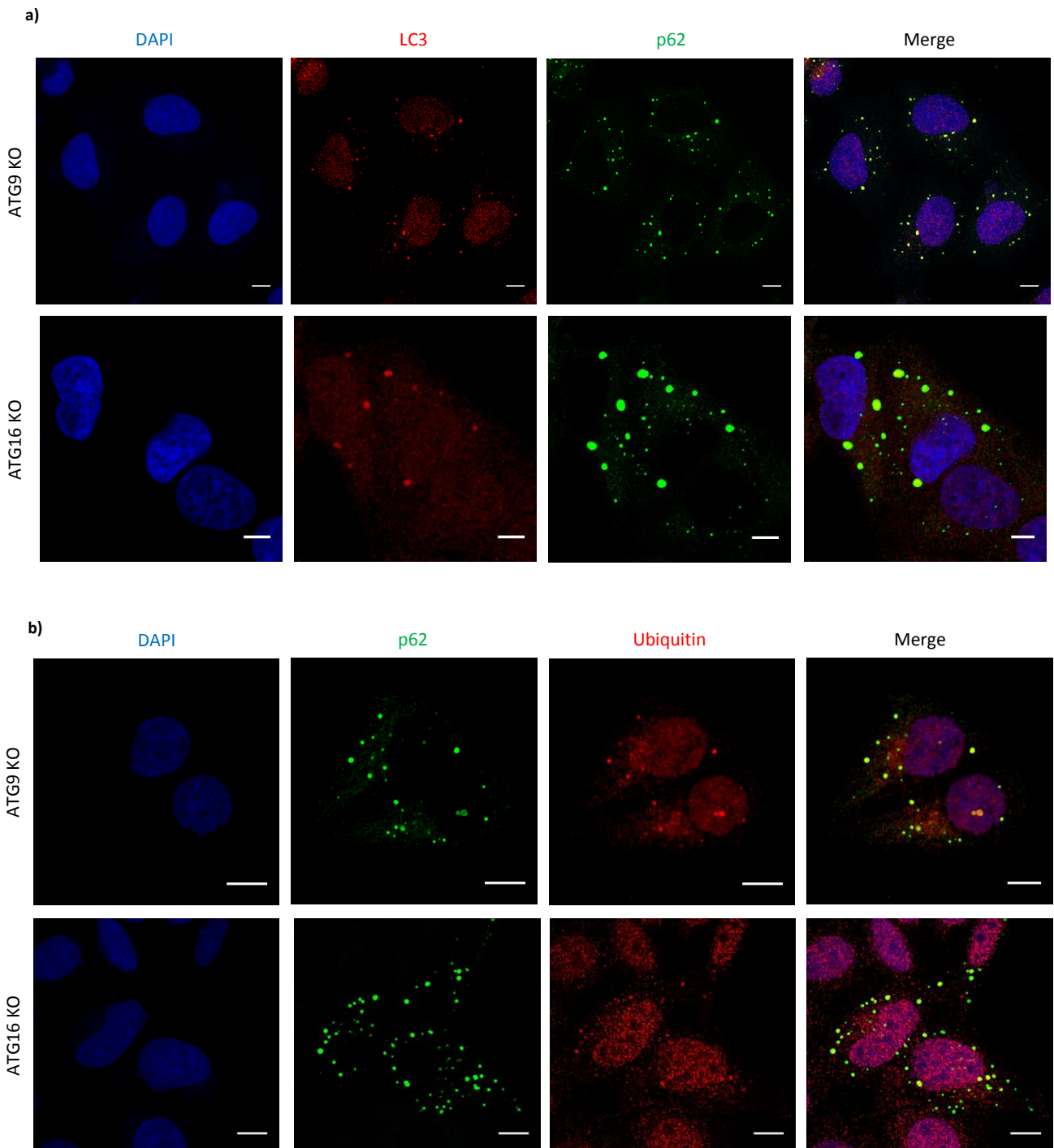
Fig 5.4: a) Representative immunofluorescence images showing the co-localisation of LC3-positive structures in autophagy-impaired cells with p62. Cells were fixed with PFA and stained with antibodies against endogenous LC3 and p62. Please note that the LC3 antibody used here is the rabbit monoclonal antibody (Abcam) which needs the samples to be fixed with PFA **b)** Representative immunofluorescence images showing the co-localisation of p62 structures in autophagy-impaired cells with ubiquitin. Cells were fixed with PFA and stained with antibodies against endogenous p62 and ubiquitin. The scale bar represents a distance of 10 µm.

a) ATG9 KO

DAPI
LC3
p62
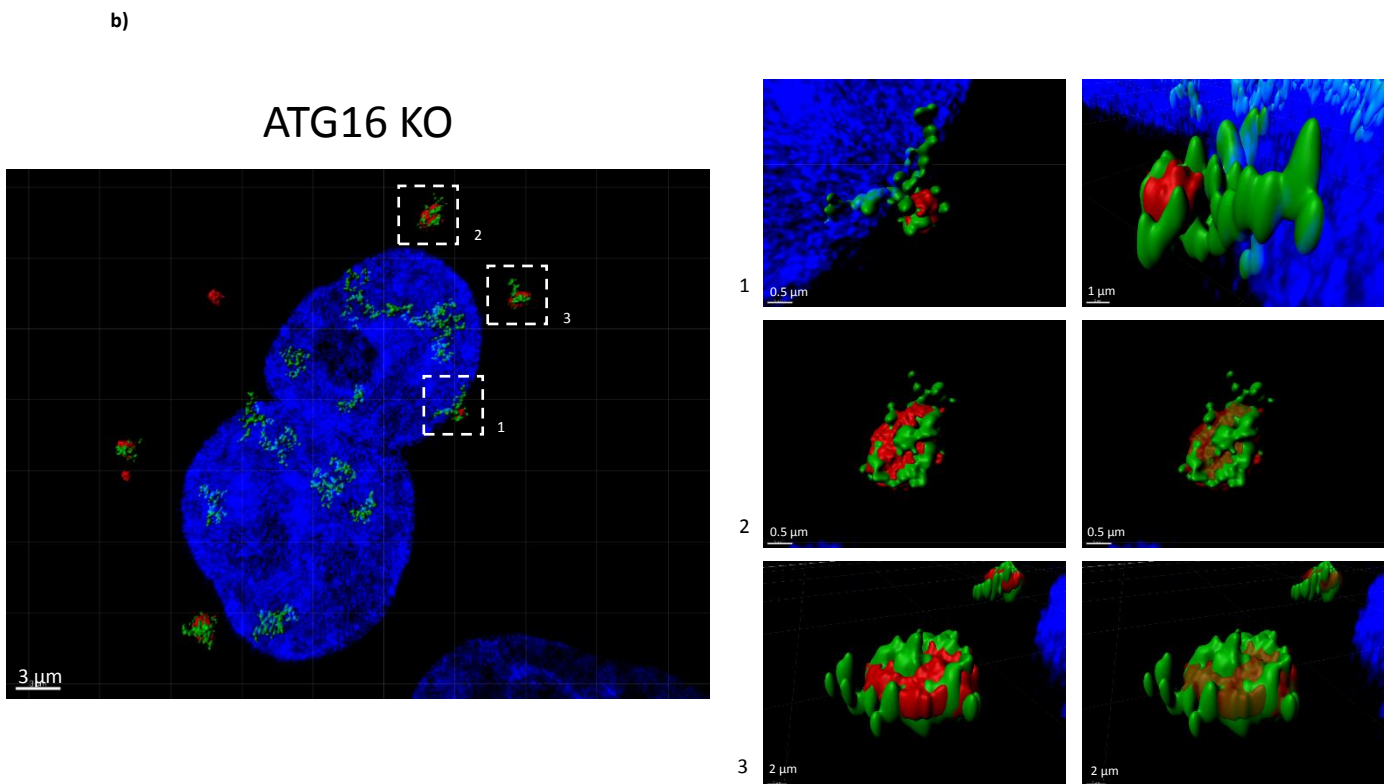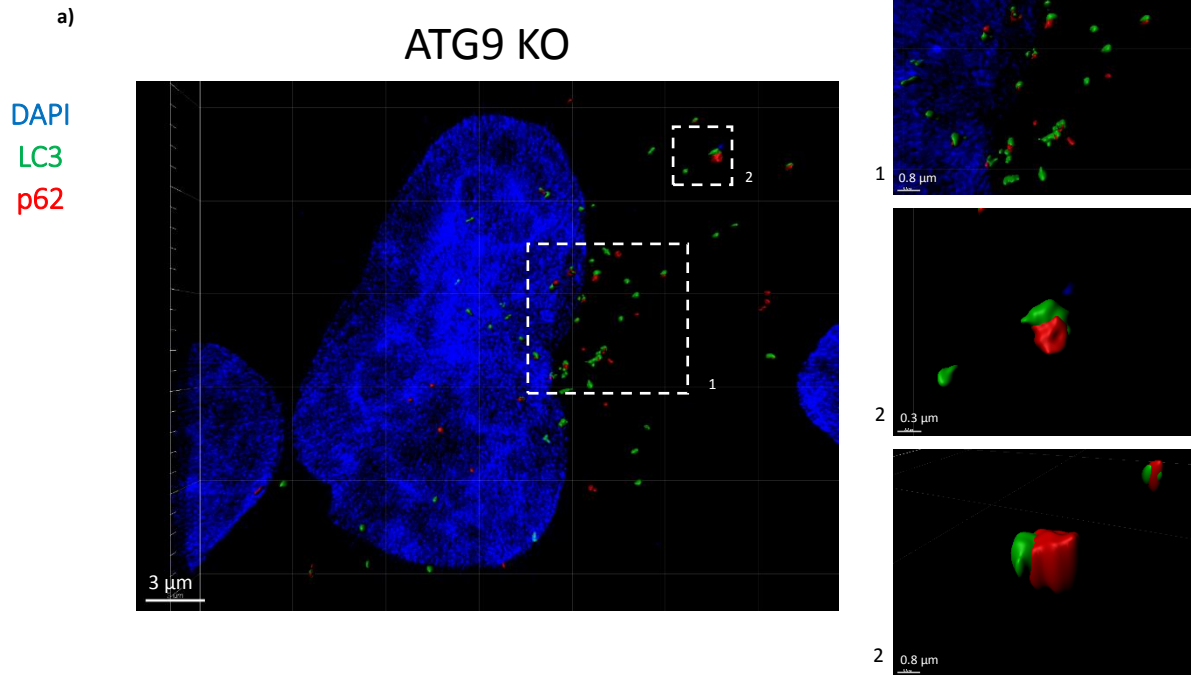
b) ATG16 KO
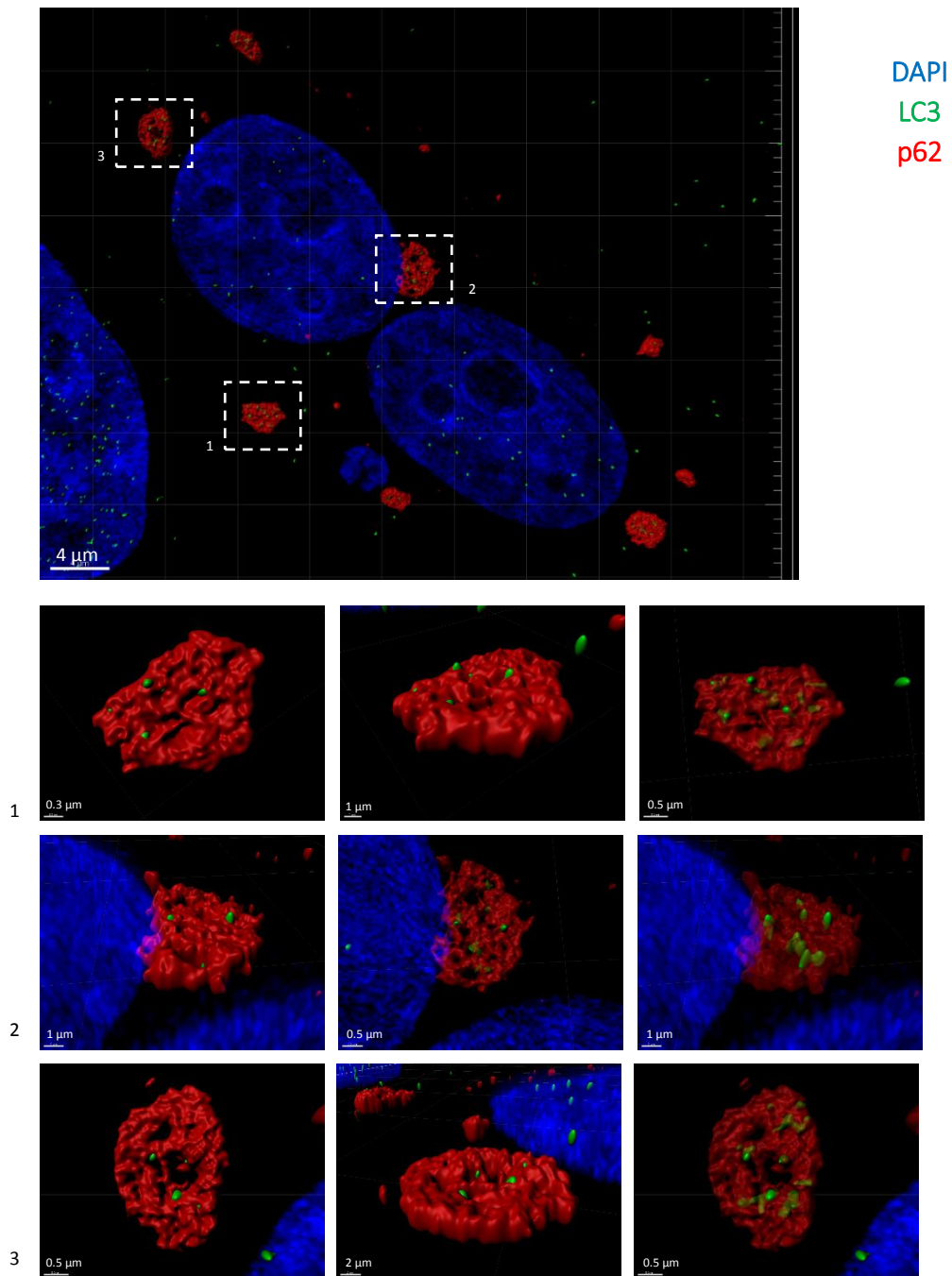
Fig 5.5: a) Representative super-resolution immunofluorescence images showing the co-localisation of LC3-positive structures with p62 in ATG9 knockout cells. Cells were fixed with PFA and stained with antibodies against endogenous LC3 (Abcam®) and p62. **b)** Representative super-resolution immunofluorescence images showing the co-localisation of LC3-positive structures with p62 in ATG16 knockout cells. Cells were fixed with PFA and stained with antibodies against endogenous LC3 and p62. **c)** Representative super-resolution immunofluorescence images showing the co-localisation of LC3-positive structures with p62 in ATG16 knockout cells. Cells were fixed with PFA and stained with antibodies against endogenous LC3 and p62.

5.5.   p62 depletion reduces the number and decreases the size of the LC3-positive puncta

To understand whether p62 is responsible for formation of these LC3-I puncta under autophagy-impaired conditions, I depleted the levels of the endogenous p62 using SMARTpool siRNA and checked the size and number of LC3 positive structures in ATG9 and ATG16 knockout cells.

Interestingly, the observed LC3-I positive structures under autophagy-impaired conditions decrease in number and size upon p62 depletion (Figs 5.6 and 5.7 a, b and c). The effect was more pronounced in ATG16 knockout cells where the cells show only cytosolic LC3 staining and no LC3-I structures whatsoever. This observation indicates that p62 aggregates formed under autophagy-impaired conditions are able to bind to LC3-I and form LC3-positive structures. It is worth noting that while the levels of p62 in ATG9 knockout cells are lower than control cells in this western blot other repeats of the experiment show the levels to be the same. This possibly indicates that ATG9 knockout cells show the presence of residual autophagy and ATG9 is not absolutely essential for autophagy. On the contrary, the levels of p62 in ATG16 knockout cells show a clear increase compared to control indicating that ATG16 is indispensable for the process.

My results, therefore, show the drawbacks of LC3 immunofluorescence as an autophagy assay when designing experiments involving autophagy-impaired conditions or autophagy-null cells.

5.6.   p62 overexpression increases the number of LC3-I positive vesicles in ATG16 knockout cells

To assess whether the effect of p62 knockdown on LC3-I positive structures is specific, a reverse approach involving the p62 overexpression was used. The idea behind this experiment was that if p62 aggregation results in the LC3-I binding and vesicle formation, overexpression of a functional p62 protein in the cells would result in an accumulation of these LC3-I positive structures, thereby leading to an increase in the observed number of LC3-I vesicles. As expected the number of LC3-I positive structures increased dramatically on p62 overexpression

and it was observed that the area of the p62 aggregates and LC3-I vesicles also increased (Fig 5.8 a and b). Furthermore, a lot more smaller aggregates led to the formation of smaller LC3-I structures, which led to an overall decrease in the average size of the LC3-I vesicles, owing to which I observed no apparent change in the average size of the LC3-I vesicles on p62 overexpression (Fig 5.8 b).

Overall my results identify a novel potential homeostatic role of p62 in autophagy-impaired cells. While p62 has been shown to aid cytoplasmic inclusion formation in autophagy-impaired conditions (Komatsu et al., 2007), in this situation the cytoplasmic inclusions formed by the excess LC3-I due to its association with p62 is being targeted for degradation to maintain cellular homeostasis. This mechanism, therefore, regulates the cellular levels of LC3 under autophagy-impaired conditions via its sequestration into aggregates by p62 and hence, its probable degradation by the proteasomal pathway.
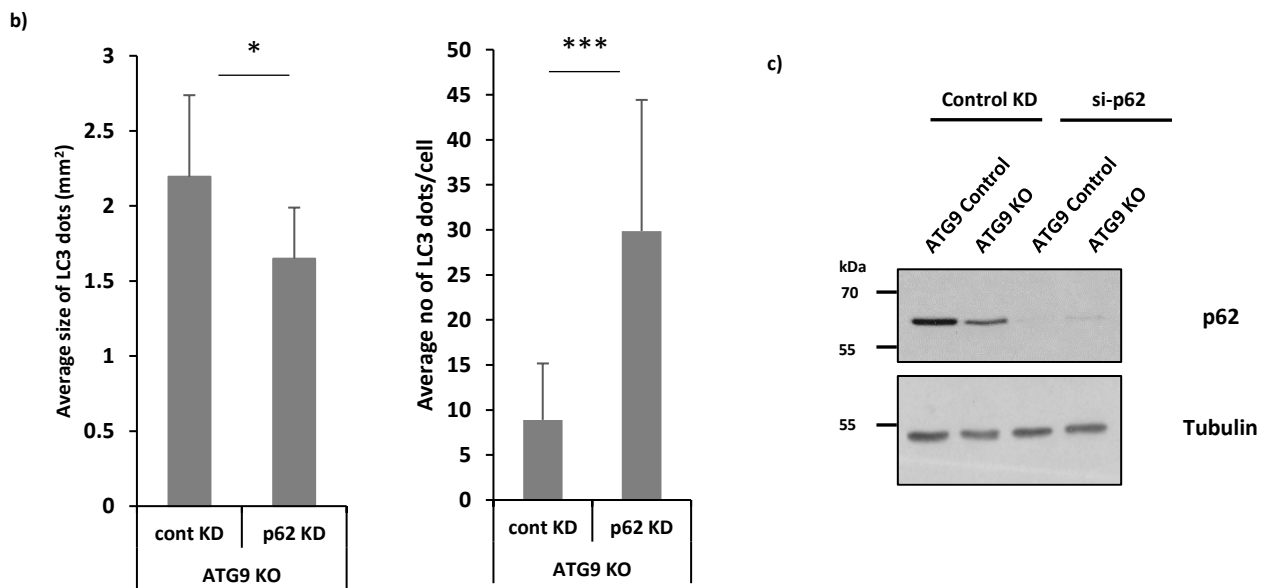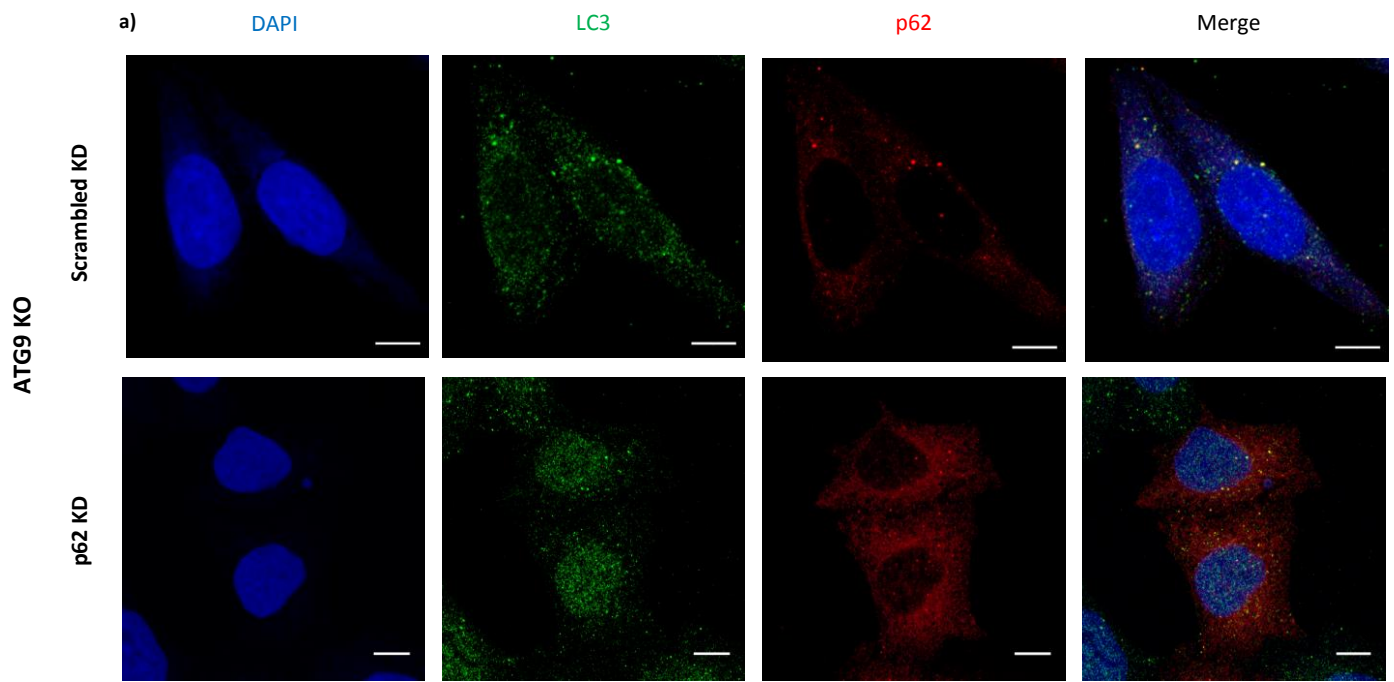
Fig 5.6: a) Representative immunofluorescence images showing the morphology of LC3-I positive structures under control and p62 knockdown conditions in representative ATG9 knockout cells. Cells were fixed with PFA and stained with antibodies against endogenous LC3 and p62. **b)** Quantification of the LC3-positive structures' size and number under control and p62 knockdown conditions using ImageJ quantification tool (** = $p < 0.01$, *** = $p < 0.001$). Quantification performed from 3 experiments with at least 25 cells quantified for each condition. The error bars represent standard deviation (SD). **c)** Western blot showing that the knockdown of p62 was successful in ATG9 control and knockout cells. It is worth noting that while the level of p62 in ATG9 knockout cells are lower than control cells in this western blot, similar repeats show the levels to be the same. This possibly indicates that ATG9 knockout cells show the presence of residual autophagy and ATG9 is not absolutely essential for autophagy. The scale bar represents a distance of 10 µm.
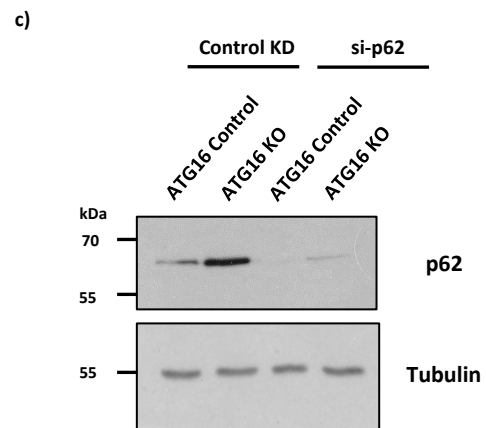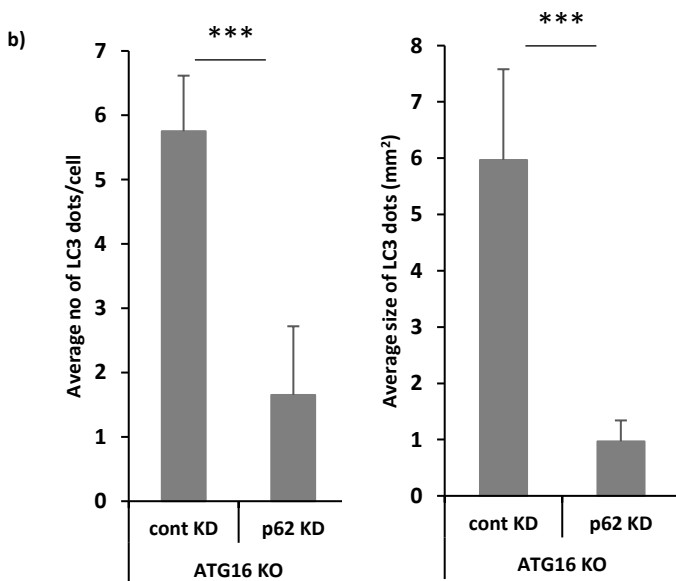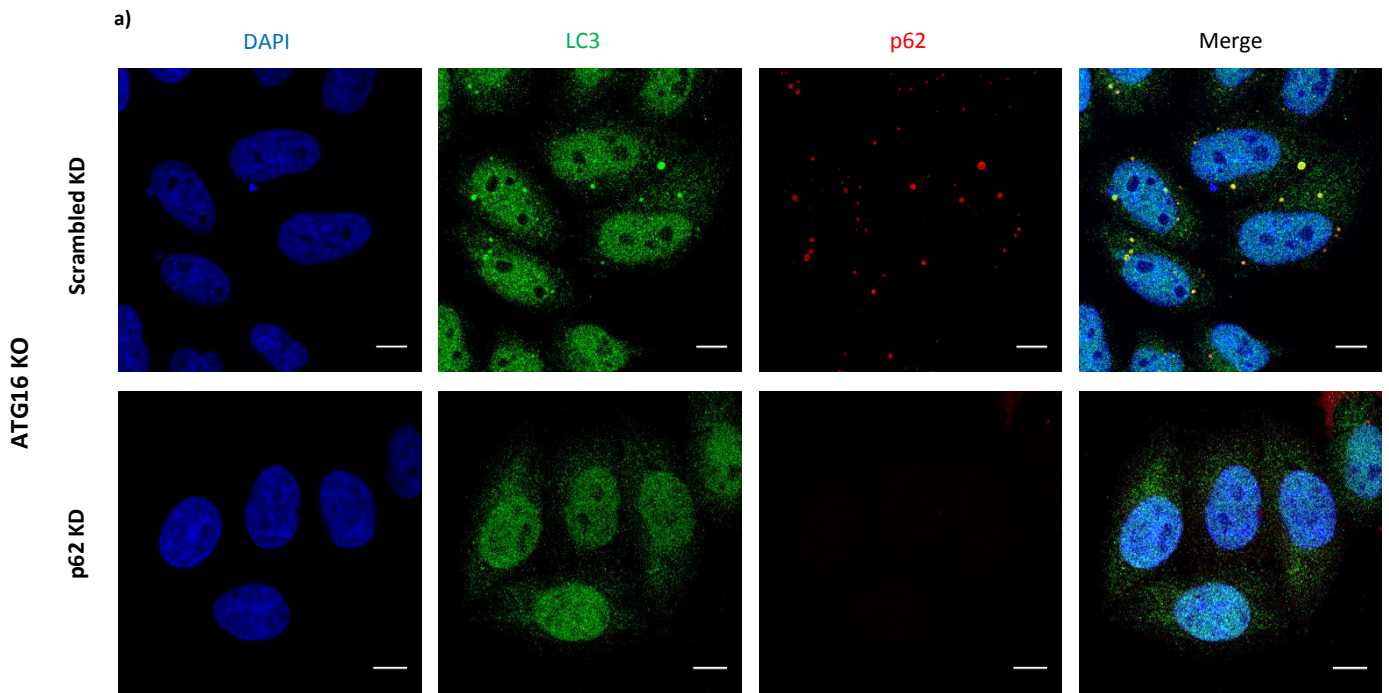
Fig 5.7: a) Representative immunofluorescence images showing the morphology of LC3-I positive structures under control and p62 knockdown conditions in ATG16 knockout cells. Cells were fixed with PFA and stained with antibodies against endogenous LC3 and p62. **b)** Quantification of the LC3-positive structures' size and number under control and p62 knockdown conditions using ImageJ quantification tool (** = p < 0.01, *** = p < 0.001). Quantification performed from 3 experiments with at least 25 cells quantified for each condition. The error bars represent standard deviation (SD). **c)** Western blot showing that the knockdown of p62 was successful in ATG16 control and knockout cells. The levels of p62 are higher in the ATG16 knockout cells confirming that ATG16 is indispensable for autophagy. The scale bar represents a distance of 10 µm.
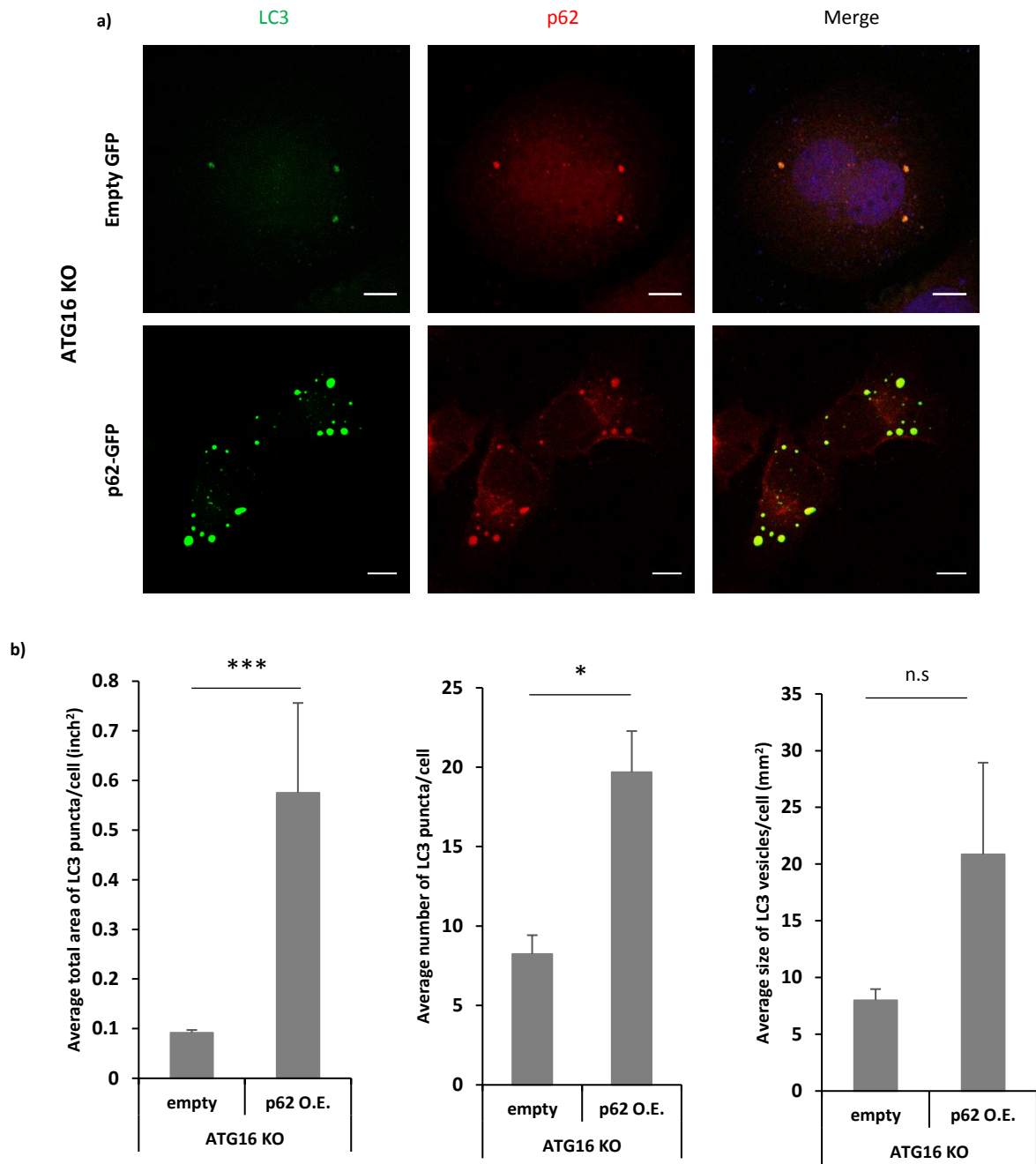
Fig 5.8: a) Representative immunofluorescence images showing the morphology of LC3-I positive structures under control and p62 overexpression conditions in representative ATG16 knockout cells. Cells were fixed with PFA and stained with antibody against endogenous LC3. **b)** Quantification of the LC3-positive structures' total area and number under control and p62 overexpression conditions using ImageJ quantification tool (* = $p < 0.05$, *** = $p < 0.001$, n.s = non-significant). Quantification performed from 3 experiments with at least 25 cells quantified for each condition. The error bars represent standard deviation (SD). The scale bar represents a distance of 10 µm.

a)

	p62	LC3	Merge
Control KD			
si-ATG7/si-ATG10			

b)

(-) BAF   (+) BAF

Control, Control, Control, si-ATG7/si-ATG10, si-ATG7/si-ATG10, si-ATG7/si-ATG10, Control, Control, Control, si-ATG7/si-ATG10, si-ATG7/si-ATG10, si-ATG7/si-ATG10

kDa

55 — GAPDH

16 — LC3-II (Low exposure)

LC3-I
16 — LC3-II (High exposure)

c)

Control, Control, Control, si-ATG7/si-ATG10, si-ATG7/si-ATG10, si-ATG7/si-ATG10

kDa

100 —
70 — ATG7

55 — ATG10

55 — GAPDH
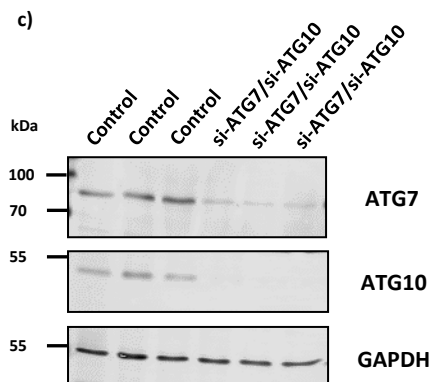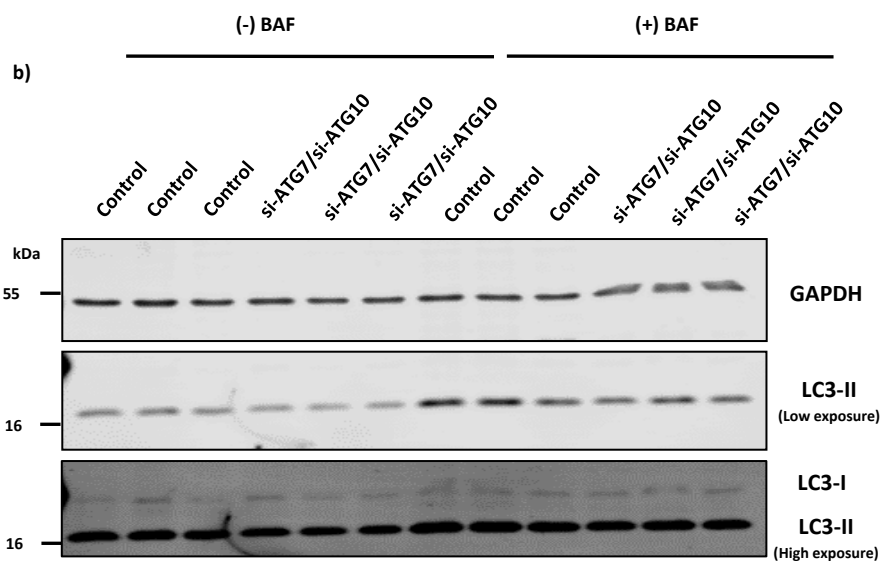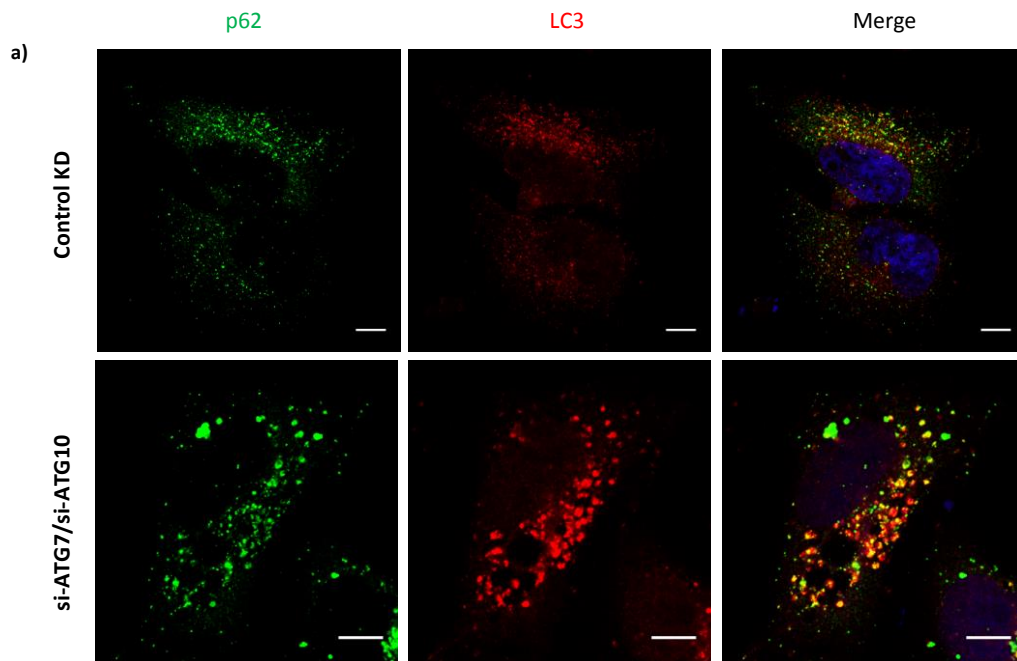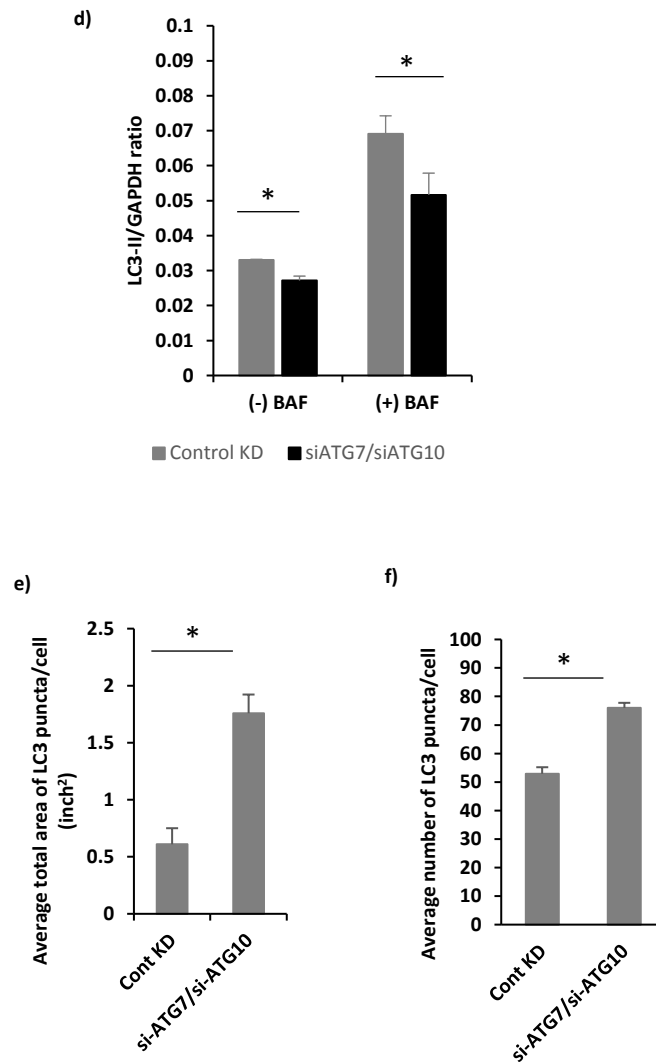
Fig 5.9: a) Representative immunofluorescence images showing the morphology of LC3-positive structures under control and ATG7/10 knockdown conditions in representative HeLa cells. Cells were fixed with PFA and stained with antibody against endogenous LC3 (Abcam®) and p62. **b)** Representative western blot showing the changes in the levels of LC3-I and LC3-II in HeLa cells upon ATG7/ATG10 knockdown compared to control. The longer exposure of the blot is shown to facilitate the visualisation of the LC3-I band. **c)** Representative western blot showing the efficiency of ATG7/ATG10 knockdown. **d)** Quantification of the LC3-II/GAPDH ratio for the control and ATG7/10 knockdown conditions in the absence and presence of BAF showing an impaired autophagic response upon ATG7/10 knockdown in HeLa cells. **e), f)** Quantification of the LC3-positive structures' area and number, respectively, under control and ATG7/10 knockdown conditions using ImageJ quantification tool (* = p < 0.05). Quantification was performed from 3 experiments with at least 20 cells quantified for each condition. The error bars represent standard deviation (SD). The scale bar represents a distance of 10 µm.

5.7. The number and area of LC3-positive structures increase upon autophagy impairment in HeLa cells

To further test whether the cells knocked down for essential autophagy genes would show similar phenotype, I knocked down the ATG7 and ATG10 autophagy proteins. These two proteins, as mentioned in the introduction section, are responsible for the conjugation of ATG5-ATG12, which is indispensable for LC3 lipidation and hence autophagosome biogenesis. As mentioned earlier, p62 aggregates have been shown to sequester the E1-like ATG7 enzyme. It has also been shown that this sequestration is mediated via the interaction of LC3-I with ATG7 and that while p62 shows preferential binding towards LC3-II, it is indeed capable of binding to the lipidation defective LC3-G120A mutant (Gao et al., 2013). Therefore, my observations and results of the experiments mentioned so far in this chapter together with the existing literature point towards the LC3-I association with p62 under autophagy-impaired conditions. And if this hypotheses were correct, I would expect a decrease in the levels of LC3-II on western blot but an increase in the number and overall area of LC3 puncta in the cells. Indeed, upon siRNA mediated depletion of two core autophagy proteins ATG7 and ATG10 for 48 hours the levels of LC3-II, tested using western blotting, under knockdown conditions decrease compared to control (scrambled siRNA) (Fig 5.9 a, b, c and d). Interestingly, on imaging these cells for LC3-puncta there was a corresponding increase in the number of LC3-positive structures and the overall area of these structures under knockdown conditions was much higher (Fig 5.9 e and f). The results of this experiment thereby depict why immunofluorescence studies on cells knocked down for essential autophagic genes can be potentially misleading.

The possible scenarios of LC3-I sequestration by p62 in cells with functional, impaired or abrogated autophagy have been described schematically in Fig 5.10 for reference. Conventionally, the LC3-I molecules are lipidated to LC3-II that marks the autophagosomes and hence, as mentioned above, LC3 immunocytochemistry is a widely technique used for quantifying the number of autophagosomes in the cells at a given time. Upon autophagy impairment or abrogation, however, the p62 levels increase that lead to the sequestration of excess of LC3-I from the cytosol into the insoluble aggregates. While these structures show an increase in the size compared to conventional autophagosomes, they still could easily be confused for mature autophagosomes to an untrained eye while performing LC3 immunocytochemistry, thereby confounding the recorded results.
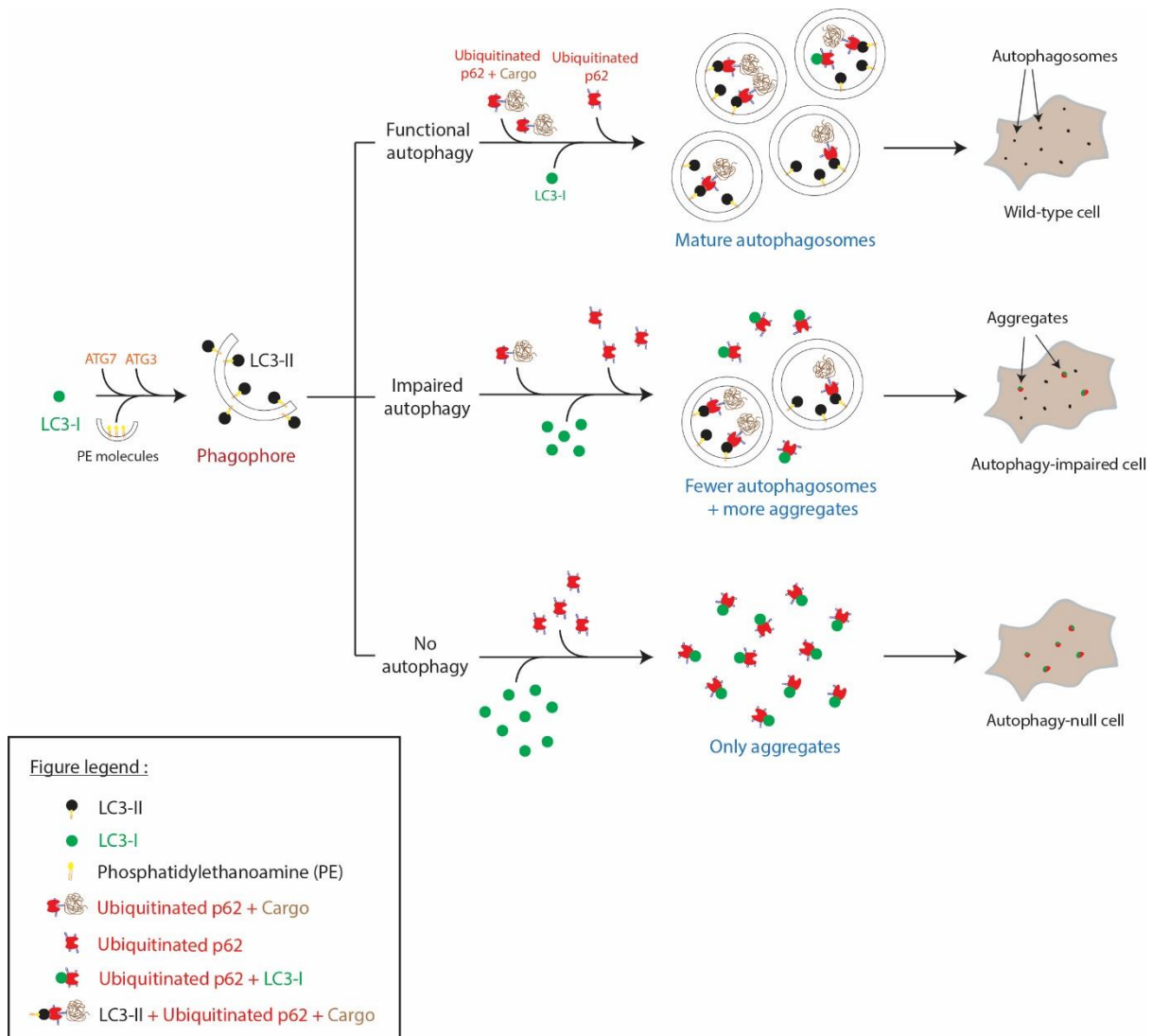
Fig 5.10: A schematic describing the process of LC3-I molecule sequestration by the p62 aggregates in autophagy-impaired and autophagy-null cells. The process of autophagy involves the lipidation of the cytosolic form of LC3 viz. LC3-I on to a phosphotidylethanolamine molecule (located on the growing phagophore) to form LC3-II. The visualisation of LC3-II molecules using immunocytochemistry techniques are therefore considered to be a gold-standard assay to assess the autophagosome number in cells. Under conditions where autophagy is fully functional, LC3-I molecules get lipidated to form LC3-II, which primarily results in the recruitment of ubiquitinated p62 molecules attached to cargoes destined for degradation to the growing autophagosomes. The LC3-II molecules then get recycled/degraded to replenish the pool of cytosolic LC3-I in these cells. However, under conditions where LC3-I accumulates in cells as a result of autophagic impairment or complete abrogation, p62 aggregates formed as a result of dysfunctional autophagy sequester the excess LC3-I molecules forming structures that resemble mature autophagosomes in autophagy-impaired and autophagy-null cells. While these strcutures show an increased size compared to conventional autophagosomes, their presence might mislead an untrained eye and might result in recording of confounding results.

To summarize, my results in this chapter identify a new role for p62 in autophagy-impaired cells. I begin with showing the aberrant accumulation of LC3-positive structures in autophagy-impaired cells. I confirm this observation by exogenously expressing non-conjugatable forms of LC3 in autophagy-null cells. I then proceed to show that these LC3-positive structures show co-localisation with p62 in autophagy-null cells and depletion of endogenous p62 in these cells abrogates formation of the LC3-positive structures. I then show that overexpression of p62 in autophagy-null cells increase the number and area of the LC3-positive structures observed. Finally, I show that an experimental setup involving depletion of core autophagy proteins ATG7 and ATG10 results in lower levels of LC3-II on blots but higher number and total area of LC3-positive structures in cells. These results together suggest that p62 associates with LC3-I under autophagy-impaired conditions that results in the formation of LC3-positive structures in these cells. Therefore, one must be careful while interpreting results from an LC3 immunofluorescence experiment since these LC3-I structures could be mistaken for mature autophagosomes confounding the outcome of the experiment.

6. Studying ATG9 and VMP1 trafficking in HeLa cells

As mentioned earlier in the introduction section, the trafficking of ATG9 and VMP1 remains to be completely explored and understood. Moreover, the relationship between these two transmembrane proteins has not been described yet. Therefore, I aimed to explore new trafficking route for these proteins and understand the relation between these proteins. The results will now be described in this chapter.

6.1. VMP1 traffics through the plasma membrane

VMP1 is a transmembrane protein with a noticeable cytosolic domain, similar to the core autophagy protein, ATG9 (Fig 1.4). It has been shown that ATG9 traffics via plasma membrane to early and recycling endosomes during autophagosome formation (Puri et al., 2013; Puri et al., 2018). Therefore, I checked whether VMP1 traffics via the same route. To begin with, I performed plasma membrane protein extraction (see methods) and checked for the presence of VMP1 in the extracted fraction. It was observed that VMP1 is present in the protein pool extracted from the plasma membrane (Fig 6.1 a). Next, to confirm the above observation, I performed a cell-surface biotinylation experiment to test the presence of VMP1 on the plasma membrane. In this experiment, I also tested whether the levels of VMP1 change when the cells were treated with different conditions like basal, starvation and the dynamin inhibitors, dynasore and dyngo. The rationale behind using dynamin-inhibitors was to identify whether VMP1 travels from the plasma membrane into the cells via trafficking route similar to ATG9. Consistent with the above observation, it was seen that VMP1 is present on the plasma membrane (Fig 6.1 b). Unfortunately, the beads showed some non-specific affinity towards VMP1 which can be seen in the negative control and was consistent across the repeats. However, since the positive control for the experiment, NHE1 – a plasma membrane resident sodium-hydrogen antiporter 1, showed no pull down in the negative control (Fig 6.1 c) and the observed difference in the levels of pulled-down VMP1 was significantly higher in biotinylated samples compared to negative control, the pull down of biotinylated VMP1 was specific. It is also worth noting that the levels of VMP1 at the plasma membrane in cells treated with the inhibitors of dynamin showed no difference (Fig 6.1 b).

6.2. VMP1 traffics through early and recycling endosomes

The next step towards the characterisation of VMP1 trafficking was to check the co-localisation of VMP1 with the endosomal markers for early and recycling endosomes, viz. EEA1 and RAB11A respectively. In addition, based on a recent study that proposes recycling endosomes as the platform for autophagosome formation (Puri et al., 2018), the co-localisation of VMP1 with RAB11A and BECN1 would also indicate its role in autophagosome formation. It was observed that VMP1 co-localises with the endosomal markers EEA1 and RAB11A (Fig 6.2 a and b). At the recycling endosomes, VMP1 was also seen to co-localise with BECN1, an early autophagy protein known to be associated with recycling endosomes. (Puri et al., 2018). The co-localisation between VMP1, RAB11A and BECN1 could be clearly visualised by plotting the intensities of various channels as a function of distance using the ZEN imaging software (Fig 6.2 c). The results from the section 6.1 and 6.2 therefore suggest that VMP1 may follow a similar trafficking route like ATG9 as it localises to plasma membrane, early and recycling endosomes.

6.3. VMP1 interacts with ATG9

After confirming that both ATG9 and VMP1 traffic through the endosomal pathway and the plasma membrane, I speculated whether the two proteins would physically interact. I, therefore, immunoprecipitated endogenous VMP1 and the checked the IP sample for the presence of ATG9. Interestingly, ATG9 was seen to co-immunoprecipitate with VMP1. The immunoprecipitation was then performed the other way around and it was seen that VMP1 co-immunoprecipitates with ATG9 in the IP sample (Fig 6.3 a and b). In addition, when VMP1-GFP was overexpressed in HeLa cells, endogenous ATG9 co-immunoprecipitates with VMP1-GFP and similarly, overexpressed VMP1-GFP co-immunoprecipitates with endogenous ATG9, further confirming the interaction between the two proteins (Fig 6.3 c and d). It was also observed that overexpressed VMP1 showed varying mobility/molecular weight on western blots between various experimental repeats. Upon excluding the obvious possibilities such as non-specific antibody binding and breakdown products, it was concluded that the overexpressed VMP1 potentially undergoes reversible post-translational modifications that affect its mobility on the gel. Based on the molecular weight shift, it could be likely that overexpressed VMP1 is glycosylated in HeLa cells.
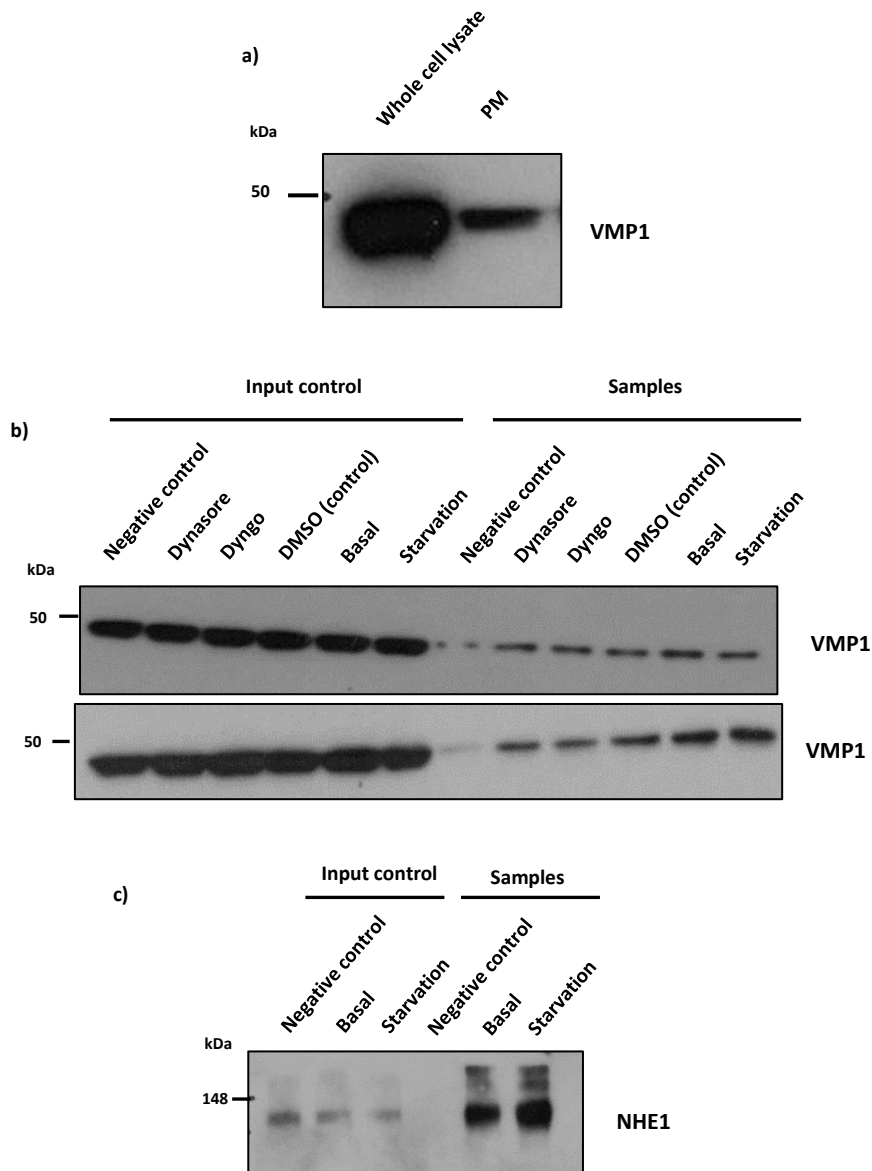
Fig 6.1 a) Representative western blot depicting the presence of VMP1 in plasma membrane fraction after extraction using the Abcam® plasma membrane protein extraction kit. **b)** Representative western blots of the repeats showing the presence of VMP1 on the plasma membrane using the cell-surface biotinylation assay. The experiment is based on isolating the biotinylated proteins on the plasma membrane by exploiting the high affinity interaction between biotin and streptavidin. Different conditions were tested to check enrichment of VMP1 on the plasma membrane upon varying stimuli. **c)** Representative western blot depicting the pull-down of the biotinylated cell-surface sodium-hydrogen antiporter1 (NHE1), acting as a positive control for the biotinylation experiment.
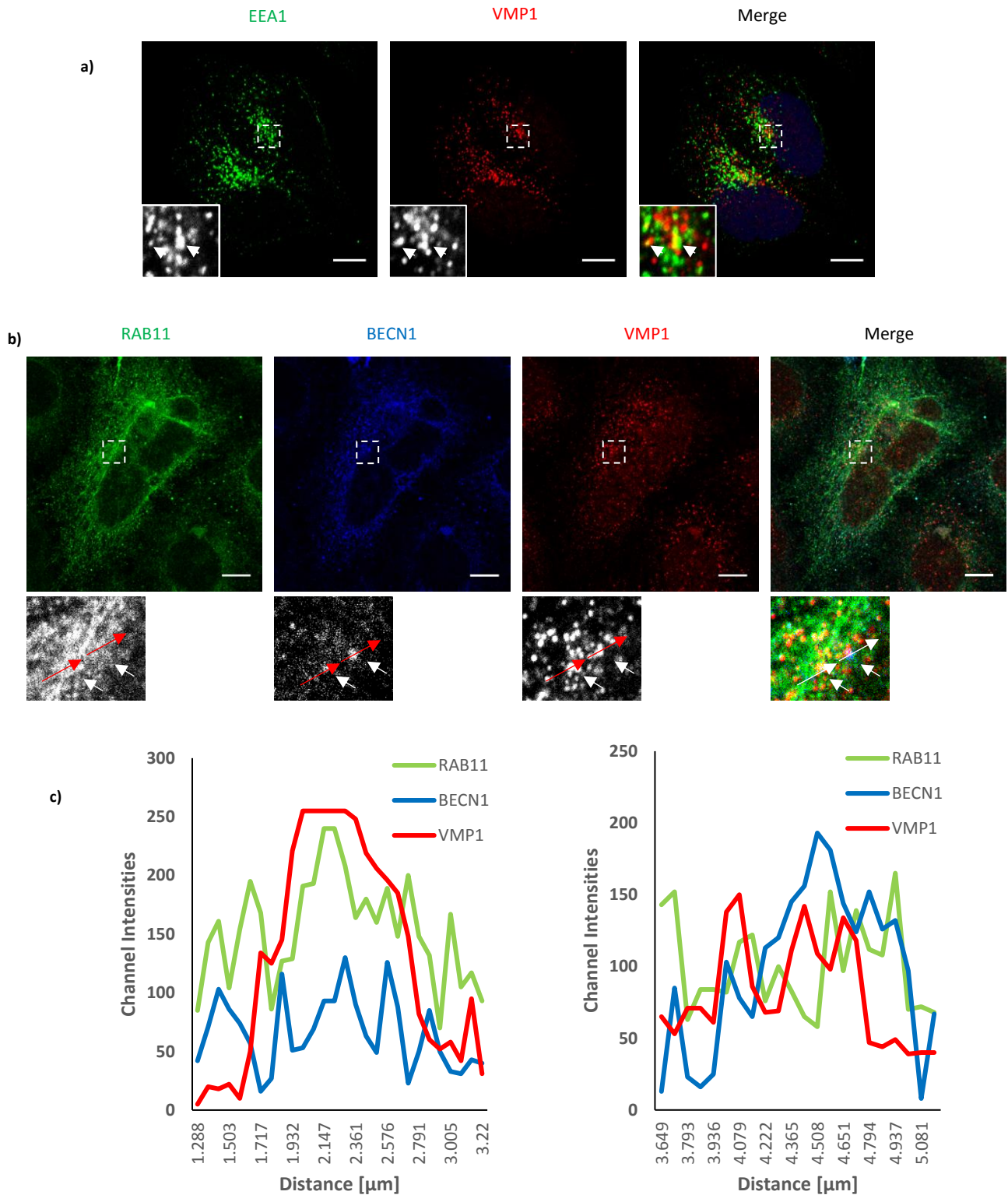
Fig 6.2 a) Representative immunofluorescence images showing the co-localisation of VMP1 with the early endosomal marker, EEA1. **b)** Representative immunofluorescence images showing the co-localisation of VMP1 with the recycling endosomal marker, RAB11 and the core autophagy protein, BECN1. c) Intensities of RAB11, BECN1 and VMP1 channels plotted as a function of distance, measured using ZEN Imaging software by Zeiss. The scale bar represents a distance of 10µm.

6.4. VMP1 overexpression induced autophagy is ATG9-dependent

The first study that described VMP1 as an autophagy protein, also showed that its overexpression results in the induction of autophagy. The studies were conducted in the context of a condition called acute pancreatitis, which shows higher levels of VMP1 expression (Ropolo et al., 2007). However, since then, not much has been described about VMP1 overexpression induced autophagy. I show that not only does VMP1 physically interact with ATG9 (Section 6.3), but also that the VMP1-overexpression induced autophagy is ATG9-dependent. When VMP1 was overexpressed in the ATG9 knockout cells, there was no increase in the autophagic flux compared to control cells (Fig 6.4 a and b).
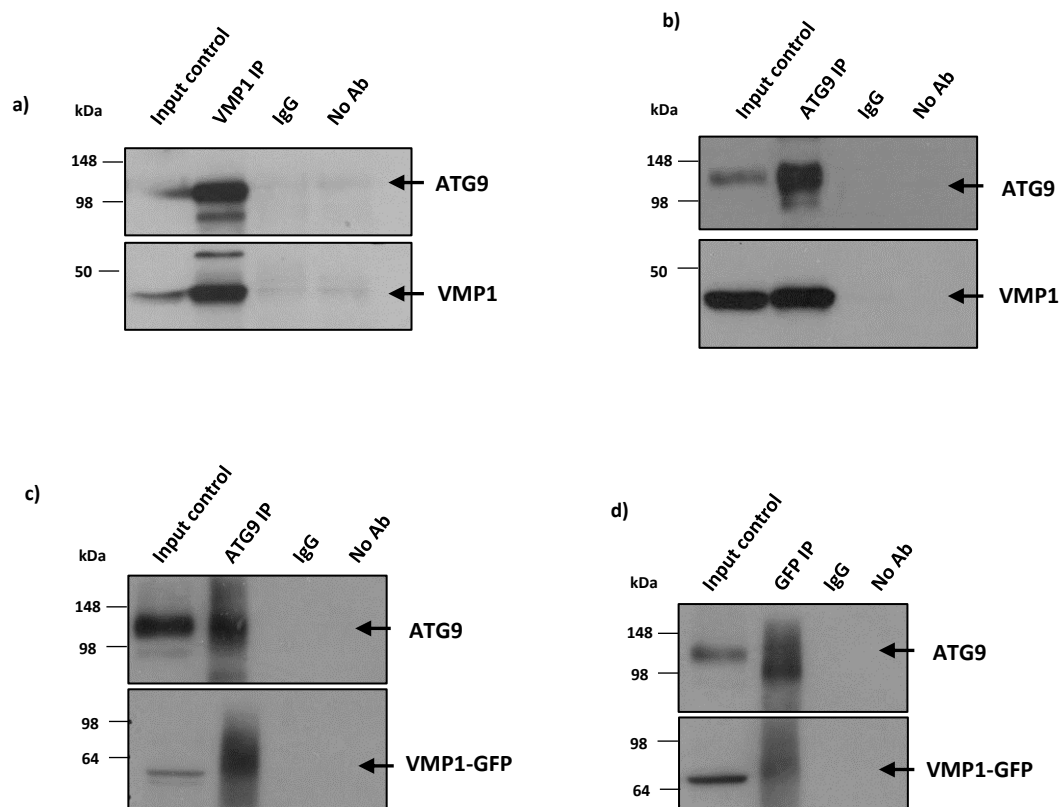
Fig 6.3 a) Representative western blot showing the co-immunoprecipitation of VMP1 with ATG9. **b)** Representative western blot showing the co-immunoprecipitation of ATG9 with VMP1. **c)** Representative western blot showing the co-immunoprecipitation of ATG9 with VMP1-GFP. **d)** Representative western blot showing the co-immunoprecipitation of VMP1-GFP with ATG9. It is worth noting that the band of VMP1-GFP shows a slight variation in the size between experiments. This observation potentially indicates that VMP1 undergoes some post-translational modifications in the cell, with glycosylation being a primary form of modification.
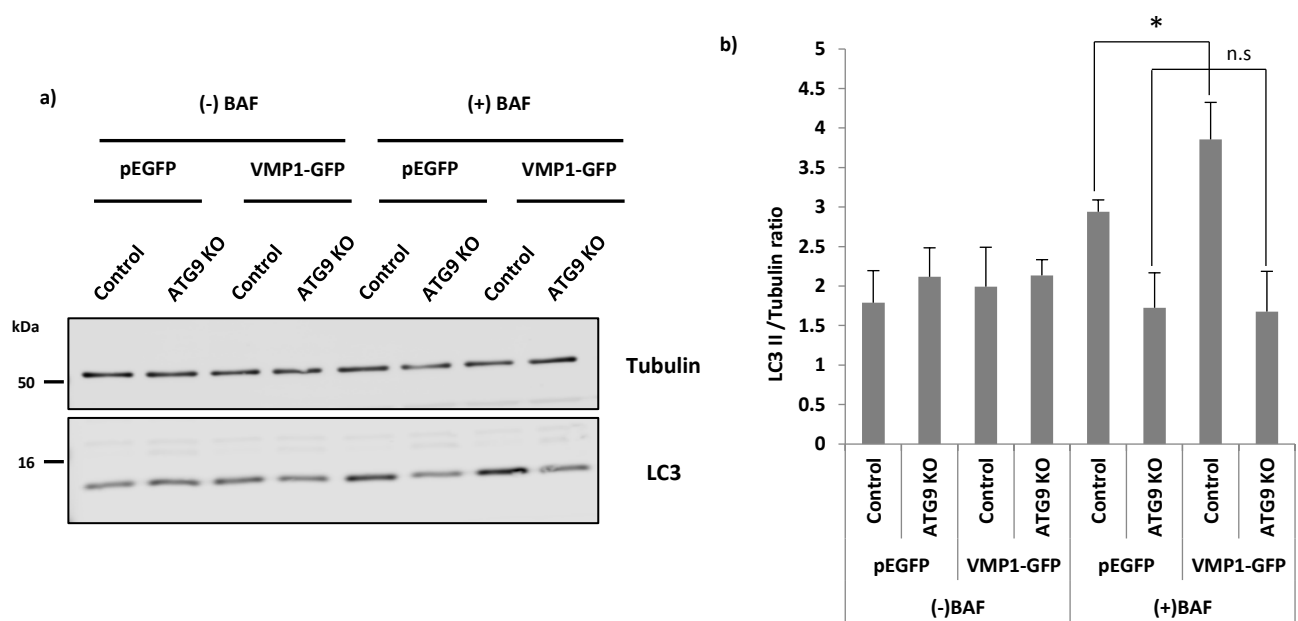
Fig 6.4 a) Representative western blot showing that the induction of autophagy on VMP1 overexpression is ATG9 dependent and can be seen in the presence of BAF. **b)** Quantification of the western blot performed using the LICOR-imaging software. The data is from the quantification of two experiments in triplicates and the error bars represent SEM. (* = $p < 0.05$, n.s = non-significant)

6.5. VMP1 trafficking is dynamin-independent

As observed in Fig 6.1 b, VMP1 does not accumulate on the plasma membrane under conditions of dynamin inhibition. I confirmed this observation by treating the cells with the dynamin inhibitor, dynasore, and checking the co-localisation between the adaptor protein AP2 and endogenous VMP1, using TIRF microscopy. The protein AP2 is a member of the clathrin adaptor-family of proteins that is known to help with the endocytic trafficking of transmembrane and membrane-associated proteins together with the help of clathrin. Consistent with the previous observation, VMP1 did not seem to accumulate on the plasma membrane and co-localise with AP2 on dynasore treatment (Fig 6.5 a and b). The inhibitory effect of dynasore was confirmed by checking the uptake of labelled transferrin ligand into the cells (Fig 6.5 c). Since dynamin is an important component of the pathways like clathrin-mediated and caveolin-mediated endocytosis, I tested whether VMP1 traffics through dynamin-independent endocytic pathways. There are 2 major dynamin-independent endocytic pathways identified till date, namely ARF6-associated and the CLIC/GEEC pathway.

ARF6-pathway relies on the activation and inactivation of ARF6, a small molecule GTPase. More specifically, it was shown that in most cases, ARF6 activation was required for the recycling cargo whereas its inactivation is required for the sorting of the cargo after its internalisation. The CLIC/GEEC pathway on the other hand, requires the activities of GRAF1 and ARF1. This pathway is mainly responsible for the internalisation of lipid-anchored proteins such as GPI-anchored proteins and fluid phase endocytosis (Mayor et al., 2014).

Based on this information, I tested if VMP1 traffics via one of these dynamin-independent endocytic pathways. The standard method used to detect whether a protein traffics via the ARF6 pathway is to check whether the protein of interest co-localises with ARF6 and its mutants. The GTP-binding defective mutant, ARF6-T27N, localises to tubular membrane compartment while the constitutively active mutant, ARF6-Q67L, localises to internal vacuolar compartment enriched in PIP2 (phosphatidylinositol-4,5-bisphosphate). Additionally, the cells could be treated with the actin inhibitor cytochalasinD (cytoD) which shifts the distribution of ARF6 to a tubular membrane compartment that origins from juxtanuclear region of the cells, that resembles the phenotype observed on the overexpression of ARF6-T27N (Radhakrishna and Donaldson, 1997). A control that is also quite commonly used to test the ARF6-pathway is to treat the cells with the inhibitor, BrefeldinA (BFA). BFA is known to inhibit ARF1 but not ARF6, therefore, the localisation of the protein of interest should not change (Donaldson, 2003; Mayor et al., 2014; Radhakrishna and Donaldson, 1997). Based on the above information, I observed that VMP1 co-localises with ARF6-GFP, ARF6-T27N-GFP and ARF6-Q67L-GFP. It was also observed that VMP1 co-localises with overexpressed ARF6-GFP under cytoD treated conditions and its localisation does not change under BFA treated conditions (Fig 6.6). Furthermore, VMP1 co-localises with MHC-I, which is a known cargo protein that traffics via ARF6-associated pathway (Radhakrishna and Donaldson, 1997) and the co-localisation of VMP1 with MHC-I does not change upon its treatment with cytoD (Fig 6.7 a). In addition, the co-localisation of VMP1 with endogenous ARF6 under cytoD treated conditions shows a small but non-significant increase compared to DMSO (Fig 6.7 b). However, it is important to note that the antibodies for both endogenous MHC-I and ARF6 have a very diffuse cytosolic staining, skewing the co-localisation under untreated conditions towards higher levels, thereby making the magnitude of difference in co-localisation between proteins lower (Fig 6.7 a and b).

6.6. ATG9 also traffics via ARF6-associated endocytic pathway

Since I identified that VMP1 traffics through the dynamin-independent ARF6-associated endocytic pathway and that it physically interacts with ATG9, I tested whether ATG9 traffics through the ARF6-associated pathway too. Studies till date have identified ATG9 trafficking only through the dynamin and clathrin-dependent endocytic routes from the plasma membrane (Puri et al., 2013). Interestingly, ATG9 co-localises with ARF6-GFP, ARF6-T27N-GFP and ARF6-Q67L-GFP, indicating that it also traffics through the ARF6-associated dynamin-independent endocytic pathway (Fig 6.8). In addition, the distribution of ATG9 changes completely on treatment of cells with cytoD and it resembles the distribution pattern of ARF6-GFP, with no change in this distribution on treatment with brefeldin A (Fig 6.8). Furthermore, ATG9 also co-localises with MHC-I under DMSO and cytoD treatment, with the co-localisation increasing under the cytoD treated conditions (Fig 6.9 a). However, since the co-localisation of ATG9 and MHC-I under basal state is very high, the magnitude of increase in co-localisation between ATG9 and MHC-I is non-significant. Furthermore, ATG9 was also seen to co-localise with endogenous ARF6. However, when the cells were treated with cytoD to disrupt ARF6 pathway the co-localisation of ATG9 with ARF6 decreased, indicating that this might not be the predominant trafficking pathway for ATG9 in the cells (Fig 6.9 b). Finally, ATG9 was also seen to co-localise with VMP1-GFP and ARF6-T27N-HA confirming they co-traffic via this pathway (Fig 6.10 a).

Finally, in addition to the ARF6-mediated endocytic pathway, VMP1 was also seen to co-localise with GRAF1-BAR-PH-GFP (GRAF1 missing the GAP, proline rich and SH3 domain), a protein that acts in dominant-negative fashion and labels stabilised early endosomal tubular structures (Fig 6.10 b) (Lundmark et al., 2008). However, further experiments need to be performed to confirm if VMP1 traffics via the CLIC/GEEC pathway in addition to ARF6-associated endocytic pathway. It is also worth noting that these observations are consistent with the previous study showing the role of ARF6 and GRAF1 proteins in autophagy regulation (Moreau et al., 2012).

a) AP2   VMP1   Merge

DMSO

Dynasore

Transferrin-488

b)

c)
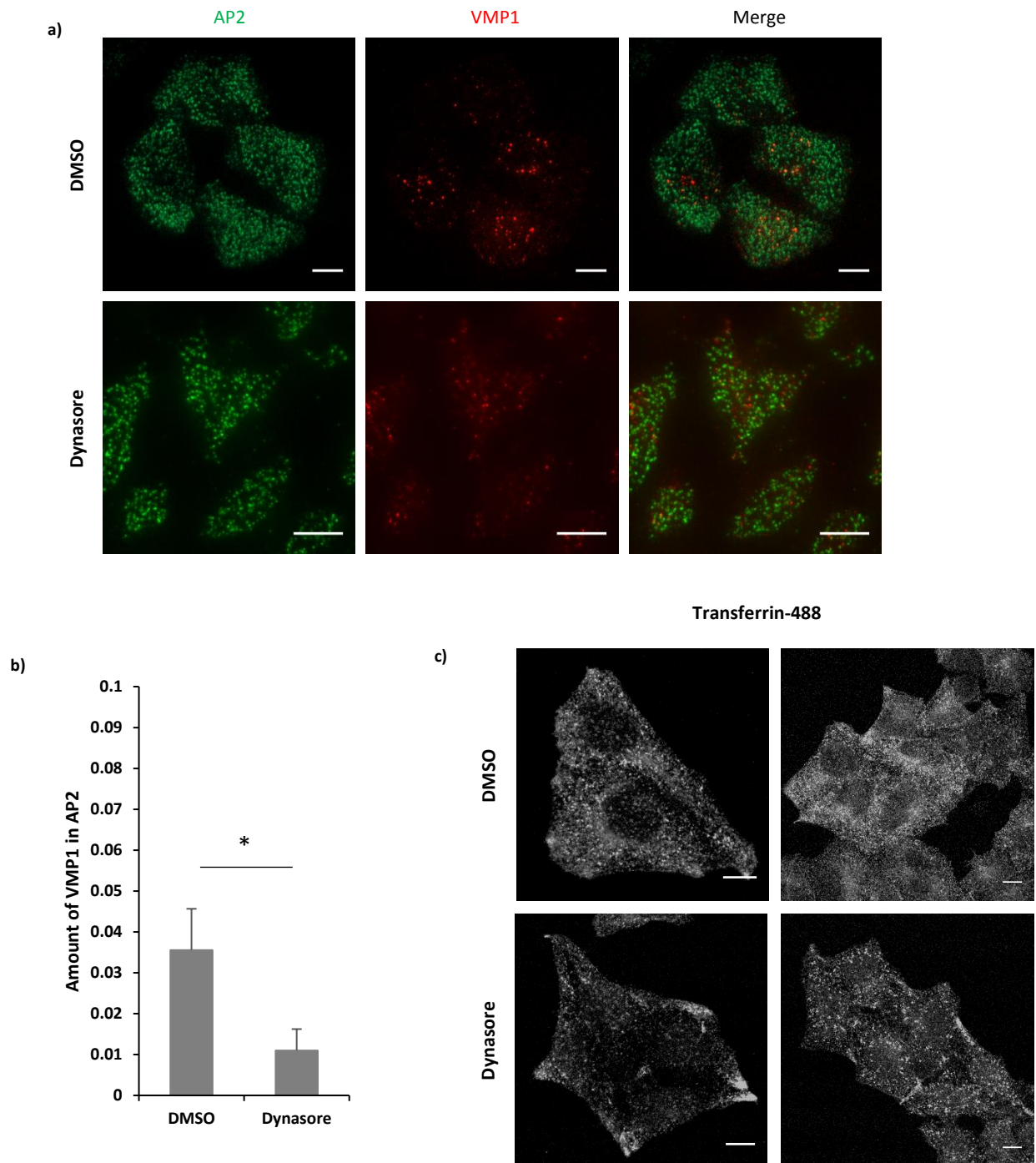
DMSO

Dynasore

Fig 6.5 a) Representative immunofluorescence images showing the localisation of VMP1 and AP2 under DMSO and dynasore treated conditions using TIRF microscopy. **b)** Quantification of the mander's co-localisation co-efficient was performed using the Volocity quantification tool and the data was plotted ($* = p < 0.05$). Quantification performed from 3 experiments with at least 25 cells quantified for each condition. The error bars represent standard deviation (SD). c) Representative immunofluorescence images showing the effect of dynasore on labelled transferrin uptake. The scale bar represents a distance of 10µm.
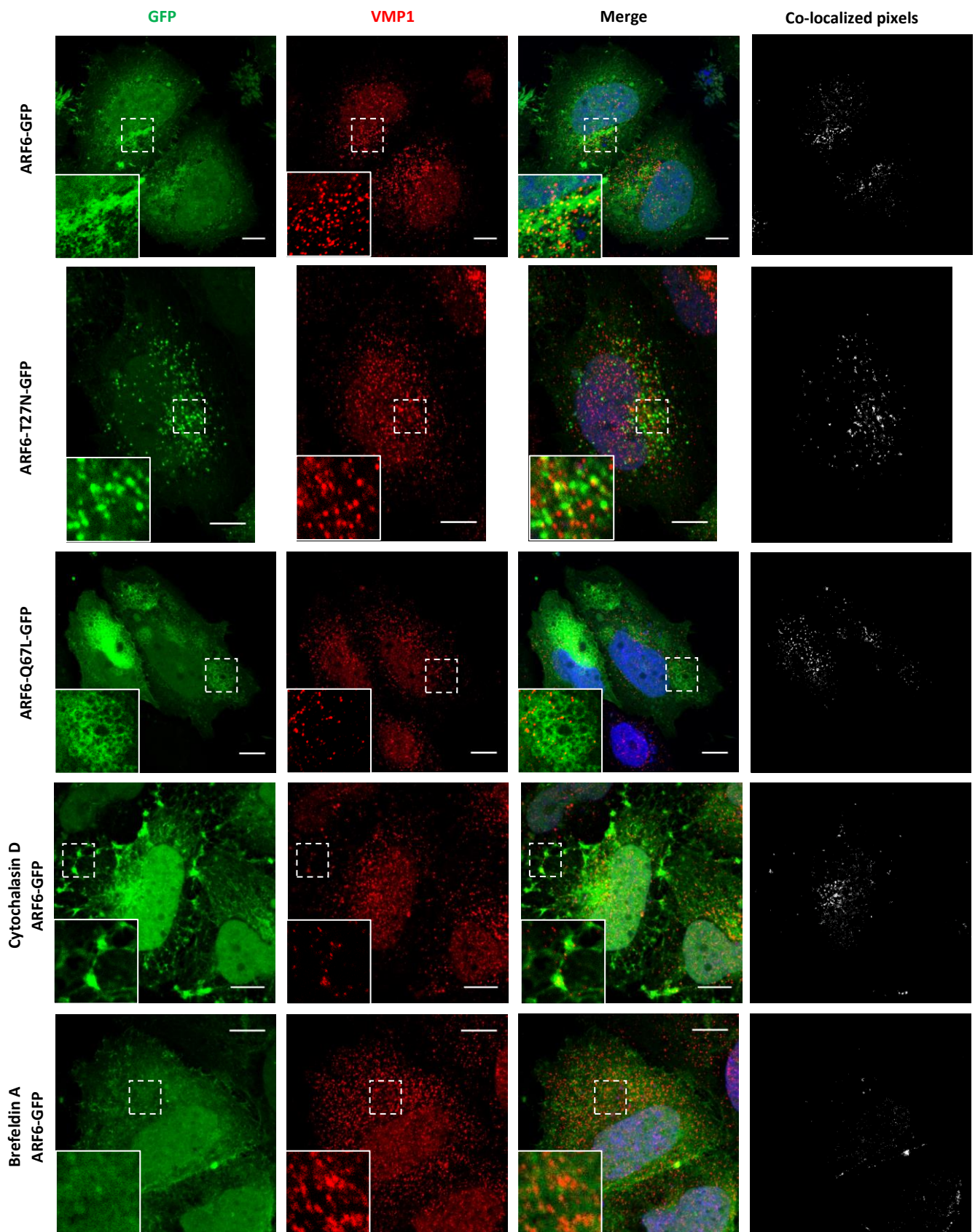
Fig 6.6 Representative immunofluorescence images showing the localisation of VMP1 with ARF6-GFP, ARF6-T27N-GFP, ARF6-Q67L-GFP and with ARF6-GFP under cytochalasinD and brefeldinA treated conditions. The

cytochalasinD treatment is known to resemble the phenotype of the cells upon ARF6-T27N-GFP overexpression, whereas treatment with brefeldinA was used as a control due to its specificity against ARF1 and not ARF6. The co-localisation pixels were identified and a profile was generated using an unsupervised ImageJ plugin algorithm called colocalization, which was developed by Pierre Bourdoncle (Institut Jacques Monod, Service Imagerie, Paris; 2003-2004). The algorithm allows manual thresholding of the acquired images that facilitates the elimination of background noise based on pixel intensities of different channels to generate a profile with grey pixels representing co-localisation of the markers. Briefly, the cells were fixed with PFA, labelled and imaged for endogenous VMP1 and the overexpressed GFP signal. The co-localisation between the two channels was then visualised by looking at the grey pixels in the co-localisation pixels panel. As mentioned above, the grey pixels represent the identified pixels above threshold that are present in both green and red channels and therefore, represents co-localisation between the used markers. The scale bar represents a distance of 10µm.
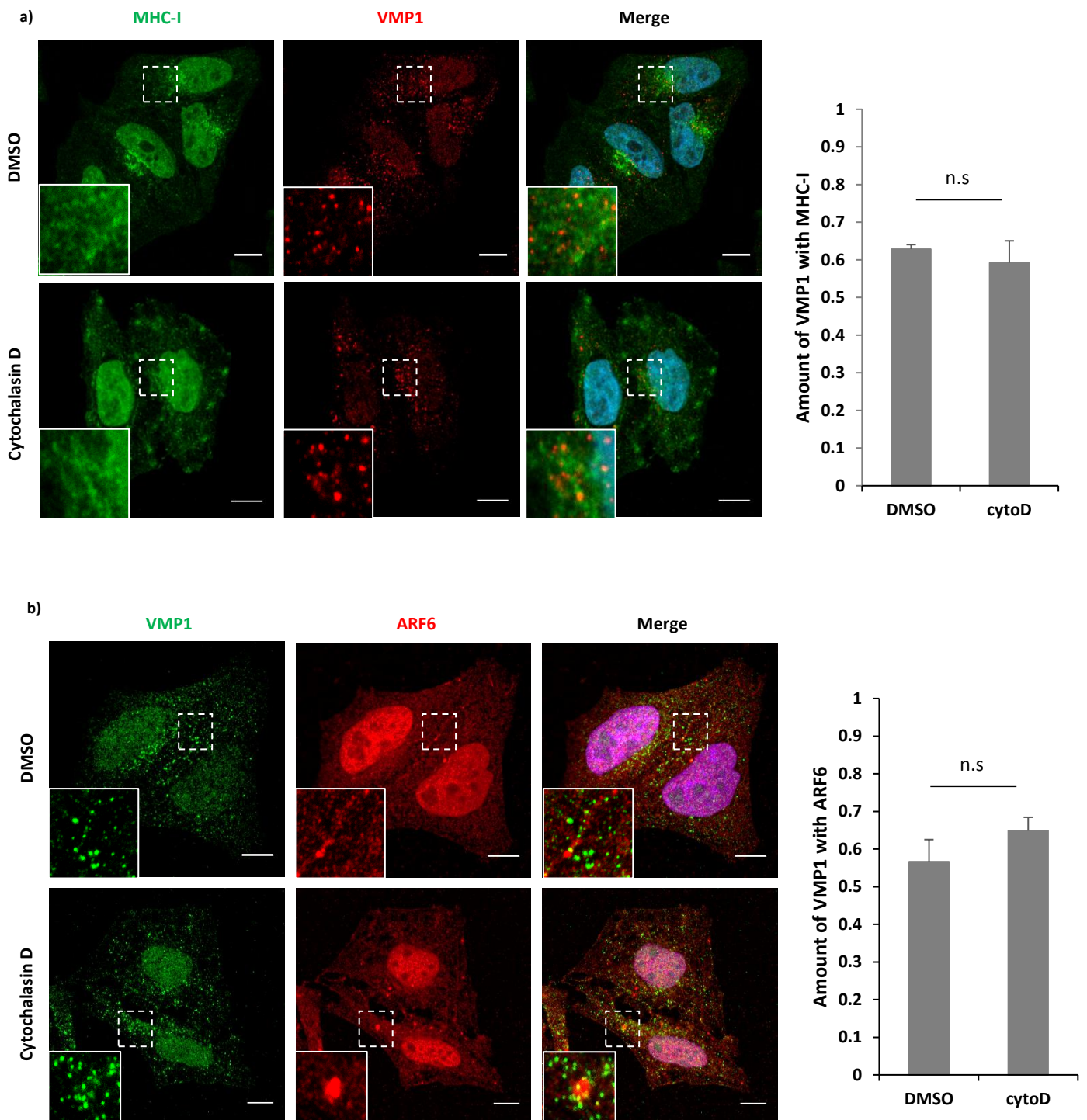
Fig 6.7 a) Representative immunofluorescence images showing the co-localisation of VMP1 with MHC-I under DMSO and cytochalasinD treated conditions. **b)** Representative immunofluorescence images showing the co-localisation of VMP1 with endogenous ARF6 under DMSO and cytochalasinD treated conditions (n.s = non-significant). Quantification performed from 3 experiments with at least 25 cells quantified for each condition. The error bars represent standard deviation (SD). The scale bar represents a distance of 10µm.
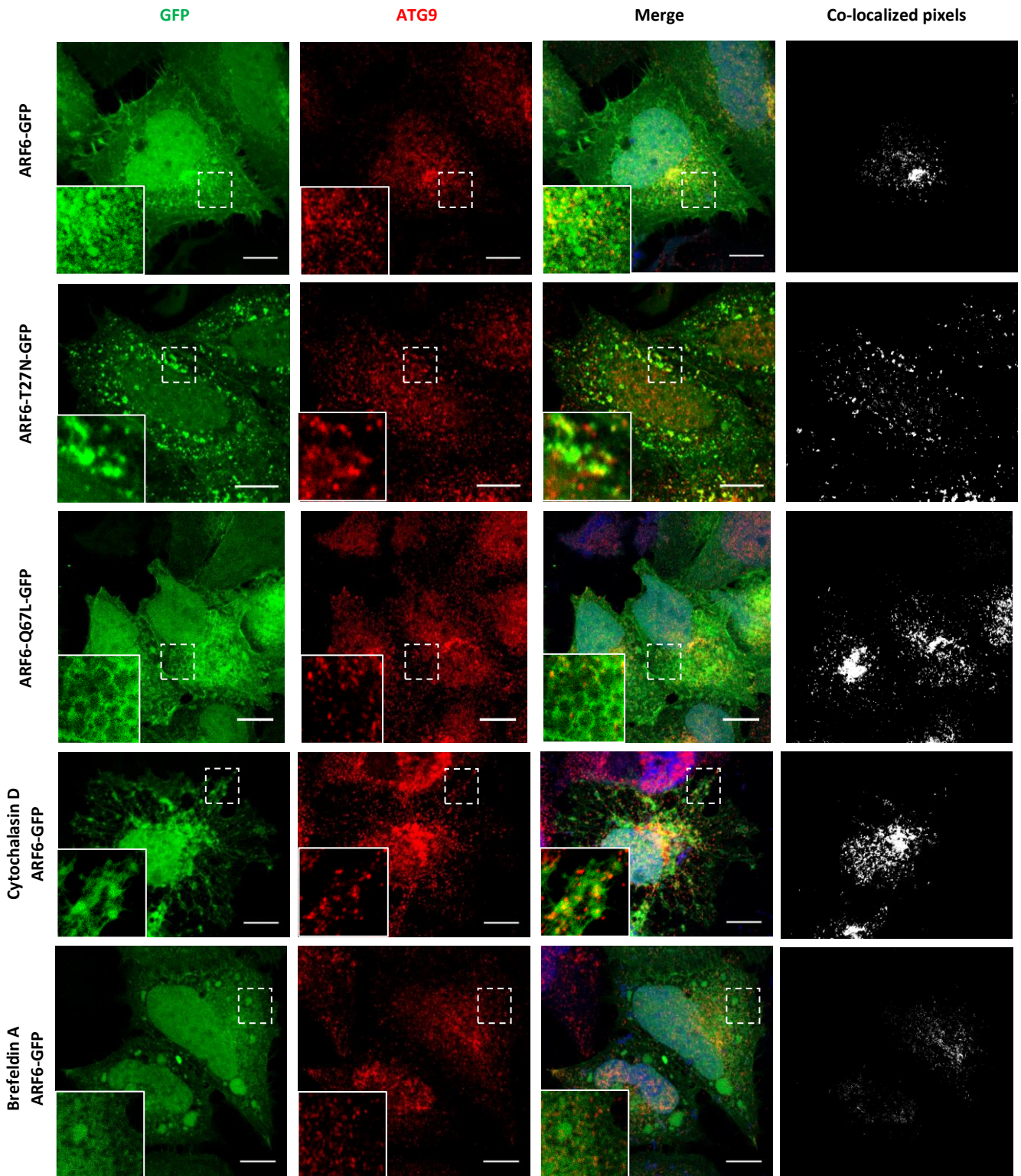
Fig 6.8 Representative immunofluorescence images showing the localisation of ATG9 with ARF6-GFP, ARF6-T27N-GFP, ARF6-Q67L-GFP and with ARF6-GFP under cytochalasinD and brefeldinA treated conditions. The cytochalasinD treatment is known to resemble the phenotype of the cells upon ARF6-T27N-GFP overexpression, whereas treatment with brefeldinA was used as a control due to its specificity against ARF1 and not ARF6. The

co-localisation pixels were identified and a profile was generated using an unsupervised ImageJ plugin algorithm called colocalization, which was developed by Pierre Bourdoncle (Institut Jacques Monod, Service Imagerie, Paris; 2003-2004). The algorithm allows manual thresholding of the acquired images that facilitates the elimination of background noise based on pixel intensities of different channels to generate a profile with grey pixels representing co-localisation of the markers. Briefly, the cells were fixed with PFA, labelled and imaged for endogenous ATG9 and the overexpressed GFP signal. The co-localisation between the two channels was then visualised by looking at the grey pixels in the co-localisation pixels panel. As mentioned above, the grey pixels represent the identified pixels above threshold that are present in both green and red channels and therefore, represents co-localisation between the used markers. The scale bar represents a distance of 10µm.
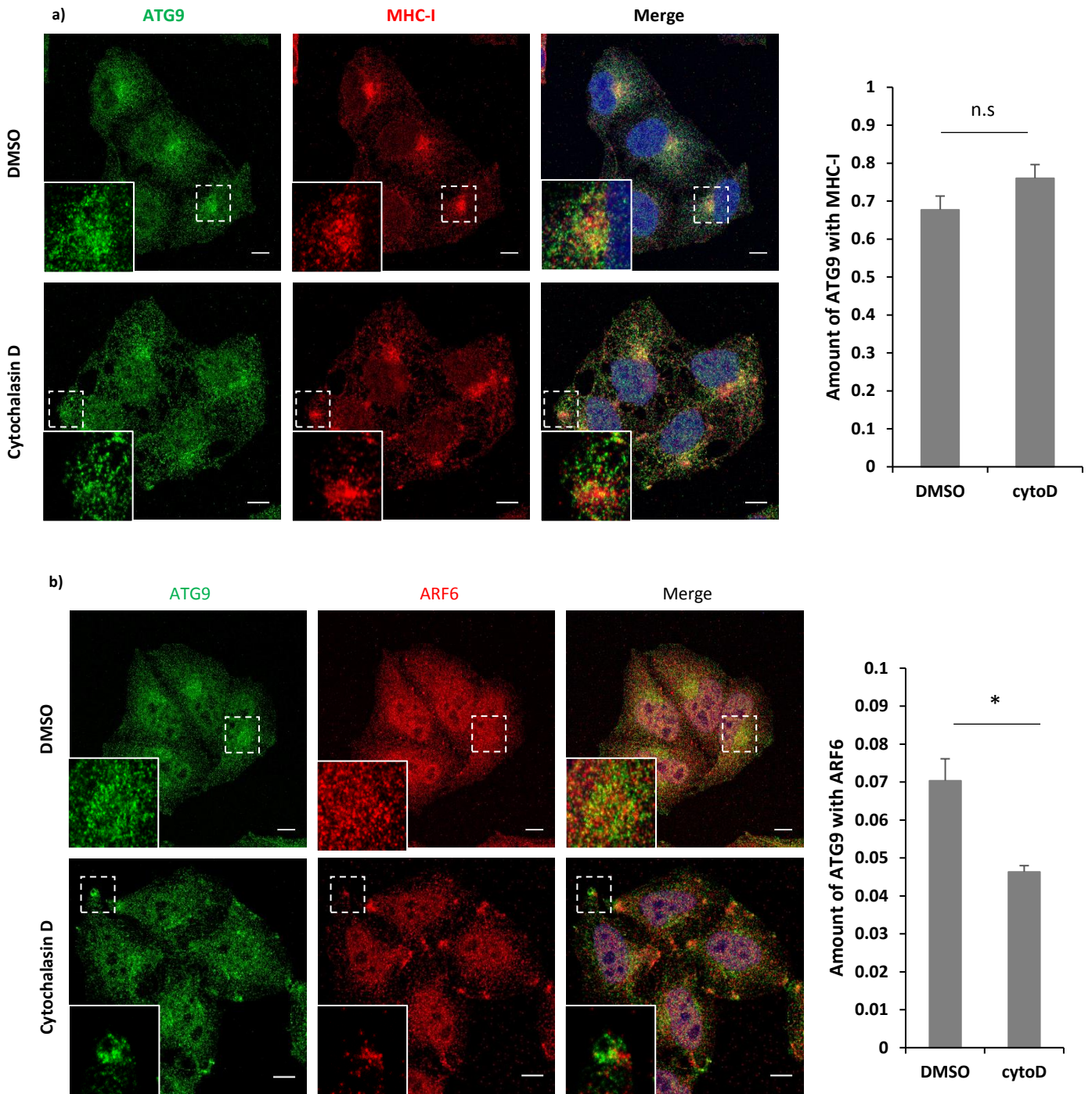
Fig 6.9 a) Representative immunofluorescence images showing the co-localisation of ATG9 with MHC-I under DMSO and cytochalasinD treated conditions. **b)** Representative immunofluorescence images showing the co-localisation of ATG9 with endogenous ARF6 under DMSO and cytochalasinD treated conditions (* = p <0.05, n.s = non-significant). Quantification performed from 3 experiments with at least 25 cells quantified for each condition. The error bars represent standard deviation (SD). The scale bar represents a distance of 10µm.
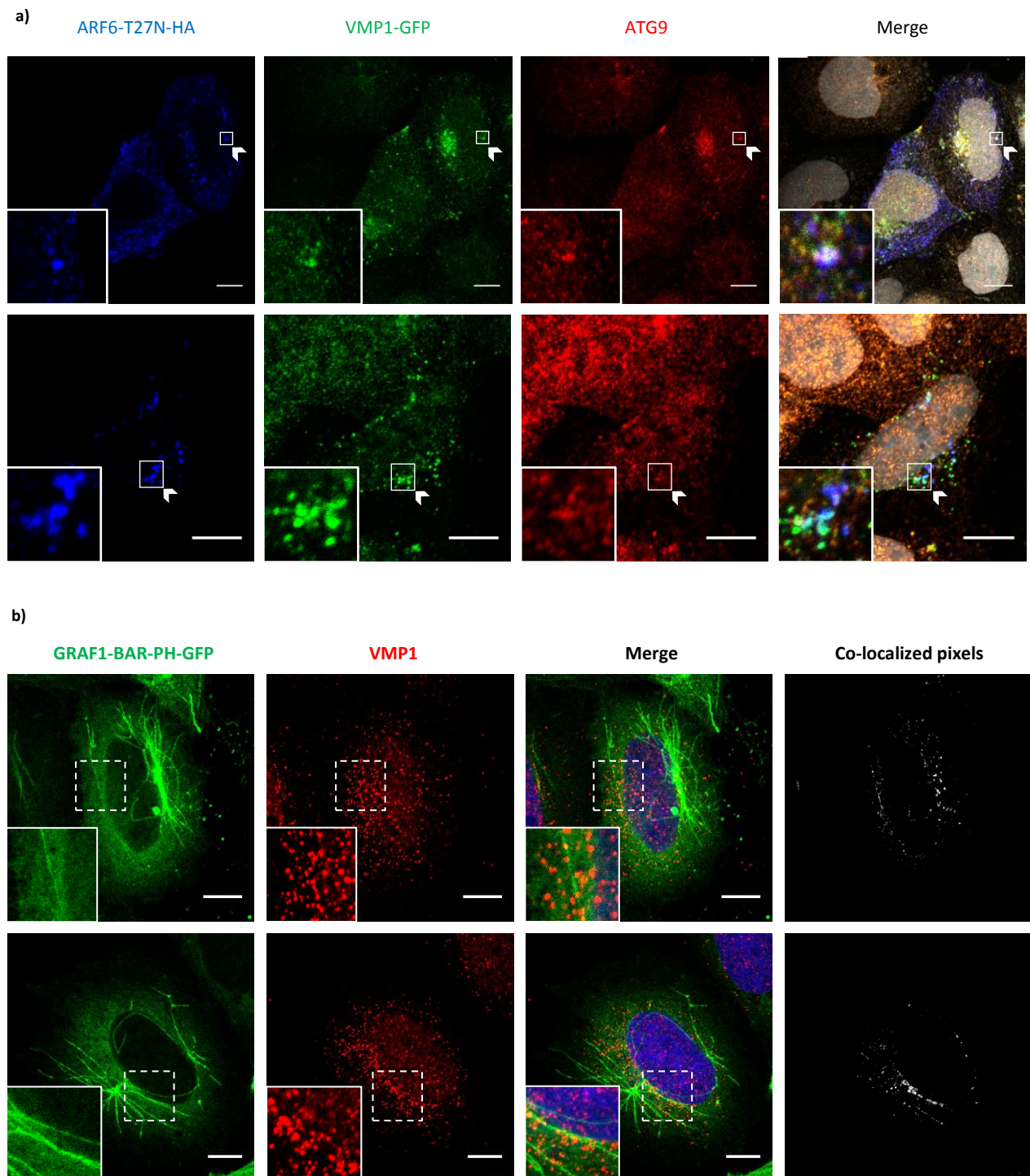
Fig 6.10 a) Representative immunofluorescence images showing the co-localisation of ATG9 with VMP1-GFP and ARF6-T27N-HA. **b)** Representative immunofluorescence images showing the co-localisation of VMP1 with GRAF1-BAR-PH-GFP. The GRAF1-BAR-PH-GFP (GRAF1 missing the GAP, proline rich and SH3 domain) protein overexpression acts in dominant-negative fashion and labels stabilised early endosomal tubular structures. The scale bar represents a distance of 10µm.

To summarize, in this chapter I show that VMP1 traffics in the cell through plasma membrane, early endosomes and recycling endosomes. This trafficking pathway highly resembles the trafficking route of ATG9. I then show that these two transmembrane proteins physically interact with each other in the cell. Next, I show that the induction of autophagy on VMP1 overexpression, as shown by previous studies, is dependent on the expression of ATG9 in the cells, since ATG9 knockout cells show no autophagy induction on VMP1 overexpression. Finally, I show that VMP1 trafficking is unaffected on dynamin-inhibition and that it traffics in the cells via dynamin-independent ARF6-associated pathway. I also show that ATG9 traffics via the same pathway and both ATG9 and VMP1 co-localise with ARF6-T27N mutant, MHC-I and endogenous ARF6. A schematic depicting the proposed trafficking for ATG9 and VMP1 via the ARF6-associated endocytic pathway has been shown in the Fig 6.11.
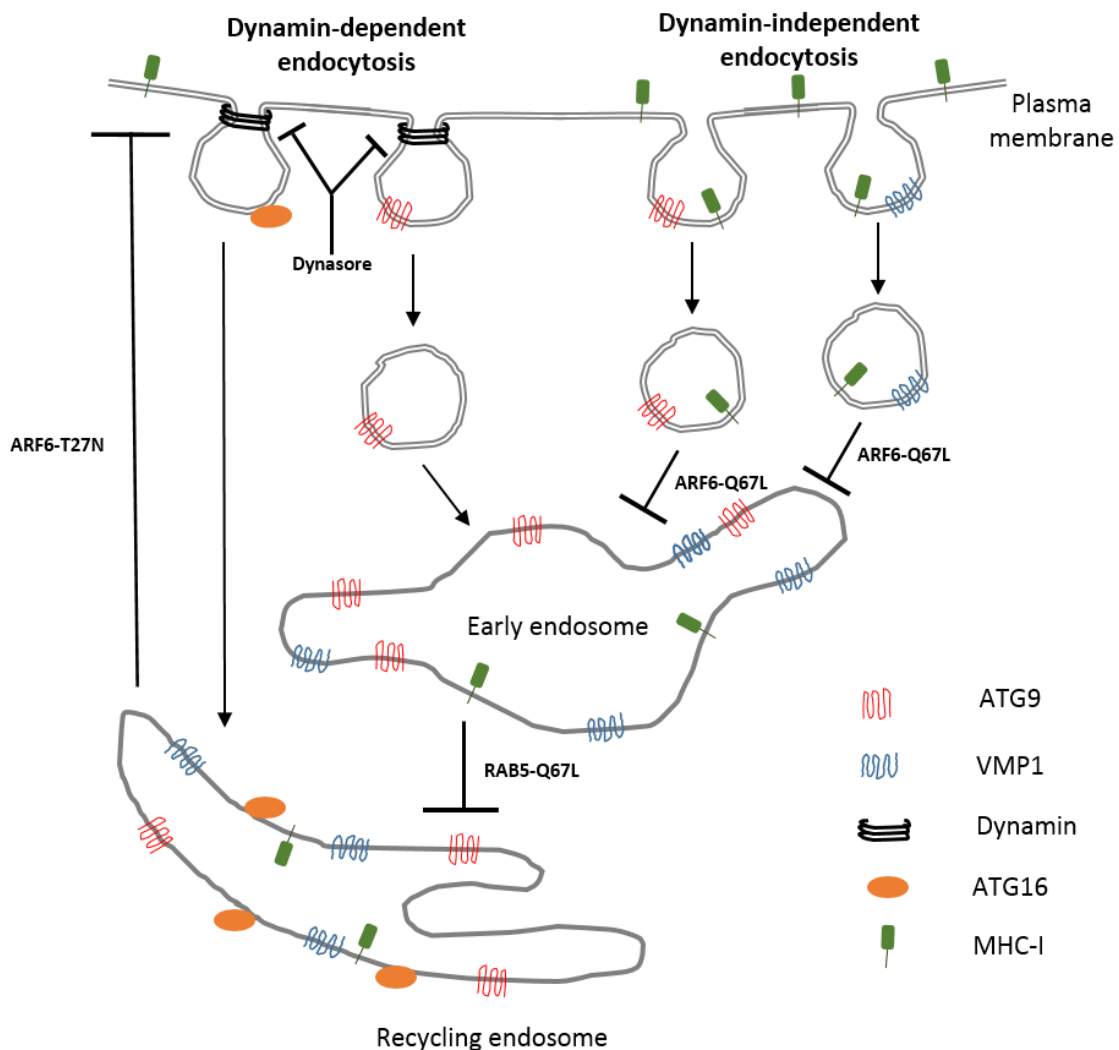
Fig 6.11 A schematic depicting the proposed trafficking route for the two transmembrane proteins ATG9 and VMP1. Current literature has established the trafficking of ATG9 via the dynamin-dependent pathway from the plasma membrane to early endosomes to recycling endosomes. At recycling endosomes, ATG9 was shown to meet ATG16 which also travels from the plasma membrane via a different route that was seen to be clathrin-dependent and hence, dynamin-dependent, directly to recycling endosomes (Puri et al., 2013). My results from this thesis identify a dynamin-independent route for the trafficking of the autophagy proteins ATG9 and VMP1 (a protein whose trafficking pathway remains unexplored). Different mutants were used during the study to block specific ARF6-mediated trafficking routes and their corresponding sites of action to block trafficking have therefore been shown in the schematic. Finally, MHC-I which is a known protein that traffics via ARF6-mediated pathway has been shown for better understanding of the process. Please refer to the legend for description of the various symbols used in the schematic. This schematic has been adapted from Sannerud et al. (2011).

7.   Discussion

In this chapter, I will discuss the results in context of the published literature and its impact on some of the hypotheses that exist in the field of autophagy. I will also try to present a few ideas based on my results that would need further experimentation for consolidation.

7.1. Human ATG9 has multiple serine residues that undergo phosphorylation upon autophagic stimulation

The role of various post-translational modifications, especially phosphorylation, in protein trafficking and function has been well-documented in the literature and some of the key phosphorylation events affecting the autophagic process have also been briefly described in section 1.6 of this thesis. The trafficking of the transmembrane autophagy protein, ATG9, was recently characterised and was shown to involve its movement from the plasma membrane to early endosomes, to finally meet ATG16 in recycling endosomes (Puri et al., 2013). Subsequent studies have then hypothesised recycling endosomes as a platform for de-novo autophagosome formation indicating a potential role of ATG9 and ATG16 in autophagosome formation (Puri et al., 2018). Therefore, understanding the regulation of trafficking of ATG9 from the plasma membrane to recycling endosomes could provide vital information about the events that regulate early stages of autophagosome formation.

I, therefore, decided to test the role of phosphorylation in the regulation of ATG9 trafficking and my results from chapter 3 of this thesis indicate the presence of multiple phosphorylation sites on ATG9 which are potentially regulated by various stimuli, differentially. The results showed that under basal conditions, ATG9 was found to be potentially phosphorylated on 5 different residues namely serine 14, 656, 735, 741 and 828. Similarly, under starvation, ATG9 was observed to be phosphorylated on 4 different residues, namely serine 14, 656, 735, and 828. Furthermore, upon stimulating the cells with trehalose, ATG9 was observed to be phosphorylated on 7 different residues namely serine 14, 18, 635, 735, 738, 741, and 828. Of these sites, only two residues (serine 14 and 18) were observed to be located on the N-terminus of ATG9 while the rest of the sites (serine 635, 735, 738, 741, and 828) were located at the C-terminus. This might be in correlation with the shorter length of the N-terminal of ATG9 as opposed to the much longer C-terminal tail of the protein. It is also worth noting that ATG9

was observed to be phosphorylated on one residue less upon stimulating the cells with starvation compared to basal conditions. This might indicate towards a potential upregulation of the ATG9 function, and thereby autophagy, via dephosphorylation of a site. The role of phosphorylation, in general, implies an activation upon phosphorylation and deactivation upon dephosphorylation, of the substrate. Therefore, activation of ATG9 upon starvation via dephosphorylation could potentially indicate a rather unusual mode of regulation of ATG9 function/activity.

To test the importance of identified phosphorylation sites on ATG9, various non-phosphorylatable and phospho-mimetic mutants were generated. These were then transfected in ATG9 CRISPR knockout cells to identify mutants that could rescue the LC3-II or LC3-I levels of these cells. However, upon examination of the expression levels of various ATG9 mutants in these cells, it was observed that the level of expression of the mutant ATG9 proteins is affected by the state of phosphorylation of these sites. The results indicated that while these sites were thought to be the primary regulators of the trafficking, they might also be responsible for maintaining the stability of ATG9. Indeed, regulation of protein stability via phosphorylation of proteins has also been widely considered as an important cellular pathway regulating processes such as cell proliferation, apoptosis, etc (Xu et al., 2009). Therefore, studying the phosphorylation of ATG9 might provide us with information more than just the regulation of trafficking and could implicate ATG9 as a potential substrate for an important kinase in the various cellular signalling axes.

Finally, my results, through mass spectrometry, indicated towards a kinase (PRKDC) that might be responsible for the potential phosphorylation of one or more sites on ATG9. This interaction was seen to be highly specific based when confirmed using other biochemical and immunofluorescence techniques. Interestingly, the identified kinase is known to be an important player regulating the repair mechanism upon DNA-damage and therefore, is known to primarily localise to the nucleus of the cell. However, the function of the cytosolic population of PRKDC remains unexplored. The specific interaction of PRKDC with the transmembrane protein ATG9 could therefore potentially hint towards one of its function in the cytosol. Furthermore, upon testing the ATG9 sequence for potential consensus sequences for various kinases, a potential site that resembles the consensus sequence for PRKDC was also found supporting the hypothesis of ATG9 phosphorylation by PRKDC under certain conditions. However, as the kinase performs an essential function in cell survival, various strategies to

decrease the activity of the kinase resulted either in cell death or accumulation of non-specific phenotypes in cells, thereby making the study of the effect of the potential phosphorylation by PRKDC on ATG9 difficult. Further experiments, perhaps involving the use of inducible PRKDC-knockout systems could facilitate the investigation of involvement of the kinase in the regulation of autophagy via ATG9 phosphorylation.

7.2. p62 – a homeostasis maintaining protein in autophagy-impaired cells

One of the key requirements for maintaining cellular homeostasis is the removal of aggregated proteins since aggregated proteins are associated with the pathologies of various neurodegenerative conditions (Bento et al., 2016b). The eukaryotic cells remove the aggregated proteins via two primary pathways namely the ubiquitin-proteasome system (UPS) and autophagy. The UPS involves ubiquitination of the cargo destined for degradation, which is recognised by the proteasome and subsequently degraded. Autophagy, on the other hand, is known to engulf proteins and other cellular constituents, that could also be ubiquitinated, destined for degradation with the help of autophagy receptor proteins like p62 and their subsequent delivery to lysosomes for degradation. The ubiquitin linkage pattern on the substrate determines its fate of degradation either by UPS or autophagy. The current knowledge indicates that K48 linkage, the primary form of ubiquitination, is associated with UPS while K63 linkage is associated with autophagic degradation of the cargo. Studies have also shown that these degradative processes work together to maintain homeostasis, acting as a backup for each other (Lilienbaum, 2013). It is worth noting that while p62 plays a defined role in cells with functional autophagy (Bento et al., 2016b), its role in cells lacking autophagy remains unknown. In cells with functional autophagy, p62 as autophagy receptors but the autophagy receptor proteins also act as a substrate for autophagy themselves. A lack of functional autophagy, therefore, results in the accumulation of autophagy receptors such as p62.

My results in chapter 5 of this thesis identify a potential role for p62 in autophagy-impaired cells. It was observed that cells with defective autophagy, due to lack of a core autophagy protein expression like ATG9 or ATG16, accumulate a lot more of the unconjugated-form (LC3-I) compared to PE-conjugated form (LC3-II). This effect is more pronounced in ATG16 null cells due to the lack of functional lipidation machinery. Since LC3 is primarily degraded

by the autophagosomes fusing with lysosomes, a cell with defective autophagy would lead to a large accumulation of LC3. This could potentially result in formation of large aggregates in the cells that interfere with various cellular processes and homeostasis. My results show that under conditions where the ever-growing pool of LC3 cannot be degraded by autophagy, LC3 (more specifically LC3-I) associates itself with p62. Since p62 forms aggregates which were seen to be ubiquitinated, it is likely that these aggregates are then directed for degradation by the UPS; however, more experiments need to be performed in order to confirm this hypothesis. This, therefore could be another example of the interplay between the process of autophagy and UPS to maintain cellular homeostasis.

A gold standard way of measuring the autophagic synthesis in cells is to test the levels of LC3-II in cells treated with or without drugs that block autophagosome-lysosome fusion such bafilomycin A1 (BAF). Autophagic flux measures the autophagic degradation activity and treating the cells with BAF inhibits the degradation and therefore, resulting in an accumulation of autophagosomes, making it a suitable assay to measure autophagic flux (Rubinsztein et al., 2009). Another gold standard assay to check the effect of various experimental conditions/treatments on autophagy is via the staining, visualisation and subsequent quantification of endogenous LC3 vesicles in the cell using immunofluorescence assay (Klionsky et al., 2016). However, the only known limitation of this assay is that it cannot be used to assess the autophagic flux. My results from chapter 4 highlight another important drawback of the LC3-immunofluorescence assay. Under conditions where the autophagic activity decreases, I show that LC3-I appears on discrete structures that are associated with p62. Although at first sight these structures might resemble the canonical morphology of LC3-II puncta, these structures tend to be larger and were exclusively dependent on the levels of p62 in these cells. These LC3-I positive structures in autophagy-impaired cells could easily be confused as mature autophagosomes. Thus, my results highlight that LC3 immunofluorescence assays are unsuitable under conditions where the cells being tested lack autophagy partially (ATG9 knockout) or completely (ATG16 knockout).

A recent study characterising the p62 filaments show that while the presence of LIR (LC3-interacting region) motif in p62 is crucial for its cluster formation, in the presence of mCherry-LC3B cluster formation of p62 is inhibited (Zaffagnini et al., 2018). In line with these observations, my results potentially show that larger p62 aggregates show much lower levels of LC3 association with them compared to 'growing' p62 aggregates. This can be visualised in

the super-resolution images of ATG16 null cells (Fig 5.5 b and c), where larger p62 aggregates show lower levels of association with LC3 compared to smaller 'growing' p62 aggregates. However, further experimentation is needed to show that this indeed is the case. A schematic representing the possible homeostatic role of p62 is shown in Fig 7.1

I will now try to present some of the open questions relevant to my study with potential answers in context of the existing literature. The study that describes the p62 cluster formation propensities in the presence of LC3 and ubiquitin molecules explains the broader phenomenon of p62 aggregate formation/nucleation very clearly (Zaffagnini et al., 2018). However, it would be interesting to understand how p62 differentiates between the forms of LC3 viz. LC3-I and LC3-II and understand their respective binding affinities with p62. Furthermore, if under steady state there exists an equilibrium between the levels of two forms of LC3, that dictates their binding with p62, how does it get perturbed under conditions where autophagy is affected under conditions such as rare form of hereditary spastic paraplegia caused due to AP-4 deficiency. Moreover, while my results show that p62 acts as a platform that associates with LC3-I, it would be interesting to understand the requirement of LC3 for the growth of p62 aggregates. It could be possible that LC3-I molecules binding to p62 facilitate its aggregation dynamics and act as potential nucleators for the process but are also counter-productive at later stages due to steric hindrance between these proteins. Another interesting idea, which could potentially resolve the problem of ambiguous LC3 recognition in immunofluorescence assays, is whether the topology/conformation of PE-conjugated LC3 molecule could be used as an epitope to develop antibodies that can effectively distinguish between the two forms of LC3.

Another important question to answer would be whether this phenomenon is exclusive to p62 amongst other autophagy receptors and is this observation cell-line specific. The family of autophagy receptors in the mammalian system includes several members like p62/SQSTM1, NBR1 (neighbour of BRCA1), optineurin (OPTN), NDP52, etc. These members show presence of conserved UBD and LIR motifs to facilitate the engulfment of the cargo into the autophagosomes (Rogov et al., 2014; Stolz et al., 2014). Therefore, it is possible that the homologous partners of the autophagy receptors spread across different species might perform a homeostatic role similar to the one discussed above for p62 under autophagy-impaired conditions.
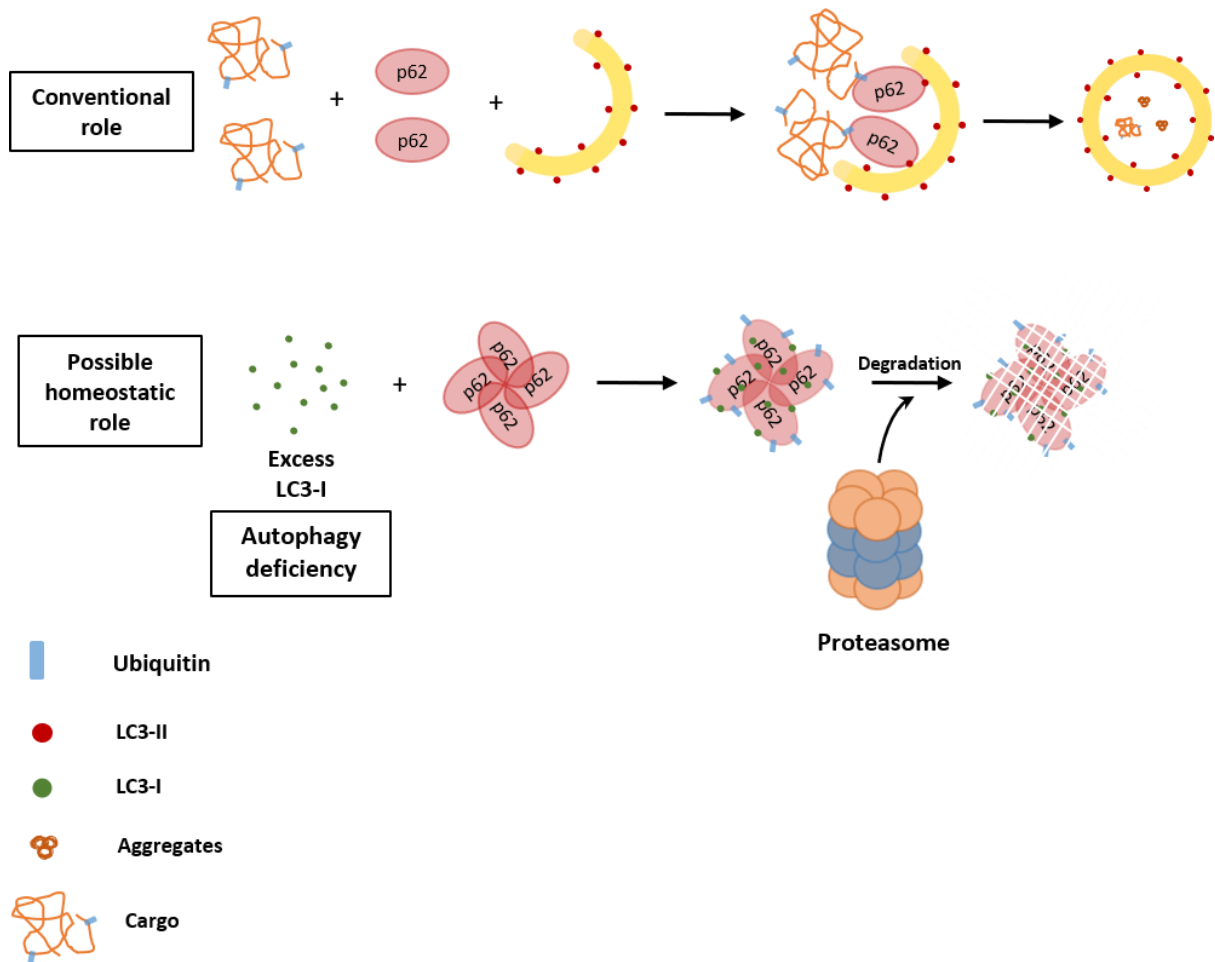
Fig 7.1 A schematic depicting the possible roles of p62 in cells. The homeostatic role of p62 is likely activated under conditions where autophagic degradation of substrate/cargo is affected. Under these conditions, p62 associates with the excess LC3-I and possibly helps towards its degradation via the ubiquitin-proteasomal pathway. The possible functions played by p62 also point towards the possible interplay between the two major protein degradation pathways viz. autophagy and ubiquitin-proteasomal pathway. Please refer to the legend for description of the various symbols used in the schematic.

7.3. Possible functions of ATG9

Although ATG9 has been described as a core-autophagy protein for almost two decades, the understanding of its function remains limited. My results in chapter 3 provide some insight towards the possible functions of ATG9. I will now discuss some of the possible functions of ATG9 based on my observations and mention potential experiments that could provide us with more information about ATG9 function.

An important observation in ATG9 knockout cells was the high levels of LC3-I compared to control cells. During the process of autophagosome formation, LC3-I gets converted to LC3-II by its conjugation to a phosphatidylethanolamine molecule (please refer to section 1.2.4 of this thesis for more details). LC3-II is considered as the primary marker for the autophagosomes in cells. After the autophagosomes are fused with the lysosomes, some of the LC3-II molecules on the autophagosome are recycled back via its deconjugation to the cytosolic LC3-I pool and these molecules can then re-enter the process of conjugation as needed (Yu et al., 2012). The observation of higher levels of LC3-I in ATG9 knockout cells could therefore either indicate a defect in the lipidation capability of the cells or an increased/premature recycling of LC3-II from the autophagosomes. It is also worth noting that depending on stage of autophagy where ATG9 acts would also give us information about its activity at either early stages of autophagosome formation or at later stages of autophagosome maturation/fusion. Simple tests such as checking the levels of ATG5-ATG12-ATG16 complex, WIPI2 localisation, ATG4B levels could provide us with information if the lipidation machinery is intact in ATG9 knockout cells. Another experiment that could potentially identify if ATG9 facilitates the LC3-lipidation directly would be an in-vitro liposome lipidation experiment (Zens et al., 2015). This experiment could potentially be setup in the presence or absence of ATG9 and the lipidation machinery with a C-terminal GFP-tagged LC3 as a substrate for the reaction. As the LC3-gets conjugated, it would lose its GFP-tag and the fluorescence of the free GFP molecules can be used to estimate the efficiency of the reaction in the presence or absence of ATG9. These experiments could provide us with the information about the role of ATG9 in lipidation. The role of ATG9 in the recycling of LC3-II from the autophagosomes could be studied by the live-cell imaging of cells transfected with GFP-LC3. Tracking the start and endpoints of lipidation events in the cells based on puncta appearance and disappearance could provide us with the

information about the dynamics of the autophagic process in general together with the time-points where LC3-II gets recycled to LC3-I in the presence or absence of ATG9.

Another interesting observation associated with the ATG9 knockout cells was their lack of a response to bafilomycin-A1 (BAF) treatment. BAF is a lysosomal V-type H^+ ATPase inhibitor that increases the lysosomal pH (inhibiting its acidification) thereby inhibiting the fusion between autophagosomes and lysosomes. The observation might therefore indicate towards impaired fusion between the autophagosomes and lysosomes in ATG9 knockout cells. Indeed, a recent study has shown that ATG9, present at the TGN, plays an important role in the exit of the newly synthesised lysosomal hydrolases from the TGN. They support the claim by showing that ATG9 expression in mammalian system is required for the lysosomal degradation activity using EGFR degradation assay and cathepsin D and L maturation. They also show that this reduced degradation was not a result of lysosomal pH since the pH was seen to be unchanged upon ATG9 knockdown (Jia et al., 2017). These results together with the observation of unchanged lysosomal pH upon ATG9 knockdown might also hint towards a mechanism that involves regulation of autophagosome fusion depending on the maturation of lysosomal hydrolases. Furthermore, it is worth noting that compared to ATG16 knockout cells, ATG9 knockout cells show some amounts of residual autophagy, indicating that ATG9 is not essential for basal levels of autophagy and might only be needed when the autophagic process needs to be upregulated under conditions like starvation.

7.4. Novel trafficking routes for ATG9 and VMP1

The presence of multiple transmembrane domains in ATG9 and VMP1 make them unique in the autophagic system. The trafficking of ATG9 has been studied to a great extent as described in the section 1.3.1 of introduction, and my research identifies a novel trafficking pathway for ATG9 that it shares with VMP1. This identified pathway is a dynamin-independent and ARF6-associated endocytic pathway that eventually merges with the conventional destinations of the endocytic pathway i.e. early and recycling endosomes.

The current understanding of ATG9 trafficking shows it to traffic from the plasma membrane to early endosomes and finally recycling endosomes (Puri et al., 2013). Additionally, ATG9 was also seen to localise in the trans-Golgi network and it possibly redistributes on autophagy

induction to the plasma membrane and eventually endosomes from the TGN (Young et al., 2006). It is worth noting that all these trafficking events rely on the activity of dynamin for their functioning. My results in chapter 6 identify a novel clathrin and dynamin-independent trafficking pathway for ATG9 (Fig 6.11). Furthermore, I also show that VMP1, trafficking of which remains unknown to date, shares its trafficking route with ATG9 and both these transmembrane autophagy proteins traffic through the ARF6-associated pathway. Interestingly, a published study has shown the ARF6 and GRAF1 proteins to regulate autophagosome biogenesis mainly by regulating endocytosis, PIP2 levels and phospholipase D activation. Interestingly, the same study also identified ATG16 to co-localise with overexpressed ARF6-GFP, hinting towards its trafficking via the ARF6-associated pathway (Moreau et al., 2012). In the light of these results, an important challenge would be therefore to understand the functional significance of trafficking of these autophagic proteins through this mode of dynamin-independent endocytosis. My results in conjunction with the published observations might indicate one of the additional ways through which ARF6 could potentially regulate autophagosome biogenesis. Depletion of ARF6, leading to disruption of this pathway, might lead to mislocalisation of the pool of ATG9, VMP1 and ATG16 trafficking through this pathway. This mislocalisation could prevent the proteins from being trafficked to their respective destinations and could therefore be responsible for lower autophagosome biogenesis. Another question raised due to the identification of this pathway would be to understand whether this pathway traffics a unique pool of ATG9 that performs an exclusive function or does it simply act as a backup pathway in case of the primary endocytic pathway failure. This also opens the possibility of regulation of the process of autophagy by a specific class of proteins involved in dynamin-independent endocytosis.

VMP1 overexpression has been shown to induce autophagy (Ropolo et al., 2007). My results extend the observation by showing that VMP1 overexpression needs ATG9 expression in cells to induce autophagy. My results also show that ATG9 and VMP1 physically interact with each other in the cell. It would therefore be interesting to identify which domains in each of these proteins are involved in this physical interaction. It could also be then checked how expression of specific-peptide representing various domains, for ATG9 and VMP1, would affect the autophagy induction on VMP1 overexpression. While the domain structure for human ATG9 is partially known (Fig 1.4) (Tooze, 2010), the domain organisation of VMP1 is relatively unclear. It is also important to note that VMP1 showed a physical interaction with GFP-tagged ATG9 that was cloned from the mouse genome. The mouse ATG9 protein when studied for

conserved domains compared to other species, shows the lack of the long C-terminal tail that is a characteristic of human ATG9 (Fig 1.4), indicating that this region might not be important towards the interaction with VMP1. An experiment involving the cloning of various domains of ATG9 and VMP1 and checking their interactions would provide us with valuable information about the importance of different peptide sequences in these proteins. Importantly, this experiment could also give us information about the nature of the interaction between ATG9 and VMP1. It could be possible that these proteins do not interact with each other directly and involves a third-party that facilitates the interaction between these two. It would also be very interesting to check whether ATG9 interacts with VMP1 while they co-traffic together though their newly identified dynamin-independent trafficking routes and whether that interaction plays a specific function towards autophagic regulation. If it does, this might hint towards a specialised pool of ATG9 that regulates autophagy together with VMP1 by trafficking through ARF-6 associated pathway. Additionally, ATG16 trafficking through the ARF6 pathway (Moreau et al., 2012) could play an important role in facilitating the ATG9, VMP1 interaction.

Finally, I also show that it is highly likely that VMP1 also traffics via the CLIC/GEEC pathway in addition to ARF6-assoicated pathway. This pathway functions independently of the AR6-associated pathway and is mainly responsible for fluid phase and GPI-linked protein endocytosis (Mayor et al., 2014). This raises questions about VMP1 trafficking, similar to ATG9, of whether there are two distinct pools of VMP1 which perform two independent functions. Also, which of these pathways act as a dominant pathway for VMP1 trafficking. The identification of the dynamin-independent pathway for trafficking of some autophagy proteins opens a new avenue for exploring the regulatory components for autophagy and answers to some of these questions might provide us with a deeper insight into the regulation of autophagy. This would also provide impetus towards searching new regulators of ATG9/VMP1 trafficking and function along the dynamin-independent pathway.

8. References

Ashkenazi, A., Bento, C.F., Ricketts, T., Vicinanza, M., Siddiqi, F., Pavel, M., Squitieri, F., Hardenberg, M.C., Imarisio, S., Menzies, F.M.*, et al.* (2017). Polyglutamine tracts regulate beclin 1-dependent autophagy. Nature *545*, 108.

Ashrafi, G., and Schwarz, T.L. (2013). The pathways of mitophagy for quality control and clearance of mitochondria. Cell Death Differ *20*, 31-42.

Ballou, L.M., and Lin, R.Z. (2008). Rapamycin and mTOR kinase inhibitors. Journal of chemical biology *1*, 27-36.

Barth, S., Glick, D., and Macleod, K.F. (2010). Autophagy: assays and artifacts. The Journal of pathology *221*, 117-124.

Bento, C.F., Ashkenazi, A., Jimenez-Sanchez, M., and Rubinsztein, D.C. (2016a). The Parkinson's disease-associated genes ATP13A2 and SYT11 regulate autophagy via a common pathway. Nature Communications *7*, 11803.

Bento, C.F., Renna, M., Ghislat, G., Puri, C., Ashkenazi, A., Vicinanza, M., Menzies, F.M., and Rubinsztein, D.C. (2016b). Mammalian Autophagy: How Does It Work? Annual Review of Biochemistry *85*, 685-713.

Bjørkøy, G., Lamark, T., Brech, A., Outzen, H., Perander, M., Overvatn, A., Stenmark, H., and Johansen, T. (2005). p62/SQSTM1 forms protein aggregates degraded by autophagy and has a protective effect on huntingtin-induced cell death. The Journal of cell biology *171*, 603-614.

Blommaart, E.F., Krause, U., Schellens, J.P., Vreeling-Sindelarova, H., and Meijer, A.J. (1997). The phosphatidylinositol 3-kinase inhibitors wortmannin and LY294002 inhibit autophagy in isolated rat hepatocytes. European journal of biochemistry *243*, 240-246.

Calvo-Garrido, J., Carilla-Latorre, S., Lázaro-Diéguez, F., Egea, G., Escalante, R., and Barr, F.A. (2008). Vacuole Membrane Protein 1 Is an Endoplasmic Reticulum Protein Required for Organelle Biogenesis, Protein Secretion, and Development. Molecular Biology of the Cell *19*, 3442-3453.

Choy, A., Dancourt, J., Mugo, B., O'Connor, T.J., Isberg, R.R., Melia, T.J., and Roy, C.R. (2012). The *Legionella* Effector RavZ Inhibits Host Autophagy Through Irreversible Atg8 Deconjugation. Science *338*, 1072.

Ciuffa, R., Lamark, T., Tarafder, Abul K., Guesdon, A., Rybina, S., Hagen, Wim J.H., Johansen, T., and Sachse, C. (2015). The Selective Autophagy Receptor p62 Forms a Flexible Filamentous Helical Scaffold. Cell Reports *11*, 748-758.

Codogno, P., Mehrpour, M., and Proikas-Cezanne, T. (2011). Canonical and non-canonical autophagy: variations on a common theme of self-eating? Nat Rev Mol Cell Biol *13*, 7-12.

Cuervo, A.M., Knecht, E., Terlecky, S.R., and Dice, J.F. (1995). Activation of a selective pathway of lysosomal proteolysis in rat liver by prolonged starvation. The American journal of physiology *269*, C1200-1208.

DeBosch, B.J., Heitmeier, M.R., Mayer, A.L., Higgins, C.B., Crowley, J.R., Kraft, T.E., Chi, M., Newberry, E.P., Chen, Z., Finck, B.N.*, et al.* (2016). Trehalose inhibits solute carrier 2A (SLC2A) proteins to induce autophagy and prevent hepatic steatosis. Science signaling *9*, ra21.

Deretic, V., Saitoh, T., and Akira, S. (2013). Autophagy in infection, inflammation and immunity. Nature Reviews Immunology *13*, 722.

Donaldson, J.G. (2003). Multiple roles for Arf6: sorting, structuring, and signaling at the plasma membrane. J Biol Chem *278*, 41573-41576.

Dooley, H.C., Razi, M., Polson, H.E.J., Girardin, S.E., Wilson, M.I., and Tooze, S.A. (2014). WIPI2 Links LC3 Conjugation with PI3P, Autophagosome Formation, and Pathogen Clearance by Recruiting Atg12-5-16L1. Molecular cell *55*, 238-252.

Dowdle, W.E., Nyfeler, B., Nagel, J., Elling, R.A., Liu, S., Triantafellow, E., Menon, S., Wang, Z., Honda, A., Pardee, G.*, et al.* (2014). Selective VPS34 inhibitor blocks autophagy and uncovers a role for NCOA4 in ferritin degradation and iron homeostasis in vivo. Nat Cell Biol *16*, 1069-1079.

Du, Y., Wooten, M.C., and Wooten, M.W. (2009). Oxidative damage to the promoter region of SQSTM1/p62 is common to neurodegenerative disease. Neurobiology of disease *35*, 302-310.

Dubouloz, F., Deloche, O., Wanke, V., Cameroni, E., and De Virgilio, C. (2005). The TOR and EGO protein complexes orchestrate microautophagy in yeast. Mol Cell *19*, 15-26.

Ebrahimi-Fakhari, D. (2018). Congenital Disorders of Autophagy: What a Pediatric Neurologist Should Know. Neuropediatrics *49*, 018-025.

Ebrahimi-Fakhari, D., Cantuti-Castelvetri, I., Fan, Z., Rockenstein, E., Masliah, E., Hyman, B.T., McLean, P.J., and Unni, V.K. (2011). Distinct Roles *In Vivo* for the Ubiquitin–Proteasome System and the Autophagy–Lysosomal Pathway in the Degradation of α-Synuclein. The Journal of Neuroscience *31*, 14508.

Ebrahimi-Fakhari, D., Saffari, A., Wahlster, L., Lu, J., Byrne, S., Hoffmann, G.F., Jungbluth, H., and Sahin, M. (2016). Congenital disorders of autophagy: an emerging novel class of inborn errors of neuro-metabolism. Brain *139*, 317-337.

El, A., Sa, W., Manifava, M., and Axe, E.L. (2008). Autophagosome formation from membrane compartments enriched in phosphatidylinositol 3-phosphate and dynamically connected to the endoplasmic reticulum. J Cell Biol *182*, 685-701.

Fabre, B., Lambour, T., Bouyssié, D., Menneteau, T., Monsarrat, B., Burlet-Schiltz, O., and Bousquet-Dubouch, M.-P. (2014). Comparison of label-free quantification methods for the determination of protein complexes subunits stoichiometry. EuPA Open Proteomics *4*, 82-86.

Feng, Y., He, D., Yao, Z., and Klionsky, D.J. (2014). The machinery of macroautophagy. Cell research *24*, 24-41.

Fimia, G.M., Stoykova, A., Romagnoli, A., Giunta, L., Di Bartolomeo, S., Nardacci, R., Corazzari, M., Fuoco, C., Ucar, A., Schwartz, P*., et al.* (2007). Ambra1 regulates autophagy and development of the nervous system. Nature *447*, 1121-1125.

Fujita, N., Itoh, T., Omori, H., Fukuda, M., Noda, T., and Yoshimori, T. (2008). The Atg16L complex specifies the site of LC3 lipidation for membrane biogenesis in autophagy. Mol Biol Cell *19*, 2092-2100.

Gao, W., Chen, Z., Wang, W., and Stang, M.T. (2013). E1-Like Activating Enzyme Atg7 Is Preferentially Sequestered into p62 Aggregates via Its Interaction with LC3-I. PLOS ONE *8*, e73229.

Gilabert, M., Vaccaro, M.I., Fernandez-Zapico, M.E., Calvo, E.L., Turrini, O., Secq, V., Garcia, S., Moutardier, V., Lomberk, G., Dusetti, N.*, et al.* (2013). Novel role of VMP1 as modifier of the pancreatic tumor cell response to chemotherapeutic drugs. Journal of Cellular Physiology *228*, 1834-1843.

Gómez-Sánchez, R., Rose, J., Guimarães, R., Mari, M., Papinski, D., Rieter, E., Geerts, W.J., Hardenberg, R., Kraft, C., Ungermann, C.*, et al.* (2018). Atg9 establishes Atg2-dependent contact sites between the endoplasmic reticulum and phagophores. The Journal of Cell Biology.

Grasso, D., Ropolo, A., Lo Re, A., Boggio, V., Molejon, M.I., Iovanna, J.L., Gonzalez, C.D., Urrutia, R., and Vaccaro, M.I. (2011). Zymophagy, a novel selective autophagy pathway mediated by VMP1-USP9x-p62, prevents pancreatic cell death. J Biol Chem *286*, 8308-8324.

Grasso, D., Sacchetti, M.L., Bruno, L., Lo Ré, A., Iovanna, J.L., Gonzalez, C.D., and Vaccaro, M.I. (2009). Autophagy and VMP1 Expression Are Early Cellular Events in Experimental Diabetes. Pancreatology *9*, 81-88.

Hailey, D.W., Rambold, A.S., Satpute-Krishnan, P., Mitra, K., Sougrat, R., Kim, P.K., and Lippincott-Schwartz, J. (2010). Mitochondria supply membranes for autophagosome biogenesis during starvation. Cell *141*, 656-667.

Hamasaki, M. (2013). Autophagosomes form at ER−mitochondria contact sites. Nature *495*, 389-393.

Hammond, Gerald R V., Schiavo, G., and Irvine, Robin F. (2009). Immunocytochemical techniques reveal multiple, distinct cellular pools of PtdIns4P and PtdIns(4,5)P(2). Biochemical Journal *422*, 23-35.

Hayashi-Nishino, M. (2009). A subdomain of the endoplasmic reticulum forms a cradle for autophagosome formation. Nature Cell Biol *11*, 1433-1437.

Hayashi-Nishino, M., Fujita, N., Noda, T., Yamaguchi, A., Yoshimori, T., and Yamamoto, A. (2010). Electron tomography reveals the endoplasmic reticulum as a membrane source for autophagosome formation. Autophagy *6*, 301-303.

Hegedűs, K., Takáts, S., Kovács, A.L., and Juhász, G. (2013). Evolutionarily conserved role and physiological relevance of a STX17/Syx17 (syntaxin 17)-containing SNARE complex in autophagosome fusion with endosomes and lysosomes. Autophagy *9*, 1642-1646.

Hosokawa, N., Hara, T., and Kaizuka, T. (2009). Nutrient-dependent mTORC1 association with the ULK1-Atg13-FIP200 complex required for autophagy. Mol Biol Cell *20*, 1981-1991.

Hsu, P.D., Scott, D.A., Weinstein, J.A., Ran, F.A., Konermann, S., Agarwala, V., Li, Y., Fine, E.J., Wu, X., Shalem, O.*, et al.* (2013). DNA targeting specificity of RNA-guided Cas9 nucleases. Nature biotechnology *31*, 827-832.

Ichimura, Y. (2008). Structural basis for sorting mechanism of p62 in selective autophagy. J Biol Chem *283*, 22847-22857.

Itakura, E., Kishi, C., Inoue, K., and Mizushima, N. (2008). Beclin 1 forms two distinct phosphatidylinositol 3-kinase complexes with mammalian Atg14 and UVRAG. Mol Biol Cell *19*, 5360-5372.

Itakura, E., and Mizushima, N. (2010). Characterization of autophagosome formation site by a hierarchical analysis of mammalian Atg proteins. Autophagy *6*, 764-776.

Jia, S., Wang, Y., You, Z., Liu, B., Gao, J., and Liu, W. (2017). Mammalian Atg9 contributes to the post-Golgi transport of lysosomal hydrolases by interacting with adaptor protein-1. FEBS Letters *591*, 4027-4038.

Jiang, P., and Mizushima, N. (2014). Autophagy and human diseases. Cell Research *24*, 69.

Jimenez-Sanchez, M., Thomson, F., Zavodszky, E., and Rubinsztein, D.C. (2012). Autophagy and polyglutamine diseases. Progress in Neurobiology *97*, 67-82.

Jr, D.W.A., Jm, C., and Jakw, K. (2005). Pexophagy: the selective autophagy of peroxisomes. Autophagy *1*, 75-83.

Kaufmann, A., Beier, V., Franquelim, H.G., and Wollert, T. (2014). Molecular mechanism of autophagic membrane-scaffold assembly and disassembly. Cell *156*, 469-481.

Kaushik, S., and Cuervo, A.M. (2018). The coming of age of chaperone-mediated autophagy. Nature Reviews Molecular Cell Biology.

Kim, J., Kundu, M., Viollet, B., and Kl, G. (2011). AMPK and mTOR regulate autophagy through direct phosphorylation of Ulk1. Nat Cell Biol *13*, 132-141.

Kimmelman, A.C., and White, E. (2017). Autophagy and Tumor Metabolism. Cell Metab *25*, 1037-1043.

Klionsky, D.J., Abdelmohsen, K., Abe, A., Abedin, M.J., Abeliovich, H., Acevedo Arozena, A., Adachi, H., Adams, C.M., Adams, P.D., Adeli, K.*, et al.* (2016). Guidelines for the use and interpretation of assays for monitoring autophagy (3rd edition). Autophagy *12*, 1-222.

Knævelsrud, H. (2013). Membrane remodeling by the PX-BAR protein SNX18 promotes autophagosome formation. J Cell Biol *202*, 331-349.

Komatsu, M., Waguri, S., Koike, M., Sou, Y.-s., Ueno, T., Hara, T., Mizushima, N., Iwata, J.-i., Ezaki, J., Murata, S.*, et al.* (2007). Homeostatic Levels of p62 Control Cytoplasmic Inclusion Body Formation in Autophagy-Deficient Mice. Cell *131*, 1149-1163.

Koyama-Honda, I., Itakura, E., Fujiwara, T.K., and Mizushima, N. (2013). Temporal analysis of recruitment of mammalian ATG proteins to the autophagosome formation site. Autophagy *9*, 1491-1499.

Lamb, C.A., Yoshimori, T., and Tooze, S.A. (2013). The autophagosome: origins unknown, biogenesis complex. Nature reviews Molecular cell biology *14*, 759-774.

Laplante, M., and Sabatini, D.M. (2012a). mTOR signaling. Cold Spring Harb Perspect Biol *4*, a011593-a011593.

Laplante, M., and Sabatini, D.M. (2012b). mTOR signaling in growth control and disease. Cell *149*, 274-293.

Lee, H.-J., Yoon, Y.-S., and Lee, S.-J. (2018). Mechanism of neuroprotection by trehalose: controversy surrounding autophagy induction. Cell death & disease *9*, 712.

Lee, I.H., Cao, L., Mostoslavsky, R., Lombard, D.B., Liu, J., Bruns, N.E., Tsokos, M., Alt, F.W., and Finkel, T. (2008). A role for the NAD-dependent deacetylase Sirt1 in the regulation of autophagy. Proceedings of the National Academy of Sciences *105*, 3374.

Lee, I.H., and Finkel, T. (2009). Regulation of autophagy by the p300 acetyltransferase. The Journal of biological chemistry *284*, 6322-6328.

Lilienbaum, A. (2013). Relationship between the proteasomal system and autophagy. International Journal of Biochemistry and Molecular Biology *4*, 1-26.

Loncle, C., Molejon, M.I., Lac, S., Tellechea, J.I., Lomberk, G., Gramatica, L., Fernandez Zapico, M.F., Dusetti, N., Urrutia, R., and Iovanna, J.L. (2016). The pancreatitis-associated protein VMP1, a key regulator of inducible autophagy, promotes Kras(G12D)-mediated pancreatic cancer initiation. Cell death & disease *7*, e2295.

Lundmark, R., Doherty, G.J., Howes, M.T., Cortese, K., Vallis, Y., Parton, R.G., and McMahon, H.T. (2008). The GTPase-Activating Protein GRAF1 Regulates the CLIC/GEEC Endocytic Pathway. Current Biology *18*, 1802-1808.

Ma, J.F., Huang, Y., Chen, S.D., and Halliday, G. (2010). Immunohistochemical evidence for macroautophagy in neurones and endothelial cells in Alzheimer's disease. Neuropathology and Applied Neurobiology *36*, 312-319.

Maiuri, M.C., Le Toumelin, G., Criollo, A., Rain, J.C., Gautier, F., Juin, P., Tasdemir, E., Pierron, G., Troulinaki, K., Tavernarakis, N.*, et al.* (2007). Functional and physical interaction between Bcl-X(L) and a BH3-like domain in Beclin-1. Embo j *26*, 2527-2539.

Malik, S.A., Orhon, I., Morselli, E., Criollo, A., Shen, S., Mariño, G., BenYounes, A., Bénit, P., Rustin, P., Maiuri, M.C.*, et al.* (2011). BH3 mimetics activate multiple pro-autophagic pathways. Oncogene *30*, 3918.

Mari, M., Tooze, S.A., and Reggiori, F. (2011). The puzzling origin of the autophagosomal membrane. F1000Prime Rep *3*.

Mattera, R., Park, S.Y., De Pace, R., Guardia, C.M., and Bonifacino, J.S. (2017). AP-4 mediates export of ATG9A from the trans-Golgi network to promote autophagosome formation. Proceedings of the National Academy of Sciences *114*, E10697.

Mayor, S., Parton, R.G., and Donaldson, J.G. (2014). Clathrin-Independent Pathways of Endocytosis. Cold Spring Harbor Perspectives in Biology *6*, a016758.

McEwan, D.G., and Dikic, I. (2011). The Three Musketeers of Autophagy: phosphorylation, ubiquitylation and acetylation. Trends in cell biology *21*, 195-201.

Mealer, R.G., Murray, A.J., Shahani, N., Subramaniam, S., and Snyder, S.H. (2014). Rhes, a Striatal-selective Protein Implicated in Huntington Disease, Binds Beclin-1 and Activates Autophagy. Journal of Biological Chemistry *289*, 3547-3554.

Meek, K., Douglas, P., Cui, X., Ding, Q., and Lees-Miller, S.P. (2007). trans Autophosphorylation at DNA-dependent protein kinase's two major autophosphorylation site clusters facilitates end processing but not end joining. Mol Cell Biol *27*, 3881-3890.

Mizushima, N., Kuma, A., Kobayashi, Y., Yamamoto, A., Matsubae, M., Takao, T., Natsume, T., Ohsumi, Y., and Yoshimori, T. (2003). Mouse Apg16L, a novel WD-repeat protein, targets to the autophagic isolation membrane with the Apg12-Apg5 conjugate. J Cell Sci *116*, 1679-1688.

Mizushima, N., Noda, T., and Yoshimori, T. (1998a). A protein conjugation system essential for autophagy. Nature *395*, 395-398.

Mizushima, N., Sugita, H., Yoshimori, T., and Ohsumi, Y. (1998b). A new protein conjugation system in human. The counterpart of the yeast Apg12p conjugation system essential for autophagy. J Biol Chem *273*, 33889-33892.

Mizushima, N., Yamamoto, A., and Hatano, M. (2001). Dissection of autophagosome formation using Apg5-deficient mouse embryonic stem cells. J Cell Biol *152*, 657-668.

Molejon, M.I., Ropolo, A., Re, A.L., Boggio, V., and Vaccaro, M.I. (2013). The VMP1–Beclin 1 interaction regulates autophagy induction. Sci Rep.

Moreau, K., Ravikumar, B., Puri, C., and Rubinsztein, D.C. (2012). Arf6 promotes autophagosome formation via effects on phosphatidylinositol 4,5-bisphosphate and phospholipase D. J Cell Biol *196*, 483-496.

Moreau, K., Ravikumar, B., Renna, M., Puri, C., Rubinsztein, D.C., and Rubinsztein C, D. (2011). Autophagosome precursor maturation requires homotypic fusion. Cell *146*, 303-317.

Moscat, J., and Diaz-Meco, M.T. (2009). p62 at the Crossroads of Autophagy, Apoptosis, and Cancer. Cell *137*, 1001-1004.

Nazio, F. (2013). mTOR inhibits autophagy by controlling ULK1 ubiquitylation, self-association and function through AMBRA1 and TRAF6. Nature Cell Biol *15*, 406-416.

Nguyen, T.N., Padman, B.S., Usher, J., Oorschot, V., Ramm, G., and Lazarou, M. (2016). Atg8 family LC3/GABARAP proteins are crucial for autophagosome–lysosome fusion but not autophagosome formation during PINK1/Parkin mitophagy and starvation. The Journal of Cell Biology.

Nilsson, P., Loganathan, K., Sekiguchi, M., Matsuba, Y., Hui, K., Tsubuki, S., Tanaka, M., Iwata, N., Saito, T., and Saido, Takaomi C. (2013). Aβ Secretion and Plaque Formation Depend on Autophagy. Cell Reports *5*, 61-69.

Nishimura, T., Tamura, N., Kono, N., Shimanaka, Y., Arai, H., Yamamoto, H., and Mizushima, N. (2017). Autophagosome formation is initiated at phosphatidylinositol synthase-enriched ER subdomains. Embo j *36*, 1719-1735.

Nixon, R.A., Wegiel, J., Kumar, A., Yu, W.H., Peterhoff, C., Cataldo, A., and Cuervo, A.M. (2005). Extensive involvement of autophagy in Alzheimer disease: an immuno-electron microscopy study. Journal of neuropathology and experimental neurology *64*, 113-122.

Noda, T. (2017). Autophagy in the context of the cellular membrane-trafficking system: the enigma of Atg9 vesicles. Biochemical Society Transactions *45*, 1323.

Obenauer, J.C., Cantley, L.C., and Yaffe, M.B. (2003). Scansite 2.0: proteome-wide prediction of cell signaling interactions using short sequence motifs. Nucleic Acids Research *31*, 3635-3641.

Orsi, A., Razi, M., Dooley, H.C., Robinson, D., Weston, A.E., Collinson, L.M., Tooze, S.A., and Hc, D. (2012). Dynamic and transient interactions of Atg9 with autophagosomes, but not membrane integration, are required for autophagy. Mol Biol Cell *23*, 1860-1873.

Pankiv, S., Clausen, T.H., Lamark, T., Brech, A., Bruun, J.-A., Outzen, H., Øvervatn, A., Bjørkøy, G., and Johansen, T. (2007). p62/SQSTM1 binds directly to Atg8/LC3 to facilitate

degradation of ubiquitinated protein aggregates by autophagy. The Journal of biological chemistry *282*, 24131-24145.

Pardo, R., Lo Ré, A., Archange, C., Ropolo, A., Papademetrio, D.L., Gonzalez, C.D., Alvarez, E.M., Iovanna, J.L., and Vaccaro, M.I. (2010). Gemcitabine Induces the VMP1 - Mediated Autophagy Pathway to Promote Apoptotic Death in Human Pancreatic Cancer Cells. Pancreatology *10*, 19-26.

Popovic, D., and Dikic, I. (2014). TBC1D5 and the AP2 complex regulate ATG9 trafficking and initiation of autophagy. EMBO reports *15*, 392.

Puente, C., Hendrickson, R.C., and Jiang, X. (2016). Nutrient-regulated Phosphorylation of ATG13 Inhibits Starvation-induced Autophagy. Journal of Biological Chemistry *291*, 6026-6035.

Puri, C., Renna, M., Cf, B., Moreau, K., and Dc, R. (2013). Diverse autophagosome membrane sources coalesce in recycling endosomes. Cell *154*, 1285-1299.

Puri, C., Vicinanza, M., Ashkenazi, A., Gratian, M.J., Zhang, Q., Bento, C.F., Renna, M., Menzies, F.M., and Rubinsztein, D.C. (2018). The RAB11A-Positive Compartment Is a Primary Platform for Autophagosome Assembly Mediated by WIPI2 Recognition of PI3P-RAB11A. Dev Cell *45*, 114-131.e118.

Qian, Q., Zhou, H., Chen, Y., Shen, C., He, S., Zhao, H., Wang, L., Wan, D., and Gu, W. (2014). VMP1 related autophagy and apoptosis in colorectal cancer cells: VMP1 regulates cell death. Biochem Biophys Res Commun *443*, 1041-1047.

Radhakrishna, H., and Donaldson, J.G. (1997). ADP-Ribosylation Factor 6 Regulates a Novel Plasma Membrane Recycling Pathway. The Journal of Cell Biology *139*, 49.

Ran, F.A., Hsu, P.D., Wright, J., Agarwala, V., Scott, D.A., and Zhang, F. (2013). Genome engineering using the CRISPR-Cas9 system. Nature protocols *8*, 2281-2308.

Rao, Y., Perna, M.G., Hofmann, B., Beier, V., and Wollert, T. (2016). The Atg1–kinase complex tethers Atg9-vesicles to initiate autophagy. Nature Communications *7*, 10338.

Ravikumar, B., Futter, M., Jahreiss, L., Korolchuk, V.I., Lichtenberg, M., Luo, S., Massey, D.C.O., Menzies, F.M., Narayanan, U., Renna, M.*, et al.* (2009). Mammalian macroautophagy at a glance. Journal of cell science *122*, 1707-1711.

Ravikumar, B., Moreau, K., Jahreiss, L., Puri, C., and Rubinsztein, D.C. (2010). Plasma membrane contributes to the formation of pre-autophagosomal structures. Nature Cell Biol *12*, 747-757.

Ravikumar, B., Sarkar, S., and Rubinsztein, D.C. (2008). Clearance of Mutant Aggregate-Prone Proteins by Autophagy. In Autophagosome and Phagosome, V. Deretic, ed. (Totowa, NJ: Humana Press), pp. 195-211.

Ravikumar, B., Vacher, C., Berger, Z., Davies, J.E., Luo, S., Oroz, L.G., Scaravilli, F., Easton, D.F., Duden, R., O'Kane, C.J.*, et al.* (2004). Inhibition of mTOR induces autophagy and reduces toxicity of polyglutamine expansions in fly and mouse models of Huntington disease. Nature genetics *36*, 585-595.

Rc, R., Tian, Y., Yuan, H., and Russell, R.C. (2013). ULK1 induces autophagy by phosphorylating Beclin-1 and activating VPS34 lipid kinase. Nature Cell Biol *15*, 741-750.

Renna, M., Bento, C.F., Fleming, A., Menzies, F.M., Siddiqi, F.H., Ravikumar, B., Puri, C., Garcia-Arencibia, M., Sadiq, O., Corrochano, S.*, et al.* (2013). IGF-1 receptor antagonism inhibits autophagy. Human molecular genetics *22*, 4528-4544.

Roczniak-Ferguson, A., Petit, C.S., Froehlich, F., Qian, S., Ky, J., Angarola, B., Walther, T.C., and Ferguson, S.M. (2012). The Transcription Factor TFEB Links mTORC1 Signaling to Transcriptional Control of Lysosome Homeostasis. Science signaling *5*, ra42.

Rogov, V., Dötsch, V., Johansen, T., and Kirkin, V. (2014). Interactions between Autophagy Receptors and Ubiquitin-like Proteins Form the Molecular Basis for Selective Autophagy. Molecular Cell *53*, 167-178.

Romanov, J., Walczak, M., Ibiricu, I., Schüchner, S., Ogris, E., Kraft, C., and Martens, S. (2012). Mechanism and functions of membrane binding by the Atg5-Atg12/Atg16 complex during autophagosome formation. The EMBO journal *31*, 4304-4317.

Ronan, B., Flamand, O., Vescovi, L., Dureuil, C., Durand, L., Fassy, F., Bachelot, M.F., Lamberton, A., Mathieu, M., Bertrand, T.*, et al.* (2014). A highly potent and selective Vps34 inhibitor alters vesicle trafficking and autophagy. Nat Chem Biol *10*, 1013-1019.

Ropolo, A., Grasso, D., Pardo, R., Sacchetti, M.L., Archange, C., Re, A.L., Seux, M., Nowak, J., Gonzalez, C.D., Iovanna, J.L.*, et al.* (2007). The Pancreatitis-induced Vacuole Membrane Protein 1 Triggers Autophagy in Mammalian Cells. Journal of Biological Chemistry *282*, 37124-37133.

Rubinsztein, D.C. (2006). The roles of intracellular protein-degradation pathways in neurodegeneration. Nature *443*, 780.

Rubinsztein, D.C., Cuervo, A.M., Ravikumar, B., Sarkar, S., Korolchuk, V., Kaushik, S., and Klionsky, D.J. (2009). In search of an "autophagomometer". Autophagy *5*, 585-589.

Rubinsztein, D.C., Shpilka, T., and Elazar, Z. (2012). Mechanisms of autophagosome biogenesis. Current biology : CB *22*, R29-34.

Sannerud, R., Declerck, I., Peric, A., Raemaekers, T., Menendez, G., Zhou, L., Veerle, B., Coen, K., Munck, S., De Strooper, B.*, et al.* (2011). ADP ribosylation factor 6 (ARF6) controls amyloid precursor protein (APP) processing by mediating the endosomal sorting of BACE1. Proceedings of the National Academy of Sciences *108*, E559.

Sarkar, S. (2013). Regulation of autophagy by mTOR-dependent and mTOR-independent pathways: autophagy dysfunction in neurodegenerative diseases and therapeutic application of autophagy enhancers. Biochemical Society Transactions *41*, 1103.

Sarkar, S., Davies, J.E., Huang, Z., Tunnacliffe, A., and Rubinsztein, D.C. (2007a). Trehalose, a Novel mTOR-independent Autophagy Enhancer, Accelerates the Clearance of Mutant Huntingtin and α-Synuclein. Journal of Biological Chemistry *282*, 5641-5652.

Sarkar, S., Floto, R.A., Berger, Z., Imarisio, S., Cordenier, A., Pasco, M., Cook, L.J., and Rubinsztein, D.C. (2005). Lithium induces autophagy by inhibiting inositol monophosphatase. The Journal of Cell Biology *170*, 1101-1111.

Sarkar, S., Perlstein, E.O., Imarisio, S., Pineau, S., Cordenier, A., Maglathlin, R.L., Webster, J.A., Lewis, T.A., O'Kane, C.J., Schreiber, S.L.*, et al.* (2007b). Small molecules enhance

autophagy and reduce toxicity in Huntington's disease models. Nature Chemical Biology *3*, 331.

Saxton, R.A., and Sabatini, D.M. (2017). mTOR Signaling in Growth, Metabolism, and Disease. Cell *168*, 960-976.

Settembre, C., Zoncu, R., Medina, D.L., Vetrini, F., Erdin, S., Erdin, S., Huynh, T., Ferron, M., Karsenty, G., Vellard, M.C.*, et al.* (2012). A lysosome-to-nucleus signalling mechanism senses and regulates the lysosome via mTOR and TFEB. The EMBO Journal *31*, 1095.

Shacka, J.J., Klocke, B.J., Shibata, M., Uchiyama, Y., Datta, G., Schmidt, R.E., and Roth, K.A. (2006). Bafilomycin A1 Inhibits Chloroquine-Induced Death of Cerebellar Granule Neurons. Molecular Pharmacology *69*, 1125.

Shi, C.S., and Kehrl, J.H. (2010). TRAF6 and A20 regulate lysine 63-linked ubiquitination of Beclin-1 to control TLR4-induced autophagy. Science signaling *3*, ra42.

Söderberg, O., Gullberg, M., Jarvius, M., Ridderstråle, K., Leuchowius, K.-J., Jarvius, J., Wester, K., Hydbring, P., Bahram, F., Larsson, L.-G.*, et al.* (2006). Direct observation of individual endogenous protein complexes in situ by proximity ligation. Nature methods *3*, 995-1000.

Søreng, K., Munson, M.J., Lamb, C.A., Bjørndal, G.T., Pankiv, S., Carlsson, S.R., Tooze, S.A., and Simonsen, A. (2018). SNX18 regulates ATG9A trafficking from recycling endosomes by recruiting Dynamin-2. EMBO reports *19*.

Spencer, B., Potkar, R., Trejo, M., Rockenstein, E., Patrick, C., Gindi, R., Adame, A., Wyss-Coray, T., and Masliah, E. (2009). Beclin 1 Gene Transfer Activates Autophagy and Ameliorates the Neurodegenerative Pathology in α-Synuclein Models of Parkinson's and Lewy Body Diseases. The Journal of Neuroscience *29*, 13578.

Stolz, A., Ernst, A., and Dikic, I. (2014). Cargo recognition and trafficking in selective autophagy. Nat Cell Biol *16*, 495-501.

Tabara, L.C., Vicente, J.J., Biazik, J., Eskelinen, E.L., Vincent, O., and Escalante, R. (2018). Vacuole membrane protein 1 marks endoplasmic reticulum subdomains enriched in

phospholipid synthesizing enzymes and is required for phosphoinositide distribution. Traffic *19*, 624-638.

Takahashi, Y. (2011). Bif-1 regulates Atg9 trafficking by mediating the fission of Golgi membranes during autophagy. Autophagy *7*, 61-73.

Takahashi, Y., Coppola, D., Matsushita, N., Cualing, H.D., Sun, M., Sato, Y., Liang, C., Jung, J.U., Cheng, J.Q., Mul, J.J.*, et al.* (2007). Bif-1 interacts with Beclin 1 through UVRAG and regulates autophagy and tumorigenesis. Nature Cell Biology *9*, 1142.

Tanida, I, Tanida-Miyake, E., Ueno, T., and Kominami, E. (2001). The human homolog of Saccharomyces cerevisiae Apg7p is a protein-activating enzyme for multiple substrates including human Apg12p, GATE-16, GABARAP, and MAP-LC3. J Biol Chem *276*, 1701-1706.

Thumm, M., Egner, R., Koch, B., Schlumpberger, M., Straub, M., Veenhuis, M., and Wolf, D.H. (1994). Isolation of autophagocytosis mutants of Saccharomyces cerevisiae. FEBS Lett *349*, 275-280.

Tooze, S.A. (2010). The role of membrane proteins in mammalian autophagy. Seminars in Cell & Developmental Biology *21*, 677-682.

Tsukada, M., and Ohsumi, Y. (1993). Isolation and characterization of autophagy-defective mutants of Saccharomyces cerevisiae. FEBS Lett *333*, 169-174.

Vaccaro, M.I., Ropolo, A., Grasso, D., and Iovanna, J.L. (2008). A novel mammalian trans-membrane protein reveals an alternative initiation pathway for autophagy. Autophagy *4*, 388-390.

van Beek, N., Klionsky, D.J., and Reggiori, F. (2018). Genetic aberrations in macroautophagy genes leading to diseases. Biochimica et Biophysica Acta (BBA) - Molecular Cell Research *1865*, 803-816.

Veuger, S.J., Curtin, N.J., Richardson, C.J., Smith, G.C.M., and Durkacz, B.W. (2003). Radiosensitization and DNA Repair Inhibition by the Combined Use of Novel Inhibitors of DNA-dependent Protein Kinase and Poly(ADP-Ribose) Polymerase-1. Cancer Research *63*, 6008.

Vicinanza, M., Korolchuk, V.I., Ashkenazi, A., Puri, C., Menzies, F.M., Clarke, J.H., and Rubinsztein, D.C. (2015). PI(5)P regulates autophagosome biogenesis. Mol Cell *57*, 219-234.

Wang, W., Chen, Z., Billiar, T.R., Stang, M.T., and Gao, W. (2013). The Carboxyl-Terminal Amino Acids Render Pro-Human LC3B Migration Similar to Lipidated LC3B in SDS-PAGE. PLOS ONE *8*, e74222.

Webb, J.L., Ravikumar, B., Atkins, J., Skepper, J.N., and Rubinsztein, D.C. (2003). α-Synuclein Is Degraded by Both Autophagy and the Proteasome. Journal of Biological Chemistry *278*, 25009-25013.

Weerasekara, V.K., Panek, D.J., Broadbent, D.G., Mortenson, J.B., Mathis, A.D., Logan, G.N., Prince, J.T., Thomson, D.M., Thompson, J.W., and Andersen, J.L. (2014). Metabolic-stress-induced rearrangement of the 14-3-3zeta interactome promotes autophagy via a ULK1- and AMPK-regulated 14-3-3zeta interaction with phosphorylated Atg9. Mol Cell Biol *34*, 4379-4388.

Weidberg, H., Shvets, E., and Elazar, Z. (2011). Biogenesis and cargo selectivity of autophagosomes. Annu Rev Biochem *80*, 125-156.

Weidberg, H., Shvets, E., and Shpilka, T. (2010). LC3 and GATE-16/GABARAP subfamilies are both essential yet act differently in autophagosome biogenesis. EMBO J *29*, 1792-1802.

White, E. (2015). The role for autophagy in cancer. The Journal of Clinical Investigation *125*, 42-46.

Williams, A., Sarkar, S., Cuddon, P., Ttofi, E.K., Saiki, S., Siddiqi, F.H., Jahreiss, L., Fleming, A., Pask, D., Goldsmith, P.*, et al.* (2008). Novel targets for Huntington's disease in an mTOR-independent autophagy pathway. Nature Chemical Biology *4*, 295.

Willmore, E., de Caux, S., Sunter, N.J., Tilby, M.J., Jackson, G.H., Austin, C.A., and Durkacz, B.W. (2004). A novel DNA-dependent protein kinase inhibitor, NU7026, potentiates the cytotoxicity of topoisomerase II poisons used in the treatment of leukemia. Blood *103*, 4659-4665.

Winslow, A.R. (2010). [alpha]-synuclein impairs macroautophagy: implications for Parkinson's disease. J Cell Biol *190*, 1023-1037.

Xia, P., Wang, S., Du, Y., Zhao, Z., Shi, L., Sun, L., Huang, G., Ye, B., Li, C., Dai, Z.*, et al.* (2013). WASH inhibits autophagy through suppression of Beclin 1 ubiquitination. Embo j *32*, 2685-2696.

Xie, Y., Kang, R., Sun, X., Zhong, M., Huang, J., Klionsky, D.J., and Tang, D. (2015). Posttranslational modification of autophagy-related proteins in macroautophagy. Autophagy *11*, 28-45.

Xu, C., Kim, N.-G., and Gumbiner, B.M. (2009). Regulation of protein stability by GSK3 mediated phosphorylation. Cell cycle (Georgetown, Tex) *8*, 4032-4039.

Yang, Z., Goronzy, J.J., and Weyand, C.M. (2015). Autophagy in autoimmune disease. Journal of Molecular Medicine *93*, 707-717.

Yi, C., Ma, M., Ran, L., Zheng, J., Tong, J., Zhu, J., Ma, C., Sun, Y., Zhang, S., Feng, W.*, et al.* (2012). Function and Molecular Mechanism of Acetylation in Autophagy Regulation. Science *336*, 474.

Yoon, Y.-S., Cho, E.-D., Jung Ahn, W., Won Lee, K., Lee, S.-J., and Lee, H.-J. (2017). Is trehalose an autophagic inducer? Unraveling the roles of non-reducing disaccharides on autophagic flux and alpha-synuclein aggregation. Cell Death &Amp; Disease *8*, e3091.

Young, A.R.J., Chan, E.Y.W., Hu, X.W., Köchl, R., Crawshaw, S.G., High, S., Hailey, D.W., Lippincott-Schwartz, J., Tooze, S.A., Arj, Y.*, et al.* (2006). Starvation and ULK1-dependent cycling of mammalian Atg9 between the TGN and endosomes. J Cell Sci *119*, 3888-3900.

Yu, Z.-Q., Ni, T., Hong, B., Wang, H.-Y., Jiang, F.-J., Zou, S., Chen, Y., Zheng, X.-L., Klionsky, D.J., Liang, Y.*, et al.* (2012). Dual roles of Atg8−PE deconjugation by Atg4 in autophagy. Autophagy *8*, 883-892.

Zaffagnini, G., Savova, A., Danieli, A., Romanov, J., Tremel, S., Ebner, M., Peterbauer, T., Sztacho, M., Trapannone, R., Tarafder, A.K.*, et al.* (2018). p62 filaments capture and present ubiquitinated cargos for autophagy. The EMBO Journal.

Zavodszky, E., Seaman, M.N.J., Moreau, K., Jimenez-Sanchez, M., Breusegem, S.Y., Harbour, M.E., and Rubinsztein, D.C. (2014). Mutation in VPS35 associated with Parkinson's

disease impairs WASH complex association and inhibits autophagy. Nature communications *5*, 3828-3828.

Zavodszky, E., Vicinanza, M., and Rubinsztein, D.C. (2013). Biology and trafficking of ATG9 and ATG16L1, two proteins that regulate autophagosome formation. FEBS letters *587*, 1988-1996.

Zens, B., Sawa-Makarska, J., and Martens, S. (2015). In vitro systems for Atg8 lipidation. Methods (San Diego, Calif) *75*, 37-43.

Zhao, Y.G., Chen, Y., Miao, G., Zhao, H., Qu, W., Li, D., Wang, Z., Liu, N., Li, L., Chen, S., *et al.* (2017). The ER-Localized Transmembrane Protein EPG-3/VMP1 Regulates SERCA Activity to Control ER-Isolation Membrane Contacts for Autophagosome Formation. Mol Cell *67*, 974-989.e976.

Zhao, Y.G., Liu, N., Miao, G., Chen, Y., Zhao, H., and Zhang, H. (2018). The ER Contact Proteins VAPA/B Interact with Multiple Autophagy Proteins to Modulate Autophagosome Biogenesis. Curr Biol *28*, 1234-1245.e1234.

Zhao, Y.G., and Zhang, H. (2018). The ER-localized autophagy protein EPG-3/VMP1 regulates ER contacts with other organelles by modulating ATP2A/SERCA activity. Autophagy *14*, 362-363.

Zhao, Y.G., Zhao, H., Sun, H., and Zhang, H. (2013). Role of Epg5 in selective neurodegeneration and Vici syndrome. Autophagy *9*, 1258-1262.

Zhu, Y., Runwal, G., Obrocki, P., and Rubinsztein, D.C. (2018). Autophagy in childhood neurological disorders. Developmental Medicine & Child Neurology *0*.

Appendix

Abbreviations

AD - Alzheimer's Disease

ADP - adenosine diphosphate

AMBRA1 - activating molecular in BECN-1 regulated autophagy protein 1

AMPK - adenosine monophosphate-dependent protein kinase

AP2 – adaptor complex 2

APP - amyloid precursor protein

ATG - autophagy related protein/gene

ATG16 KO – ATG16 CRISPR knockout cell line

ATG9 KO – ATG9 CRISPR knockout cell line

ATP - adenosine triphosphate

Baf/BAF - bafilomycin A1

BECN-1 - beclin-1

Bcl-2 - B-cell lymphoma 2

4E-BP1 - eukaryotic translation initiation factor 4E-binding protein 1

BSA - bovine serum albumin

Ca^{2+} - calcium

CMA - chaperone mediated autophagy

DAPI - 4',6-diamidino-2-phenylindole

DMEM - Dulbecco's modified eagle media

DMSO - dimethyl sulfoxide

DNA - deoxyribonucleic acid

EDTA - ethylenediaminetetraacetic acid

ER - endoplasmic reticulum

FBS - foetal bovine serum

FIP200 - focal adhesion kinase family kinase-interacting protein of 200 kDa

GABARAP - γ-aminobutyric-acid-type-A-receptor-associated protein

GAPDH - glyceraldehyde 3-phosphate dehydrogenase

GATE16 - Golgi-associated ATPase enhancer of 16 kDa

GDP - guanosine diphosphate

GFP - green fluorescent protein

GTP - guanosine triphosphate

HBSS - Hank's balanced salt solution

HD - Huntington's Disease

HEK – human embryonic kidney cells

HeLa - human epithelial cervical cancer cells

Hsc- heat shock cognate

hsp – heat shock protein

IP - immunoprecipitate

K^+ - potassium

kDa - kilo Dalton

LAMP - lysosomal-associated membrane glycoprotein

LC3 - microtubule-associated protein 1A/1B-Light Chain 3

LIR - LC3-interacting region

MEFs - mouse embryonic fibroblasts

mTOR - mechanistic/mammalian target of rapamycin

mTORC - mTOR complex

NBR1 - neighbour of BRCA1 gene 1

p53 - phosphoprotein 53

p62/SQSTM1- sequestosome 1

PAS - pre-autophagosomal structure/phagophore assembly site

PBS - phosphate buffered saline

PD - Parkinson's Disease

PE - phosphatidylethanolamine

PFA - paraformaldehyde

PH - pleckstrin homology

PI3P - phosphatidylinositol 3-phosphate

PI3K - phosphatidylinositol-4,5-bisphosphate 3-kinase

PS - phosphatidylserine

PTM - post-translational modification

PVDF - polyvinylidene fluoride

Rab - Ras superfamily of monomeric G proteins

Rap - rapamycin

RAPTOR - regulatory-associated protein of mTOR

RFP - red fluorescent protein

p70 S6K1 - ribosomal protein S6 kinase, 70 kDa, polypeptide 1

RICTOR - rapamycin-insensitive companion of mammalian target of rapamycin

RNA - ribonucleic acid

SDS-PAGE - sodium dodecyl sulphate-polyacrylamide gel electrophoresis

SNAP - soluble NSF attachment protein

SNARE - SNAP receptor

TGN - trans-Golgi network

TSC1 - tuberous sclerosis 1

UBA domain - ubiquitin-associated domain

ULK1 - unc-51-like autophagy activating kinase

UPS - Ubiquitin proteasome system

UVRAG - UV radiation resistance associated is a protein-coding gene

VAMP - vesicle-associated membrane protein

VPS - vacuolar protein sorting

WD40 - tryptophan-aspartic acid repeat-containing proteins

WD - tryptophan-aspartic acid (motif)

WE - tryptophan-glutamate (motif)

WIPI - WD repeat domain phosphoinositide-interacting protein